The topology of fullerenes

Schwerdtfeger, Peter; Wirz, Lukas; Avery, James Emil

The topology of fullerenes

Peter Schwerdtfeger,[1,2]* Lukas N Wirz[1] and James Avery[3]

Fullerenes are carbon molecules that form polyhedral cages. Their bond structures are exactly the planar cubic graphs that have only pentagon and hexagon faces. Strikingly, a number of chemical properties of a fullerene can be derived from its graph structure. A rich mathematics of cubic planar graphs and fullerene graphs has grown since they were studied by Goldberg, Coxeter, and others in the early 20th century, and many mathematical properties of fullerenes have found simple and beautiful solutions. Yet many interesting chemical and mathematical problems in the field remain open. In this paper, we present a general overview of recent topological and graph theoretical developments in fullerene research over the past two decades, describing both solved and open problems. © 2014 The Authors. *WIREs Computational Molecular Science* published by John Wiley & Sons, Ltd.

INTRODUCTION

Buckminsterfullerene C_{60}-I_h is a convex and 'spherical' molecule (in the sense that the atoms lie on the surface of a sphere) with a highly symmetric icosahedral structure. It was originally conjectured independently by Ōsawa in 1970[1,2] and Stankevich, Bochvar, and Galpern in 1973,[3,4] discovered by mass spectrometry in 1985 by Kroto et al. through laser evaporation of graphite,[5–8] and synthesized in larger amounts by Krätschmer et al.[9] in 1990 (the first mass-spectroscopic studies on small carbon cluster were performed by Mattauch et al.[10] in 1943). Fullerenes are the polyhedral analogs to the two-dimensional graphene sheets.[a] They occur in nature and have been detected in interstellar space,

albeit in minute amounts.[11–14] In general, (classical) fullerenes are cage-like, hollow molecules of pseudo-spherical symmetry consisting of pentagons and hexagons only, resulting in a trivalent (and in the most ideal case) convex polyhedron with exactly three edges (bonds) joining every vertex occupied by carbon, idealized as sp^2 hybridized atoms.[15] In graph theoretical terms, fullerenes belong to the class of cubic, planar, three-connected, and simple graphs, consisting of 12 pentagons only (the 12 *Pentagon Theorem*) and F_6 hexagons. This gives the general formula of C_{20+2F_6} ($F_6 \geq 0$ and $F_6 \neq 1$) for carbon fullerenes, with the number of hexagonal faces $F_6 = 20$ for C_{60}. The smallest possible fullerene is C_{20} ($F_6 = 0$), a dodecahedron consisting of 12 connected pentagons, and the only Platonic solid in the family of fullerene polyhedra.[16] The truncated icosahedron C_{60} belongs to the class of Archimedean solids.[17] C_{60}-I_h is the minimal arrangement such that no two pentagons share an edge (isolated pentagons): The edges of each pentagon join only hexagons, and the edges of each hexagon alternately join pentagons and hexagons. Thus, it is the smallest member in the class of fullerenes fulfilling the so-called *isolated pentagon rule* (IPR), which brings thermodynamic stability to a fullerene cage.[18]

*Correspondence to: p.a.schwerdtfeger@massey.ac.nz

[1]Centre for Theoretical Chemistry and Physics, The New Zealand Institute for Advanced Study, Massey University Auckland, Auckland, New Zealand

[2]Fachbereich Chemie, Philipps-Universität Marburg, Marburg, Germany

[3]Niels Bohr Institute, University of Copenhagen, Copenhagen, Denmark

Conflict of interest: The authors have declared no conflicts of interest for this article.
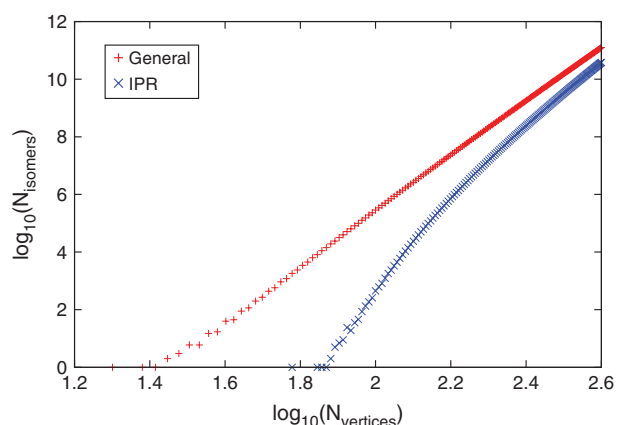
FIGURE 1 | Number of distinct (non-isomorphic) fullerene isomers C_N (with and without fulfilling the IPR) with increasing number of carbon atoms N up to $N = 400$ (double logarithmic scale). (Data taken from the House of Graphs Ref 34)

There are infinitely many fullerenes, the number of isomers growing as $\mathcal{O}(N^9)$ for N carbon atoms as shown in Figure 1.[19] The reason for the N^9 growth comes from algebraic geometry, and is discussed below. These isomers come in many different shapes depending on the distribution of the pentagons as shown in Figure 2.[b] As experimental techniques advance to synthesize new fullerene isomers[21] with many interesting chemical and physical applications,[22–25] see for example the recent bottom-up synthesis of C_{60} by Scott et al.[26] and Kabdulov et al.,[27] one naturally wants to know more about their thermodynamic stability and electronic properties.[28] As the isomer space rapidly grows into the millions and beyond, this becomes a daunting task for larger fullerenes. Even when the search is restricted to fullerenes that have isolated pentagons, known to yield the best stability, the number of candidates for most thermodynamically stable isomers is huge, many orders of magnitude too large for quantum chemical methods to be a viable means of analyzing stability. But, remarkably, the fullerene graphs contain all the information we need, and we are able to sort through the millions of isomers, finding a few candidates for the most stable, by way of simple, easily computed topological indicators,[29,30] such as the neighbor indices for pentagons or hexagons,[31] or the incremental assignment of heat of formations to certain face patches.[32,33]

There has been an intense activity in the field of topological and graph theoretical descriptions of molecules such as fullerenes[29,31,36–40] over the past 20 years, to the extent that it has become a major sub-discipline within mathematical chemistry. It comes perhaps as a surprise that graph theory applied to molecular structures has not yet made it into main-stream university teaching. Furthermore, since the publication of the standard reference work in this area, *An Atlas of Fullerenes* by Fowler and Manolopoulos,[31] there has not been a comprehensive review on this subject highlighting the many activities in recent times. In contrast, there are excellent reviews and books available on the chemistry and physics of fullerenes[22,23,41–47] or on their electronic structure calculations.[28] In this overview we aim to close this gap and report on the many new and exciting developments in the topological and graph theoretical treatment of fullerenes, which have taken place over the past decade or so.[c]

TOPOLOGICAL PROPERTIES OF FULLERENES

A Short Introduction to Graph Theory and Embeddings

A *graph* is a pair $G = (\mathcal{V}, \mathcal{E})$, where $\mathcal{V}$ defines a set of vertices, and $\mathcal{E}$ is a set of edges, each an unordered pair connecting two vertices. If a graph can be drawn in the two-dimensional plane without edge crossings, then it is called *planar*, and in this case it can also be drawn using only straight lines. A *planar embedding* is a map $\mathcal{V} \rightarrow \mathbb{R}^2$ assigning a 2D-coordinate to each vertex such that straight-line drawings of the edges do not cross. For planar graphs in general, planar embeddings are not unique. But whenever at least three vertices must be removed before the graph separates into two disconnected components, the graph is called *three-connected*, and there is essentially only one way[d] to embed it in the plane.[48] Because of this, a three-connected planar graph has a well-defined set of *faces*, $\mathcal{F}$. We can therefore represent a three-connected planar graph as $G = (\mathcal{V}, \mathcal{E}, \mathcal{F})$ without ambiguity, and will do so where convenient.

Whenever a graph is planar, it can also be embedded onto a surface of a sphere without edge crossings, and vice versa. Once again, this embedding is unique (in the same sense as for a planar embedding) if and only if the graph is three-connected, and we obtain the same faces. In fact, the graphs describing three-dimensional polyhedra are exactly the three-connected planar graphs,[49] and are therefore called *polyhedral graphs*.

The number of neighbors to a vertex v, that is, the number of edges incident to v, is called its *degree*, abbreviated as $\deg(v)$. If every vertex of a graph G has the same degree k, then G is called *k-valent* or *k-regular*. The special case of three-valent graphs is called *cubic*, and has a host of attractive mathematical
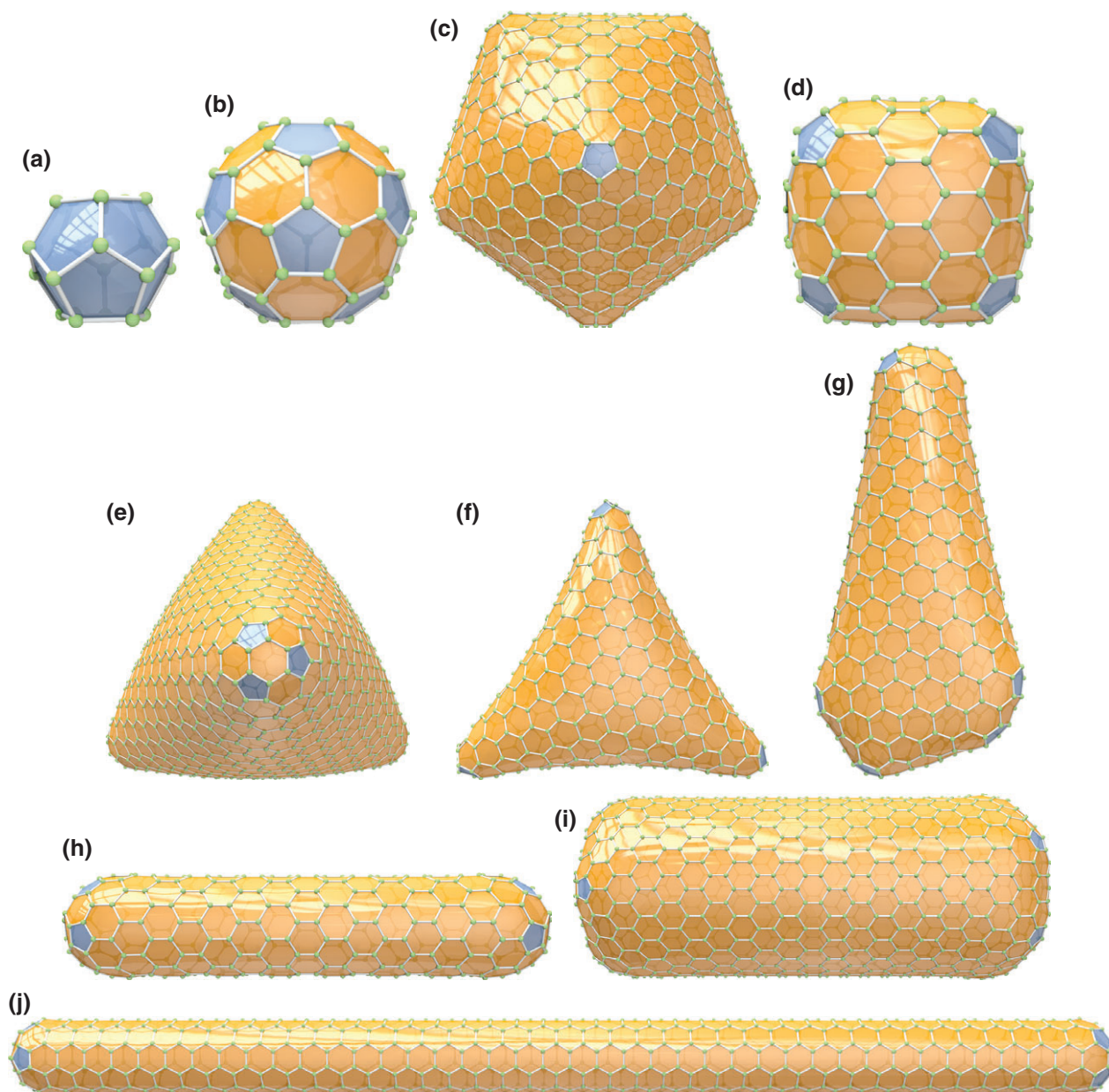
FIGURE 2 | A selection of different 3D shapes for regular fullerenes (distribution of the pentagons D_P are set in parentheses). 'Spherically' shaped (icosahedral), for example, (a) C_{20}-I_h, (b) C_{60}-I_h, and (c) C_{960}-I_h ($D_P = 12 \times 1$); barrel shaped, for example, (d) C_{140}-D_{3h} ($D_P = 6 \times 2$); trigonal pyramidally shaped (tetrahedral structures), for example, (e) C_{1140}-T_d ($D_P = 4 \times 3$); (f) trihedrally shaped C_{440}-D_3 ($D_P = 3 \times 4$); (g) nano-cone or menhir C_{524}-C_1 ($D_P = 5 + 7 \times 1$); cylindrically shaped (nanotubes), for example, (h) C_{360}-D_{5h}, (i) C_{1152}-D_{6d}, (j) C_{840}-D_{5d} ($D_P = 2 \times 6$). The fullerenes shown in this figure and throughout the paper have been generated automatically using the *Fullerene* program.[35]

properties, not least of which is their deep connections to algebraic geometry.[19]

Fullerenes have the neat property that the graphs formed by their bond structure are both cubic, planar, and three-connected, for which all faces are either pentagons or hexagons. Because of this, the mathematics describing them is in many cases both rich, simple, and elegant. We are able to derive many properties about their topologies, spatial shapes, surface,

as well as indicators of their chemical behaviors, directly from their graphs.

Planar connected graphs fulfil *Euler's polyhedron formula*,

$$N - E + F = 2 \qquad (1)$$

with $N = |\mathcal{V}|$ being the number of vertices (called the *order* of the graph), $E = |\mathcal{E}|$ the number of edges, and $F = |\mathcal{F}|$ the number of faces (for fullerenes these are
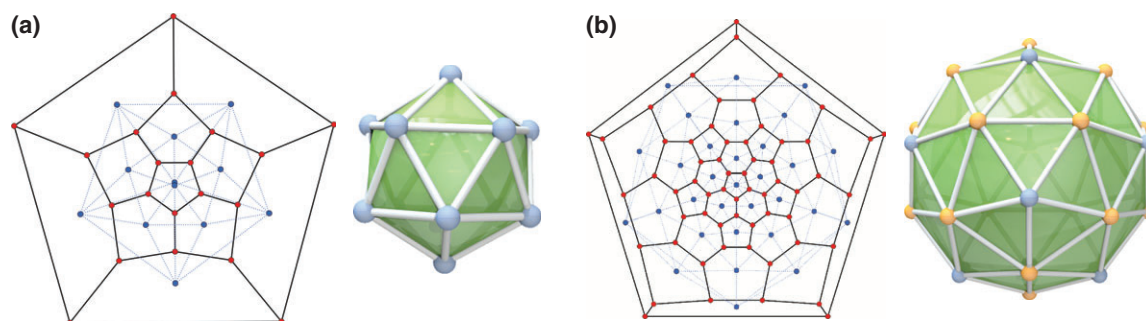
FIGURE 3 | Planar embeddings of fullerene graph and dual (blue color and dotted lines for the dual representation), and 3D embeddings of the duals: (a) C_{20}-I_h, for which the dual is the icosahedron; (b) C_{60}-I_h, for which the dual is the pentakis-dodecahedron.
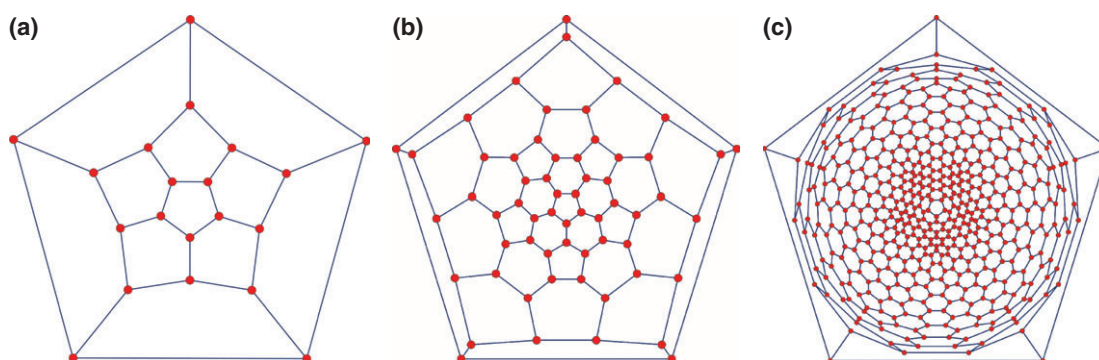

FIGURE 4 | Planar embeddings (no crossing edges) for three different fullerenes obtained from a perspective projection. (a) icosahedron C_{20}-I_h; (b) truncated icosahedron C_{60}-I_h; (c) C_{540}-I_h.

hexagons and pentagons). The hand-shaking lemma in graph theory tells us that

$$\sum_{i=1}^{N} \deg\left(v_i\right) = 2E \tag{2}$$

Since for fullerenes $\deg(v_i) = 3$ for all vertices, we obtain[50]

$$E = \frac{3}{2}N, \quad F = \frac{1}{2}N + 2 = \frac{1}{3}E + 2, \quad \text{and } E = 3F - 6 \tag{3}$$

Hence, for fullerenes and fulleroids[e] one has an even number of vertices. The total number of faces is $F = F_5 + F_6$, where F_5 and F_6 are the number of pentagons and hexagons respectively. From this we derive from Eq (3) $E = 3F_5 + 3F_6 - 6$ and $N = 2F_5 + 2F_6 - 4$. On the other hand, each pentagon (hexagon) has five (six) edges, which gives $E = (5/2)F_5 + 3F_6$. From these equations together with Eq (1) we obtain $F_5 = 12$ for regular fullerenes (the '12 Pentagon Theorem' for fullerenes), which gives the number of hexagons as $F_6 = (N - 20)/2$ with $N \geq 20$, and the general formula C_{20+2F_6} for fullerenes. Hence, from the fact that we only allow for cubic planar graphs consisting of pentagons and hexagons, we restrict the number of pentagons to exactly 12 (no more and no less!), and every

addition of a hexagon adds two new vertices. Moreover, $N = 22$ with just 1 hexagon and 12 pentagons is not valid, but every number of hexagons two or greater yields at least one fullerene.[51] The most stable C_{22} molecule is, however, a cage-like fulleroid with a four-membered ring.[52]

In this article, we will often work with the *dual graph*. The dual graph G^* of a planar connected graph G has a vertex corresponding to each face of G, and an edge joining two neighboring faces in G. By this process, the old vertices become the new faces. The dual of a planar graph is itself a planar graph, and for fullerenes it is a triangulation with 12 vertices of degree 5 and the remaining of degree 6. For planar graphs in general, the dual is not unique, but as discussed above, it is unique for three-connected graphs such as fullerenes, and hence the dual operation is well defined.[48] The dual operation is an involution, that is, $(G^*)^* = G$, so we can think of the dual as just another representation of the same graph. Figure 3 shows the duals of two representative fullerenes with their corresponding 2D graph representation discussed in the next section.

A useful representation of a graph is the *adjacency matrix* A_{ij} well known to chemists, as it is widely used in Hückel theory of conjugated organic
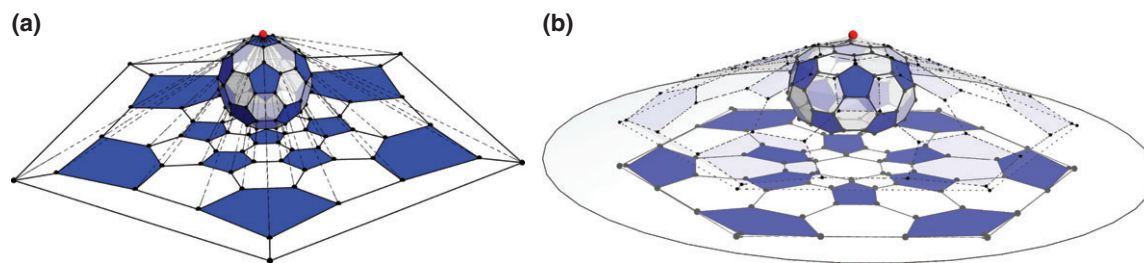
(a)   **(b)**

FIGURE 5 | (a) Schlegel projection of C_{60}-I_h. (b) Cone projection of disk-shaped C_{72}-D_{6d}.

molecules. The adjacency matrix is a symmetric matrix defined by $A_{ij} = 1$ if the graph G contains an edge $v_i - v_j$, and $A_{ij} = 0$ otherwise. It is equivalent to the edge-set representation, and is much easier to work with in many settings. As the number of edges for fullerenes is $E = 3N/2$, the adjacency matrix is very sparse. If two graphs G_1 and G_2 are isomorphic, the corresponding adjacency matrices A_1 and A_2 are related by vertex permutation, and thus share the same set of eigenvalues and eigenvectors. Matrices play a special role in chemical graph theory, and the reader is referred to Ref 53 for more details.

Drawing Fullerene Graphs: Methods for Planar Embedding

Planar embeddings can be drawn on paper and give us a way to visualize the structures of planar graphs. However, not all choices of embeddings are equally informative. We want the drawings to be simple, not too cluttered, and to expose as much as we can of the graph's structure and symmetry. In general the full symmetry group can not be realized in two dimensions, but we can find embeddings that show as much of it as possible. Figure 4 shows planar drawings of three icosahedral fullerenes, C_{20}-I_h, C_{60}-I_h, and C_{540}-I_h, exposing 10-fold D_5-symmetry out of the full I_h group. In this section, we will discuss methods for constructing good planar embeddings.

While a small graph can easily be drawn by hand, larger graphs such as C_{540} shown in Figure 4(c) require a computer algorithm and a drawing program. The first method we will discuss is called the *Schlegel projection*, and requires first an embedding of the graph as a three-dimensional polyhedron. In 1886, Victor Schlegel showed that a planar graph can be obtained from a three-dimensional polyhedron by projection in the following way: A point $\vec{x}_0$ is placed slightly above one of the faces, and a plane P is chosen to lie below the polyhedron. Lines are then drawn from $\vec{x}_0$ through each of the polyhedron's vertices. The intersection of each line $\vec{x}_0 - \vec{x}_v$ with P defines the 2D coordinate of the vertex v. If $\vec{x}_0$ is chosen

sufficiently close to the face, and if the points of the polyhedron lie on a sphere, the resulting 2D embedding will be planar. While Schlegel only proved that the projection produces a planar layout when the vertices lie on a sphere, it still works in many cases where this is not the case, and the method is widely used to the extent that planar graph embeddings sometimes (incorrectly) are called Schlegel diagrams. However, Schlegel diagrams are specifically the embeddings that result from the Schlegel projection. The Schlegel projection is illustrated in Figure 5(a).

A problem with the Schlegel projection is that it often fails, and produces crossing edges, when used with many non-spherical polyhedra or when the parameters are not well chosen. The cone-projection method, shown in Figure 5(b), which projects the vertices out on an enveloping cone of the fullerene polyhedron and then down onto a plane, seems to be more robust.[35]

Both the cone-projection and the Schlegel projection require first a polyhedral embedding of the graph, and on top of that often necessitate bit of hand-tuning to produce a planar embedding. The third method we mention is called the *Tutte embedding*,[54] and is guaranteed to always yield a planar embedding for three-connected planar graphs. In the Tutte embedding, one fixes the coordinates of a single, outer face, and solves a sparse linear system

$$\sum_j T_{ij} \vec{x}_j = \vec{y}_i \qquad (4)$$

such that in the result, every vertex is placed in the barycenter of its neighbors. For fullerenes, $T_{ij} = \delta_{ij} - A_{ij}/3$ and $\vec{y}_i = 0$ for every i where v_i is not a fixed vertex, and for the vertices v_i on the outer face, $T_{ij} = \delta_{ij}$ and $\vec{y}_i$ is the fixed coordinate. While the Tutte embedding is guaranteed to be planar, the solution to the linear system results in exponential crowding of the vertices when embedding large graphs, making the result difficult to interpret. Hence, it is useful to follow the Tutte embedding by an optimization to make the face sizes more even.[35]
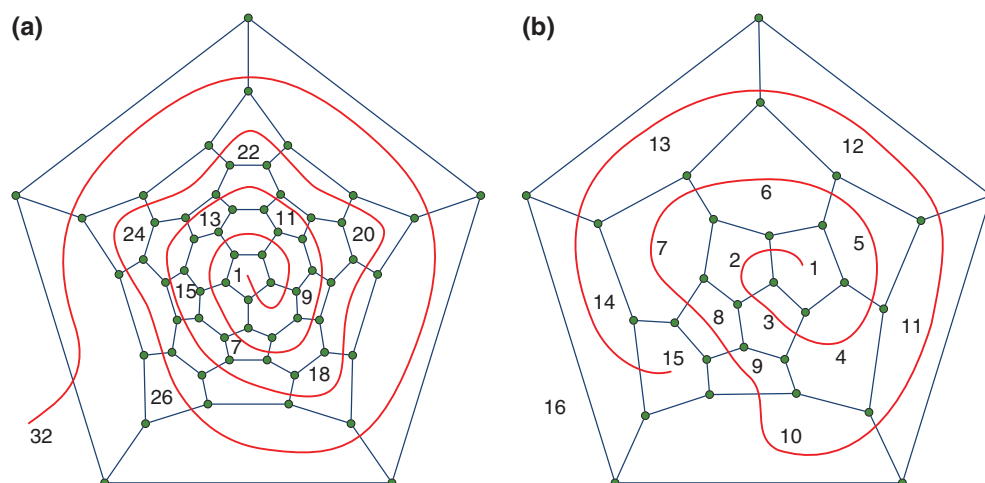
FIGURE 6 | (a) Canonical face spiral for C_{60}-I_h. (b) The first fullerene (C_{28}-D_2) with a failing face spiral.

We note that there are many different graph drawing algorithms available, each with advantages and disadvantages, but none that are guaranteed to always yield good results.[54–57]

The Large Isomer Space

How does the number of C_N-isomers grow as we increase the number of vertices N? Naively one might assume a hypothetical sphere of 'connected' hexagons (which is of course impossible because of Euler's theorem) and substitute 12 hexagons by pentagons to obtain a set containing all possible fullerene isomers fulfilling Euler's theorem (just like playing Lotto), we obtain an upper bound for the number of isomers of the order $\mathcal{O}(N^{12})$. This is, however, three orders of magnitude too large, but the proof is nontrivial. In 1998, William Thurston showed that all the triangulations of the sphere with vertex degree at most 6 form a lattice of integer points in a complex hyperbolic space $C(1,9)$ through a parameterization as described in Ref 19. The triangulations with N vertices or less correspond to the lattice points inside the intersection between a certain cone and a ball of radius $\sqrt{N}$ in this space. Hence their number is roughly proportional to N^{10}, and the number of triangulations with exactly N vertices is roughly proportional to

$$\Delta\left(N^{10}\right) = N^{10} - (N-1)^{10} = 10N^9 - 45N^8$$
$$+ 120N^7 + \cdots \quad (5)$$

or, in short, $\mathcal{O}(N^9)$. Because they are the largest class of the finitely many triangulation classes with vertex degree six or less, the fullerenes have the same asymptotic count. Hence, the number of C_N isomers grows as $\mathcal{O}(N^9)$. We note in passing that the

connection of fullerenes to combinatorial manifolds is a deep one and gives rise to many of the beautiful mathematical properties exhibited by fullerenes.

The high order polynomial growth of fullerene isomer counts makes it difficult to establish a complete database for fullerene graphs up to high vertex numbers.[34] Moreover, the proportion of IPR isomers to the total number of isomers grows with increasing N, gradually approaching 1 with increasing N, as is shown on Figure 4.

Face Spiral Representations of Fullerene Graphs

One of the first methods for encoding fullerene graphs was the *face spiral* algorithm by Manolopoulos et al.,[58] which unwinds all faces of a fullerene 'like an orange peel' (the *Manolopoulos face spiral algorithm*). More specifically, starting with a sequence of three mutually adjacent faces, new faces are added to the string such that the next face is adjacent to the previous one and the one that was added to the string earliest, and that has neighboring faces left which are not part of the spiral string (yet). As the result, one obtains a string of length F of 12 fives and $F - 12$ sixes, corresponding to the sizes of faces.

There are $6N$ possible spiral starts resulting in up to $6N$ spirals per fullerene graph. In most fullerenes, some spirals cannot be completed because the two rules for choosing the next face cannot be both fulfilled. Since a fullerene spiral always consists of 12 fives and $N/2 - 10$ sixes, this spiral string can be abbreviated as a list of the 12 pentagon positions, called the *face spiral pentagon indices* (FSPI) $\{S_n | n = 1, \ldots, 12\}$. The lexicographically smallest of all successful spirals is the *canonical spiral* representation of the graph.
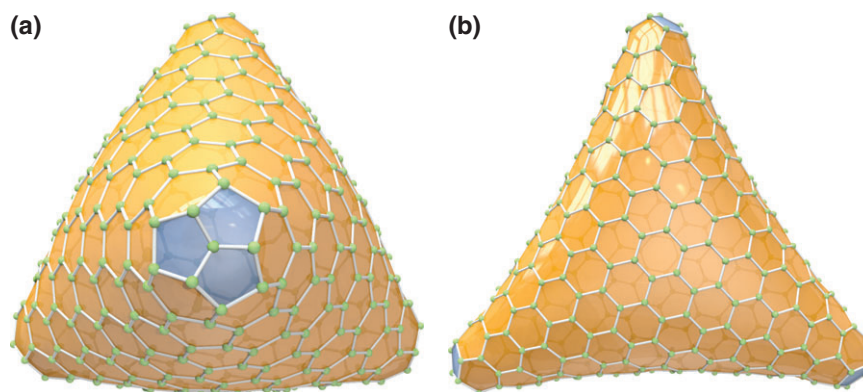
FIGURE 7 | B3LYP optimized structures for the two smallest non-spiralable fullerenes (a) C_{380}-T and (b) C_{384}-D_3 (see Ref 59 for details).

For example, for C_{60} we have the canonical FSPI of $\{1, 7, 9, 11, 13, 15, 18, 20, 22, 24, 26, 32\}$ as shown in Figure 6.[31]

While it was initially conjectured that every fullerene can be unwound into a face spiral[58] (for good reason: the first counterexample comes after over 10^{12} isomers) there is an exceedingly small proportion of fullerene graphs[59] (but infinitely many in total) that do not admit a face spiral,[60] that is, where all $6N$ spiral starts fail. See Figure 6 for a case where a face spiral fails. The smallest of these unspiralable fullerenes is C_{380}-T.[61] Manolopoulos et al.,[60] Fowler et al.,[62] Yoshida et al.,[63] and Brinkmann et al.[64] compiled lists of non-spiral fullerenes with up to 1000 atoms and selected point groups (all T_+, all isolated pentagon triple (IPT) fullerenes with D_2 and T symmetry, all D_{3+}, and all truncated IPT fullerenes respectively). Two of those are shown in Figure 7.

In order to encode any fullerene graph, it is necessary to extend the face spiral algorithm to a general version in which the spiral may 'jump' from one face to a non-adjacent face. Both Brinkmann[65] and Fowler et al.[66] published general face spiral algorithms for cubic polyhedral graphs, including fullerene graphs. Fowler's algorithm extends the two above mentioned rules such that the subgraph that has not been added to the spiral yet never gets disconnected, and as a result the spiral never gets stuck. Brinkmann's algorithm, in contrast, adds faces as defined by the non-general version, but defines how to proceed if all neighbors of the current face have been added to the spiral already. Both algorithms yield the same spiral string as the non-general algorithm if no jump is required.

For the non-general as well as both general algorithms for finding the canonical face spiral of a graph, there is an inverse algorithm that efficiently regenerates the graph from the (general) spiral string representation. With the extension to general spirals,

all fullerene isomers with any vertex number can be generated. In addition, all the information of the fullerene graph is contained in a general face spiral consisting of 12+ numbers (12 for most fullerenes). This makes it rather convenient for database storage as the face spiral uniquely defines the fullerene.

In a similar way to face-spirals we can introduce *vertex spirals* (or *Hamilton spirals*) useful for identifying locations of substituents (such as hydrogen) or reaction centers[67] (for details see Ref 68). For fullerenes with no vertex spirals the scheme can be extended to general spirals with jumps similar to general face spirals.

Generation of Fullerene Graphs

In order to explore chemical, physical, or graph theoretical properties for a wide range of fullerenes, it is important to have access to a list of (stored) fullerene graphs. For this, one requires an exhaustive and efficient generator for all fullerene isomers of a given vertex number N. The general face spiral algorithm is well suited for compactly storing and recreating specific fullerene graphs. It also allows for sorting all isomers of C_N for a given vertex number N according to their FSPIs including information about jumps if required. It is, however, extremely inefficient to generate all isomers C_N directly through a face spiral algorithm. In the non-general case one attempts to create graphs from $\binom{F}{12}$ spiral strings while the number of non-isomorphic graphs only grows $\sim N^9$. A large and quickly growing portion of all potential spiral strings are either non-canonical spirals, duplicates or are not successful for coding a fullerene. Including general spirals increases the overhead by two orders of magnitude, as jumps could be inserted at any step and with arbitrary lengths $l < N$.

A different approach to generating fullerene graphs is by adding faces to an existing graph, while

considering different sites for addition at each step. Liu et al.[69] introduced a method which grows a graph starting with a single face and thus only reaches a fullerene graph in the last step. Brinkmann et al.[70] use patches, rather than single faces, as building blocks. These patches can be obtained by subdividing existing fullerene graphs.

Further development in efficient graph generation came from transforming an existing fullerene graph into a new, larger one by adding faces. Using C_{24} as a 'seed', Brinkmann et al.[71] were able to generate almost all fullerene graphs up to C_{200}. However, three graphs were not accessible by the applied set of transformations. To cure this shortcoming, Hasheminezhad et al.[72] defined a set of patch replacements (or growth operations) which, starting from either C_{20} or C_{28} - T_d, yield every fullerene in a systematic way. The set consists of one single operation that elongates a nanotube with minimal caps, one class of linear generalized Stone-Wales transformations[73,74] that depend on one parameter, and one class of bent generalized Stone-Wales transformations that depend on two parameters. Brinkmann et al.[75] used this set of growth operations to define a fast and complete algorithm that recursively generates all fullerene isomers up to a given maximal N. The algorithm prunes the recursion tree in such a way that the only one representative of each isomorphism class is ever considered. Without such a scheme, exhaustively generating all fullerene graphs would succumb to combinatorial explosion.[76] The result is an incredibly efficient algorithm which has been used to generate an exhaustive database up to C_{400}, which is available at the House-of-Graphs website.[34] Sometimes one is not interested in generating exhaustive isomer lists (which are huge for large N), but rather to generate in a directed fashion fullerenes that have specific properties. For this, one may start with one specific isomer C_N and derive others by certain transformations. This will be discussed in the following section.

Transformation of Fullerene Graphs

Transformations of fullerene graphs can be divided into local transformations that leave all but a certain region of the graph unchanged, and global transformations such as the Goldberg-Coxeter transformation.[77,78] A planar graph can be transformed locally by replacing one fullerene patch[74,79–84] by either a different patch or the same patch in a different orientation. A *patch* is a set of faces that is bounded by a simple cycle,[82,85] that is, a cycle that traverses no vertex or edge twice. Some authors relax this condition and allow cycles that are non-selfintersecting, but are permitted to traverse any edge at most twice. This
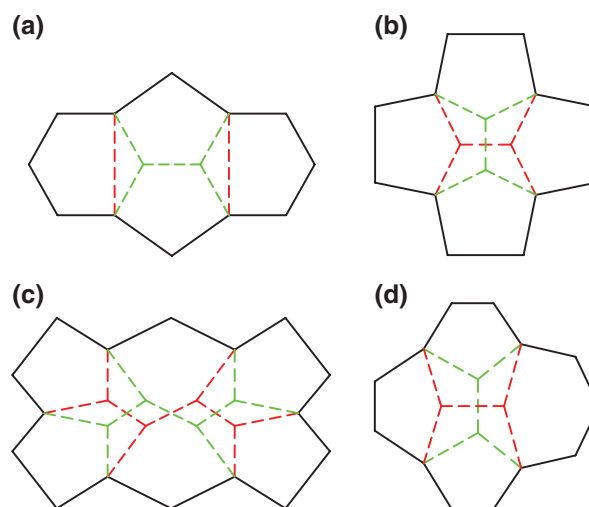

(a) **(b)**

(c) **(d)**

FIGURE 8 | (a) Endo-Kroto (EK) 2-vertex insertion. (b) Stone-Wales (SW) transformation. (c) Example of an extended Stone-Wales transformation. (d) A patch replacement which introduces one heptagon.

definition includes patches that have bridges, and is used in the complete characterization of fullerenes by Hasheminezhad et al.[72]

Two patches can be exchanged if they share the same *boundary code*. The boundary code of a patch is the sequence of free valencies of the vertices that lie on the boundary (in case of cubic graphs, a sequence of zeros and ones). A few patch replacements are shown in Figure 8.

Replacing patches of equal size can be understood as a formal isomerization, while replacement by larger or smaller patches, referred to as vertex insertion or deletion, or growth operations, formally derives a molecular graph of a different size. Two fullerene graph patches with the same boundary code contain the same number of pentagons, as can be seen from Euler's polyhedron formula. The most prominent example for formal isomerizations is the *Stone-Wales* (or pyracylene) *transformation* (SW),[86] which can be generalized[73,87] by allowing a variable distance between the two pentagons. Astakhova et al.[88] extended this rearrangement mechanism even further to higher numbers of pentagons. Brinkmann et al.[83] generated a catalog of isomerization pairs with up to five pentagons.

Isomerization operations can be reformulated as sequences of vertex-pair switches, called 2-switches.[89] According to Berge's switching theorem,[90] the whole isomer space of a given C_N is accessible by repeated application of 2-switches. However, intermediate structures of this procedure might have faces different from pentagons and hexagons, or result even in non-planar graphs.
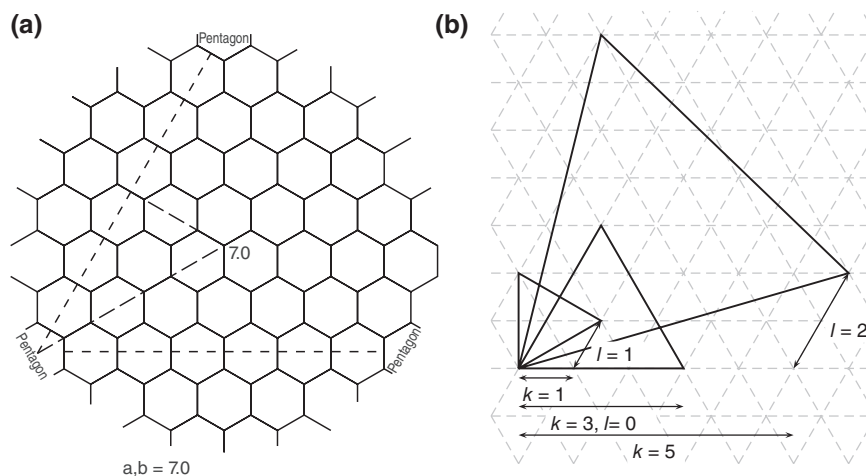
(a)

(b)

FIGURE 9 | Illustration of GC-transform. (a) Original figure of a hexagonal sheet from Goldberg's paper.[77] (b) The GC-transform acting on a face in the fullerene dual for various values of *k* and *l*.

Growth operations can be classified according to the number of pentagons and the number of vertices that are added. There are no growth operations for fullerene graphs that involve no or only one pentagon.[81] The smallest example is the *Endo-Kroto transformation* (EK),[91] which involves two pentagons and adds two vertices. Additional noteworthy examples are the addition of four and six vertices at a patch that contains three pentagons and has C_3 symmetry.[92] Brinkmann et al.[84] compiled an extensive list of growth pairs. The three classes of patch replacements defined by Hasheminezhad et al.[72] form the basis of the currently fastest fullerene graph generator, as discussed in a previous section.[75]

With respect to the polyhedral representation of a fullerene graph, growth operations can be understood as the capping of a domain by additional vertices. As a result the pentagons in that domain move toward each other. Patches in which all pentagons are fused cannot be capped. Conversely, the inverse of a growth operation corresponds to the truncation of a domain of high curvature: The distances between the affected pentagons increase.

While patch replacements are useful from a graph theoretical point of view to obtain new fullerene isomers, the EK C_2 insertion and the SW transformation have also been suggested to resemble viable reaction pathways.[86,91,93–95] As Stone and Wales pointed out in their initial article, a concerted mechanism for the SW transformation ([2+2]) is Woodward-Hoffmann forbidden in the electronic ground state.[86] Other mechanisms that involve the breaking of one bond[93,96,97] or the catalysis by additional carbon atoms[98] are therefore more likely. For a discussion of different mechanisms see Ref 93. For every suggested pathway, however, the activation

barrier is so high that SW transformations are only feasible at very high temperatures.[93,94] The SW transformation is believed to be one of the main mechanisms by which fullerene cages equilibrate during formation to form the most stable isomer.[99,100] Starting at C_{60} - I_h, 1709 out of the 1811 other isomers are accessible by consecutive SW transformations.[101]

Endo and Kroto proposed a concerted mechanism for what has since been known as the EK C_2 addition.[91] However, more recent experimental and theoretical investigations show, that the concerted reaction leads to an unstable adduct and is followed by C_2 ejection.[102] For a summary of alternative mechanisms of the C_2 addition to fullerene cages see Ref 95.

Given any fullerene, it is possible to construct an infinite series of larger ones with (essentially) the same three-dimensional shape. This is possible through the *Goldberg-Coxeter* transformation, named after an infinite series of icosahedral-symmetry polyhedra described by Goldberg in 1937.[77] By superimposing a hexagonal mesh on the surface of the dodecahedron, as shown in Figure 9(a), a new polyhedron is obtained with the same number of pentagons and an increased number of hexagons. The number of vertices in the new polyhedron is $k^2 + kl + l^2$, where k and l are integers describing the scale and orientation of the mesh, as shown for the dual in Figure 9(b). The construction used by Goldberg was discovered independently, and applied to the shapes of vira, by Caspar and Klug in the 1960s, and later popularized by Coxeter.[78]

While originally only defined for C_{20}, yielding exactly all the fullerenes of icosahedral symmetry, Dutour and Deza have shown that it is well defined for all cubic planar graphs.[103] However, it is not

trivial to determine how to automatically perform the general transform, the main difficulty lying in how to 'glue' the graph back together when the new edges cross the transformed triangles in complex ways. The general construction by Dutour and Deza is quite algebraically heavy handed, and is not easily understood, nor lends itself easily to implementation. In the case of fullerenes, however, it is quite easy to give a procedural description of the transformation in terms of the fullerene dual: Because a fullerene dual is a triangulation of the sphere with no vertices of degree more than 6, it can be unfolded onto the plane of equilateral triangles, called the *Eisenstein plane*. The unfolded surface forms a polygon in the Eisenstein plane with every degree 5 vertex on the polygon periphery, and with each edge on the periphery appearing twice, once in each direction.

The vertices in the Eisenstein triangulation is a sub-ring of the complex plane, and we can write

$$(a, b) = a + b\omega \quad \text{where} \quad \omega = e^{i\frac{2\pi}{6}} \tag{6}$$

Because it is a sub-ring, multiplication by Eisenstein integers (a, b) are exactly the operations that bring $(1, 0)$ into every other vertex point. Because $\omega^2 = \omega - 1$, we get the multiplication rule

$$(a, b) \cdot (c, d) = ac + (ad + bc) \omega + bd\omega^2$$
$$= (ac - bd, bc + (a + b) d) \tag{7}$$

and the magnitude of (a, b) is $(a + b\omega)(a + b\omega^{-1}) = a^2 + ab + b^2$. Hence, if T is an equilateral triangle with unit area, the area of $(k, l)T$ is $k^2 + kl + l^2$. This is no coincidence: multiplication in the Eisenstein ring exactly corresponds to the Goldberg-Coxeter transformation in the dual formulation. This yields a simple and practical formulation of the Goldberg-Coxeter transform of any triangulation of the sphere with $\deg(\nu) \leq 6$:

$$\text{GC}_{k,l}(G^*) = \text{fold}\left(\left(k + l\omega\right) \cdot \text{unfold}\left(G^*\right)\right) \tag{8}$$

The procedure is illustrated in Figure 10. Details for how to efficiently perform the fold and unfold operations are given in Avery (unpublished manuscript). Note that two successive GC-transformations on a graph G^* can be expressed as a single GC-transformation by multiplying the two Eisenstein numbers together. Similarly, a GC-transformation can be inverted by dividing instead of multiplying. For any particular fullerene, we can even use Euclid's algorithm to find out whether it is a GC-transform of a smaller fullerene, and to find the smallest such 'parent' fullerene.[59]

Notice, that if one were to cut out the two diagrams in Figure 10, gluing together the edges so that the numbers on the vertices match, one obtains the three dimensional structure of the given C_{32} and C_{224} fullerenes. The reader is invited to do so.

There are two special cases of the Goldberg-Coxeter transformation that warrant closer study: the case $l = 0$, named the *halma transform* (or k-inflation) for the construction's similarity to the game board of halma, or 'Chinese Checkers'; and the case $k = l = 1$, called the *leapfrog transform*. Both of these types of Goldberg-Coxeter transformations are simple to understand: every triangle is subdivided and reconnected the same way, as illustrated on Figure 11. While the GC-transform in general can introduce, reverse, or remove chirality (but otherwise preserves symmetry), both the halma and leapfrog transformation always preserve symmetry.

Geometry of Fullerenes

Many of the beautiful properties of fullerenes derive from their relation to algebraic and differential geometry. This relation is mostly out of scope for this review, but in this section we will touch on the subject informally. The subject is treated in great depth by Thurston[19] and others.

An important quantity for understanding the geometry and shapes of fullerenes is the *Gaussian curvature*. The Gaussian curvature is the product of the two principal curvatures, which for each point on the surface are the maximal and minimal curvatures in any direction through that point. By the Bertrand-Diquet-Puiseux theorem, the Gaussian curvature in a point is the same as the difference between 2π and the angle required to make a circle in a neighborhood around this point. Figure 12 illustrates three categories of surfaces with zero, positive, and negative Gaussian curvature respectively. If the Gaussian curvature is zero in a point, the surface only bends in one direction around that point. A surface that has zero Gaussian curvature everywhere is characterized by being 'flat' in the sense that it can be unwrapped onto a plane without tearing. Positive Gaussian curvature bends the same way in all directions. A positive curvature surface can be cut open and unwrapped onto a plane. Finally, negative curvature around a point constitutes a saddle point, yielding a wobbly pringle-like surface. Negative curvature surfaces cannot be unwrapped onto a plane, because there is no room: around a negative curvature point, the angle of a circle is greater than 2π. If one were to make a cut in a negative curvature surface, it could only be flattened out by allowing parts of it to overlap itself.
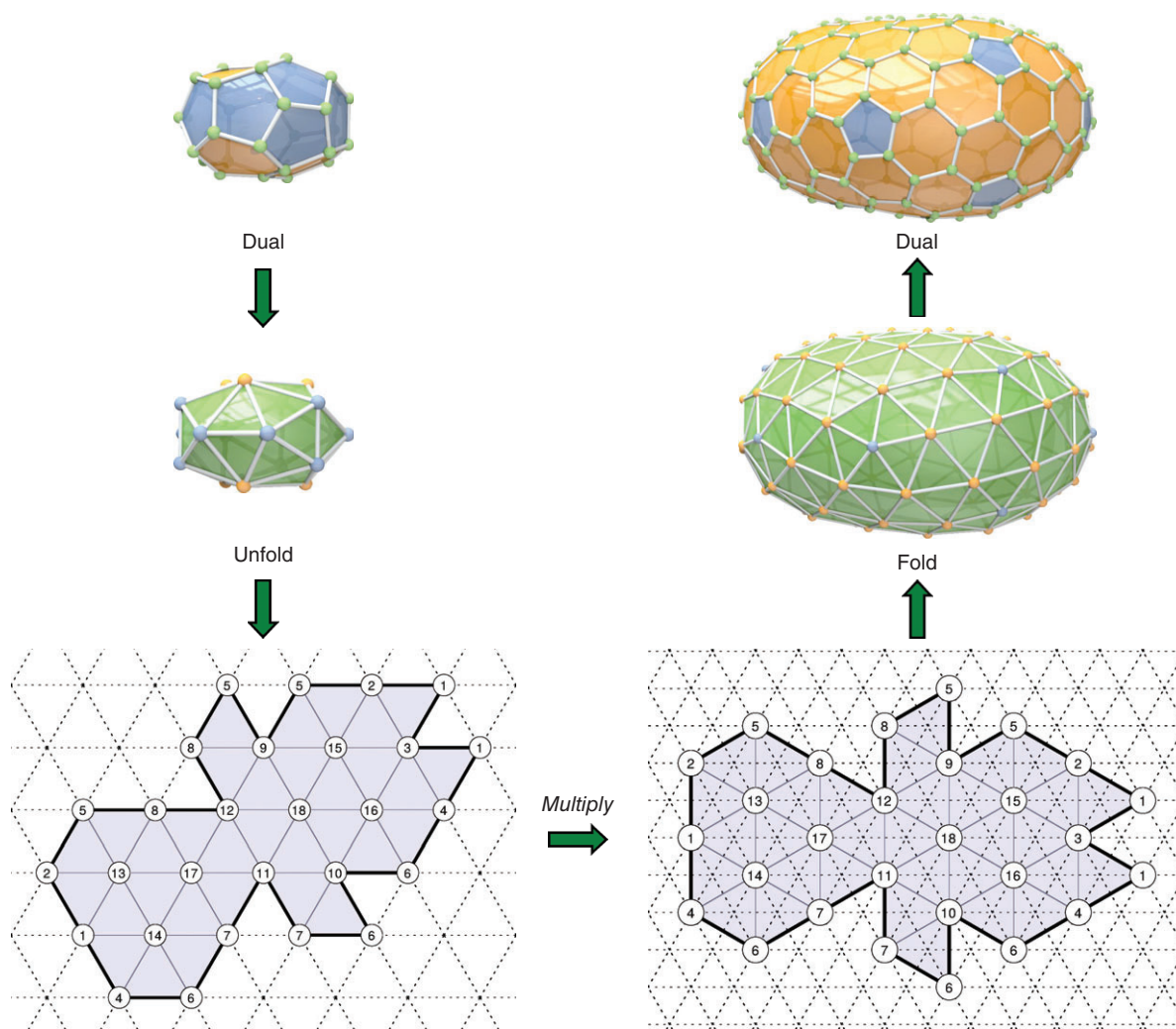
FIGURE 10 | The steps in the GC$_{2,1}$ Goldberg-Coxeter transformation from C$_{32}$-D_{3h}(5) to C$_{224}$-D_{3h}. The transform and the diagrams of the unfolded fullerenes were automatically generated using the program *Fullerene*.[35]

The Gaussian curvature only depends on the topology of the surface, and is independent of how it is isometrically embedded in space. In the same way, the surface metric (or Riemann metric), which determines the geodesics and distances between points along the surface, can be derived directly from the graph (Avery et al., unpublished manuscript), and is also independent of the spatial embedding. However, while we do not require a 3D embedding to analyze these surface properties, they themselves do determine the possible ways that the surface *can* embed isometrically into space, and what is its 'natural' three-dimensional shape.

Fullerenes are all closed surfaces with non-negative Gaussian curvature everywhere. Surprisingly, this is simply due to them having faces no larger than hexagons! In fact, the slightly larger class of three-connected cubic planar graphs with largest face size 6, and their dual triangulations, are in a sense *all* the positive curvature genus 0 surfaces.[f]

It is most easy to understand the geometry of fullerenes when considering their duals. These are equilateral triangulations of a closed surface. The equilateral triangle plane, also called the Eisenstein plane, is the dual of a hexagonal mesh. Hexagon planes (like graphene) and their dual degree-six triangulations are *flat* in the sense that they have Gaussian curvature 0 everywhere: any surface of equilateral triangles with vertex degree only six can be unwrapped into the plane without stretching or tearing. What happens now if we set the degree to 5 of a single vertex in the plane? To do this, we must cut out an infinite triangular wedge of angle $2\pi/6$. Gluing together the edges forms an infinite cone with Gaussian curvature zero everywhere except the degree 5 vertex at the cone's apex, which introduces the positive curvature $2\pi/6$.
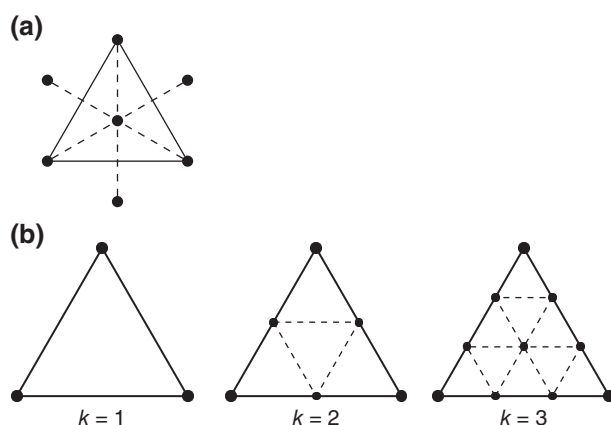
(a)

(b)

k = 1   k = 2   k = 3

FIGURE 11 | Subdivision of a triangle in the dual graph; (a) for the leapfrog transformation ($k = l = 1$), and (b) for the lowest few halmas ($l = 0$).

Every time we introduce a vertex of degree 5 (or a pentagon in the hexagonal plane), it introduces a surface cut that is glued together to locally introduce the positive Gaussian curvature $2\pi/6$ at the vertex. After 12 pentagons we reach 4π, the Gaussian curvature of the sphere, closing the surface.[g] Unfolding again along the 12 cuts would result in a polygon similar to the diagrams shown in Figure 10. Had we instead introduced, for example, degree 4 vertices, each would contribute with curvature $2\pi/3$, requiring only 6 to close the surface. The positions at which we placed the 12 pentagons determine where and how strongly the surface bends, and through that the natural shape of the fullerene, giving rise to the many interesting polyhedral shapes shown in Figure 2.

Because fullerenes always have exactly 12 curvature-$2\pi/6$ bends, with the remaining surface of Gaussian curvature zero, they adopt polyhedral shapes rather than being spherical in nature (the latter defined as atoms lying on a sphere), and the most symmetric shapes that they can achieve have icosahedral symmetry. The non-spherical nature of fullerenes was pointed out already by Bakowies and Thiel in 1995.[104,105]

The curvature of cubic graph surfaces also provides an intuitive understanding of why fullerenes, having only hexagon and pentagon faces, would be more prevalent in nature than other polyhedral carbon structures: smaller face sizes introduce much sharper bends, reducing stability. Heptagons by themselves introduce no sharper bends than pentagons, but each heptagon necessitates an extra pentagon to balance out the negative Gaussian curvature and reach a closed surface, increasing the total number of bends by two. However, with the right distribution of heptagons and pentagons, it is possible to construct quite smoothly curving near-spherical fulleroid surfaces that could potentially be stable in nature. We discuss fulleroids, a generalization of fullerenes that allow arbitrary face sizes, in the final section.

Generating Accurate 3D Geometries

The Cartesian coordinates for the ideal molecular geometry of small highly symmetric fullerenes such as C_{20}-I_h or C_{60}-I_h can be calculated directly using basic geometry.[106] This is not the case for fullerenes in general: They come in many different shapes, most of which do not have a simple mathematical formula. However, we do know that the ideal geometry (in which the faces of the dual polyhedron are equilateral triangles) can be derived directly from the fullerene graph. This is because of their special properties discussed above. However, while we know that a fullerene graph determines the ideal 3D structure as a conformal, isometric embedding of the surface into space, it is not yet known how to compute it directly. However, we can use numerical optimization methods to obtain good 3D structures—both efficiently and with results that are very close to the physical molecular geometry.

Generating Initial Structures

Before optimizing a fullerene structure by for example a force-field method, we need a reasonable initial structure. Specifically, we need an embedding of the
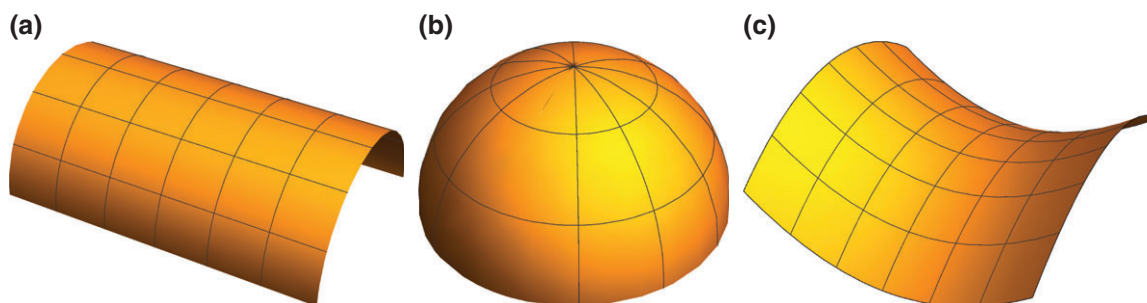
(a)   **(b)**   **(c)**

FIGURE 12 | Examples of surfaces with zero (a), positive (b), and negative (c) Gaussian curvature around a point.

graph as a polyhedron (i.e., no crossing edges) such that its faces are the same ones as in the final polyhedron, and such that the magnitude of the force experienced by the vertices does not vary too greatly, causing slow convergence or numerical instability. We here outline two methods for obtaining initial geometries that are suitable for input to the fullerene force-field optimization.

The *Fowler-Manolopoulos 3D embedding algorithm* (also called Adjacency Matrix Eigenvector or AME algorithm) diagonalizes the $N \times N$ adjacency matrix A_{ij} of the fullerene graph to obtain eigenvectors $\vec{x}_i$ ($i = 1, \ldots, N$), of which three 'P-type eigenvectors' with one nodal plane are chosen to construct the Cartesian coordinates (termed *topological coordinates* by Manolopoulus and Fowler) for the initial structure.[31,107] This often yields suitable coordinates because fullerenes can be modeled as spherical aromatic systems fulfilling approximately the Laplace differential equation with real spherical harmonics $Y_{lm}(\theta, \varphi)$ as eigenfunctions, of which the three Y_{lm} ($l = 1$) are associated with the coordinates (x_i, y_i, z_i).[31,108] Cartesian coordinates constructed in this way already reflect the space symmetry of the fullerene. The P-type eigenvectors can easily be found for near-spherical fullerenes like C_{20} or $C_{60} \cdot I_h$, because the sequence of eigenvalues mimics the spherical harmonics. However, for distorted fullerenes, or for very large fullerenes where the spectrum of the adjacency matrix becomes very dense with quasi-degeneracies, it becomes difficult to find the appropriate eigenvectors, and the assumption that the eigenvectors resemble spherical harmonics becomes decreasingly valid. For example, for large fullerene nano-tubes aligned around the z-axis, such as the one shown in Figure 2, the eigenvalues belonging to the P_x- and P_y-type eigenvectors do not lie close to the P_z eigenvalue. Hence, one must search for the appropriate set of eigenvectors, and identifying them is not always easy.[109–111] Second, the bond lengths tend to vary substantially in the constructed fullerene, leading to unreasonable large bond distances once the minimum bond distance is set to ≈ 1.4 Å, and a scaling procedure for the eigenvectors may only solve part of this problem.[31] Finally, because it is often necessary to search for the right eigenvectors and hence calculate a large number of them, the algorithm scales up to $\mathcal{O}(N^3)$, which quickly becomes a heavy operation as N grows.

We have found it useful to sacrifice some accuracy in the initial geometry for a method that is more stable, and which scales approximately as $\mathcal{O}(N)$. The fullerene force-field optimization is insensitive enough to the starting geometry that the difference

is not noticeable. The method starts with any planar embedding of the fullerene graph. We choose the *Tutte-embedding*, which is guaranteed to be planar, and can be computed in near-linear time by solving two sparse linear systems of equations.[54] The planar embedding is then mapped onto the surface of a sphere (or e.g., ellipsoid, if the fullerene is a priori known to be elongated) in the following way: For every vertex v, let the topological distance from the outer face (the 'depth' of the vertex) be d_v, and its coordinate in the Tutte-embedding be $\vec{x}_v$. Let D be the maximum depth, and $\vec{x}_c$ be the barycenter in the embedding. We assign one angle $\phi(v) = (d_v + 1/2)\pi/D + 1$, placing vertex layers equidistantly along the ϕ-angle according to their depth. The second angle $\theta(v)$ is the angle of $\vec{x}_v$ around $\vec{x}_c$. Then assigning the angles $v \mapsto (\theta(v), \phi(v))$ yields an embedding on the sphere with no crossings, since the Tutte-layout is guaranteed to be planar, but which avoids the exponential crowding of the planar Tutte-embedding, such that the vertices are distributed in a reasonable manner across the surface of the sphere.[h] It remains, however, a challenge to embed the fullerene graph on a more realistic surface.

Fullerene Force-Field

This section describes how to obtain good results for the molecular geometry numerically by way of specially tailored force-field optimization methods. This yields geometries that are very close to the ones obtained by long and computationally heavy quantum chemical calculations, as we shall see.

It is common for molecular force-field optimizations to distinguish between single and double bonds, even introducing different types of single and double bonds depending on atoms and groups in close proximity. For each bond, that is, edge in the graph, one sums over all the Kekulé structures and assigns fractional double bond character to each edge. This strategy is not practical for fullerenes, even for small cages like C_{60},[112,113] due to exponential growth in perfect matchings and hence Kekulé structures, as discussed below. Force fields for fullerenes should therefore be designed in a way that avoids explicit treatment of double bonds. As a good approximation it is assumed that the properties of bonds, angles, and dihedral angles in a fullerene are determined by the size of their neighboring faces alone. The force fields discussed below are specifically designed for fullerenes based on this assumption.

The first force field tailored to fullerenes by Wu et al.[114] was designed for $C_{60} \cdot I_h$ and uses harmonic force field terms. It distinguishes between two bond types: bonds adjacent to two hexagons, and bonds

TABLE 1 | The 28 Possible Point Groups for Fullerenes Sorted According to Their Order $|\mathcal{G}|$ of the Group $\mathcal{G}$[31]

Order	Point Groups	Order	Point Groups	Order	Point Groups
120	I_h	60	I	24	T_d, T_h, D_{6h}, D_{6d}
20	D_{5h}, D_{5d}	12	T, D_6, D_{3h}, D_{3d}	10	D_5
8	D_{2h}, D_{2d}	6	D_3, S_6, C_{3h}, C_{3v}	4	D_2, S_4, C_{2h}, C_{2v}
3	C_3	2	C_2, C_s, C_i	1	C_1

adjacent to a pentagon and a hexagon, which are optimized for bond lengths r_0 with values of 1.54 Å and 1.41 Å, respectively. Angles are either part of a pentagon ($\theta_0 = 3/5\ \pi$) or a hexagon ($\theta_0 = 2/3\ \pi$). The force constants k_1 through k_4 are given (in 10^5 dyn/cm) as 11.0, 10.0, 1.0, and 1.0. No further parameters are taken into account.

In the following years a number of extensions and modifications to the Wu force field were published, taking into account an increased number of parameters. These extensions include improved force constants,[115] torsions,[116] angles and distances to second and third neighbors,[117] mixed terms between distances and angles,[118,119] the volume of the tetrahedron defined by an atom and its three neighbors,[118] a complete force field for C_{60} - I_h,[120] and a strategy for defining complete force fields for any deltahedron or trivalent polyhedron using mixed terms of distances and angles.[121] Except for the force field by Ceulemans et al.,[121] all above mentioned force fields have been exclusively designed for and applied to C_{60} - I_h.

The program *Fullerene*[35] includes a 22-parameter force field with explicit dihedral angles. It takes into account three types of distances (bonds that are part of 0, 1, or 2 pentagons), two angles (part of a pentagon or a hexagon) and four types of improper dihedral angles, defined between a vertex and its three neighbors (where the starting vertex is part of 0, 1, 2, or 3 pentagons). It is applicable to all fullerenes and yields structures that are in very good agreement with DFT optimized structures. For example, for C_{380} - T, the rms error between the B3LYP/SVP and the force field optimized structure is only 0.038 Å. For many purposes, the force-field optimized molecular geometry, which is computed in milliseconds, is good enough to be used instead of a more computer time intensive quantum chemical optimization (although semiempirical methods including density functional based tight-binding are also very computer time efficient and have yielded good results[122]).

Fullerene Symmetry

There are two symmetry groups associated with a fullerene: the *ideal* or *topological symmetry group* of the fullerene graph, and the *real* or *physical symmetry group* of the molecule in 3D space. The physical symmetry group is a subgroup of the ideal one, due to (first or second order) Jahn-Teller distortions, variation of bond-lengths, or other effects from external perturbations. But because the shape is often only mildly altered from the ideal shape, the ideal symmetry group carries useful information about the physical system.

A surprising theorem by Mani[123] shows that any three-connected cubic planar graph can be embedded in space as a convex polyhedron, the point group of which realizes the full symmetry group of the graph. That is: every graph automorphism of a fullerene is also a rotation or reflection of its ideal polyhedral shape. In addition, it can be shown[124] that the point group for a fullerene must be one of the 28 point groups listed in Table 1. The largest group is the icosahedral group I_h of order 120, and each of the 27 remaining attainable point groups are subgroups of I_h.

Can we automatically determine the symmetry group for the fullerene directly from the graph, without referring to spatial coordinates? (The latter requires first finding a maximally symmetric 3D embedding) For general graphs, this is a difficult problem. However, in the case of cubic polyhedral graphs, for which general face spirals determine isomorphism, it is both simple and efficient to do so.

Before moving on, we take note of an ambiguity in terminology. The terms *symmetry group* and *automorphism group* often refer simply to the *group* formed by operations that leave the system invariant. In the group theoretical sense, a group is fully defined by its multiplication table. *Point groups*, however, are not just groups, but are *isometries of space* and carry additional information about how they transform space. For example, the point groups D_6, C_{6v}, D_{3d}, and D_{3h} are all the exact same group, but differ as point groups. It is unfortunate for this reason that 'point groups' are called 'groups'. To make the distinction explicit, we will use the term *abstract group* for the symmetry group in the group theoretical sense, and either *point group* or *symmetry group* for the isometries.

Assume that we are given the fullerene graph dual G^*, constructed from a generalized spiral $S = (d_1, d_2, \ldots, d_F)$, and wish to compute the automorphism group $\mathcal{G}$ of G^*. Since G^* is constructed from S, the entries in S are the degrees of vertex number $1, 2, \ldots, F$ in G^*. For every vertex v of degree d_1, we have $2d_1$ different spiral starts: d_1 for clockwise and d_1 for counter-clockwise traversal. If a spiral start (f_1, f_2, f_3) unwinds G^* to the input spiral S, there is an automorphism of G^* that maps $(1, 2, 3) \mapsto (f_1, f_2, f_3)$. These are *all* the automorphisms, and the number of starts that unwind to S is the order $|\mathcal{G}|$ of the automorphism group. This construction lets us easily obtain the actual group: The spiral start determines the entire spiral, and by simply writing down the vertex names in G^* while unwinding the spiral, we obtain a permutation representation of the group element

$$\pi_F(g) = \begin{pmatrix} 1 & 2 & 3 & \cdots & F \\ f_1 & f_2 & f_3 & \cdots & f_F \end{pmatrix} \qquad (9)$$

This is a faithful (but not irreducible) representation of the group, and if we wish, we can easily build the multiplication table by composing all pairs of the permutations. Similarly, we can calculate characters, irreducible representations, and all other properties, and we can identify the group. There are a number of ways to make this efficient. In Wirz et al. (unpublished manuscript), we present a general, but efficient, $\mathcal{O}(N)$-algorithm that works for all cubic polyhedral graphs, including all fullerenes and fulleroids.

The permutation representation π_F allows us to not only find the abstract symmetry group, but contains enough information to identify the point group, that is, the isometries of the three-dimensional fullerene polyhedron. Fowler and Manolopoulos published a program for identifying the point group of any spiralable fullerene in Ref 31, based on site symmetries and counting group orbits. The *symmetry points* of interest in a fullerene are the vertices, midpoints of edges, the barycenter of the polygons and the whole cage, the latter having the full symmetry of the point group. They have certain site symmetries according to the rotational axes or mirror planes going through these symmetry points,[31] which are collected in Table 2. The full isometry group $\mathcal{G}$, which correspond to the rotations, reflections, roto-inversions, and inversions that leave the ideal polyhedron invariant, also act as permutations of the symmetry points,[107,125,126] the action always being a subgroup of $\mathcal{G}$. The permutations of the symmetry points in fact completely determine the point group symmetry, and we can find the full point group of the graph G (or, equivalently, its dual G^*) as follows:

TABLE 2 | The Site Symmetries of the Local Symmetry Points in a Fullerene[31]

Symmetry Points	Site Symmetries (Order)
Vertices	$C_{3v}(6)$, $C_3(3)$, $C_s(2)$, $C_1(1)$
Edge centers	$C_{2v}(4)$, $C_2(2)$, $C_s(2)$, $C_1(1)$
Pentagon centers	$C_{5v}(10)$, $C_5(5)$, $C_s(2)$, $C_1(1)$
Hexagon centers	$C_{6v}(12)$, $C_6(6)$, $C_{3v}(6)$, $C_3(3)$, $C_{2v}(4)$, $C_2(2)$, $C_s(2)$, $C_1(1)$
Cage center	Full point group

The order of the site-symmetry group is given in parentheses (the maximum value of any site symmetry group order is 12).

In step 1, one computes the face permutation representation π_F of the abstract group, as described above. From this one derives vertex and edge permutation representations π_V and π_E by acting with every group operation on the dual graph.

In step 2 one computes the vertex, edge, and face *group orbits* by acting with the permutation representations on every vertex, edge, and face.[127] Each orbit belongs to a certain site-symmetry group as shown in Table 2. The site-symmetry groups are determined by the orbit sizes. For example, the site-symmetry group of the face f_i has order $|\mathcal{G}_{f_i}| = |\mathcal{G}|/|\mathcal{G}f_i|$. By counting the number of sites belonging to each site-symmetry group, we obtain a signature that uniquely identifies the point group:

$$m_F(k) = \left| \left\{ f \in \mathcal{F} \,\middle|\, k = \frac{|\mathcal{G}|}{|\mathcal{G}f|} \right\} \right|,$$

$$m_E(k) = \left| \left\{ e \in \mathcal{E} \,\middle|\, k = \frac{|\mathcal{G}|}{|\mathcal{G}e|} \right\} \right|, \quad \text{and}$$

$$m_V(k) = \left| \left\{ v \in \mathcal{V} \,\middle|\, k = \frac{|\mathcal{G}|}{|\mathcal{G}v|} \right\} \right| \qquad (10)$$

The information can be condensed to a *site-symmetry count* for each site-group order:

$$m_S(k) = m_F(k) + m_E(k) + m_V(k) \qquad (11)$$

In the final step, the point group is determined by the site-symmetry counts by the decision tree structure shown in Figure 13. The method can be extended to any fullerene and fulleroid by using general spirals. However, for every possible point group, the site-symmetry signature must be worked out and added to the decision tree.

Once the point group has been determined, the number of infra-red and Raman active lines, as well as the ^{13}C NMR pattern can be derived.[31,107] Moreover, point groups lacking an inversion center
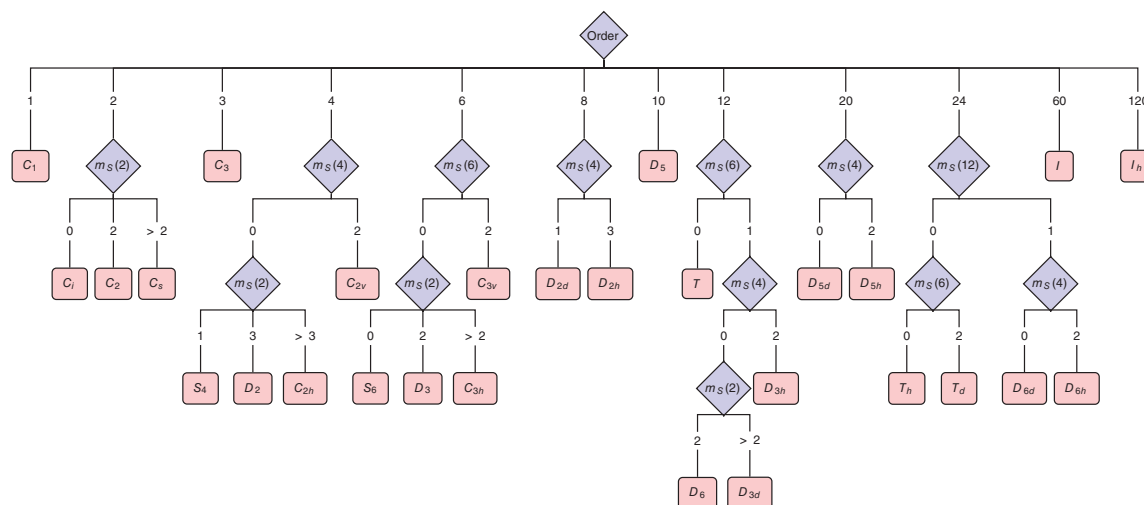
FIGURE 13 | The decision tree for determining the symmetry point group for any fullerene from the group order and orbit counts.

are further divided into polar and chiral point groups. A *chiral point group* is one without any roto-inversion symmetry elements, and a *polar point group* allows for the fullerene to have a dipole moment. A point group with an inversion center or a mirror plane perpendicular to the axis of rotation cannot be polar. The nine chiral point groups for fullerenes are $I, T, D_6, D_5, D_3, D_2, C_3, C_2,$ and C_1.[31] The polar fullerenes belong to either of the point groups $C_{3v}, C_3, C_{2v}, C_2, C_s$ or C_1.[31] For larger fullerenes, the fraction of low-symmetry to high-symmetry isomers grows rapidly, and the C_1 point group increasingly dominates. This can be intuitively understood combinatorially from distributing pentagons on a sphere. Already at C_{100}, more than 99% of the isomers are C_1.

The separation of spiral starts into equivalence classes by their spirals yields an interesting relation:

$$|\mathcal{G}| = \frac{6N}{N_S^s} \quad (12)$$

where N_S^s is the number of symmetry distinct (general) spirals. For I_h symmetry we have $|I_h| = 120$, which gives $N = 20N_S^s$. Hence, I_h-fullerenes can only occur when N is a multiple of 20. In a similar way, for I symmetry we have $N = 10N_S^s$, and for T_d, T_h, D_{6h}, or D_{6d} we obtain $N = 4N_S^s$. This explains why some of these high symmetry groups are not found in certain isomer lists.

In the case of icosahedral symmetry, we have a full characterization of when they occur: As described by Dutour and Deza,[103] every fullerene of I_h or I symmetry is a Goldberg-Coxeter transform of C_{20}.[77] This means that they occur exactly when $N = 20(k^2 + kl + l^2)$ for integers k and l. It is also

possible to determine when these are of I_h and when they are of I symmetry. Halma and leapfrog transformations, which correspond to Goldberg-Coxeter transforms of $l = 0$ and $k = l$, respectively, both preserve symmetry.[128] Hence, there is a fullerene with I_h symmetry at $N = 20j^2$ and $N = 20(3j^2)$ for every $j \in \mathbb{N}$, corresponding to a single Halma or leapfrog transformation on C_{20}. Consecutive application of the two shows that isomers with I_h symmetry are found for every $N = 20(3^i j^2)$ ($j \in \mathbb{N}$ and $i = 0, 1$). Moreover, general Goldberg-Coxeter (k, l) transforms with $k \neq l$ and $l \neq 0$ ($k > 0$) break horizontal mirror plane symmetry.

Shapes: Volume and Surface Area, Sphericity, and Convexity

For ideal C_{60} - I_h, where all edges are of equal length, the geometric volume V, and surface area A can be obtained through simple algebraic and geometric considerations. The volume and surface are of a regular 20-sided polyhedron (icosahedron, see Figure 3) made out of equilateral triangles with edge length a is,

$$V_{ico} = \frac{5}{12}\left(3 + \sqrt{5}\right)a^3 \quad \text{and} \quad A_{ico} = 5\sqrt{3}a^2 \quad (13)$$

Cutting out 12 pentagonal pyramids at length $a/3$ gives the ideal truncated icosahedron C_{60} - I_h with

$$V_{C_{60}} = \frac{1}{4}\left(5^3 + 43\sqrt{5}\right)r_e^3$$

$$\text{and} \quad A_{C_{60}} = 3r_e^2\left(\sqrt{5^2 + 10\sqrt{5}} + 10\sqrt{3}\right)$$

$$(14)$$

where $r_e = a/3$ is the length of the edge (C–C bond length). This gives the ratios $V_{ico}/V_{C_{60}} \cong 1.065$ and $A_{ico}/A_{C_{60}} \cong 1.073$ between the two volumes and surface areas. C_{60} has, however, two different bond lengths as the crystal structure shows,[129] $r_5 = 1.455$ Å (edge at pentagon-hexagon fusion) and $r_6 = 1.391$ Å (edge at hexagon-hexagon fusion). A smaller bond distance in the hexagon implies that more of the original icosahedron is cut off,

$$V_{C_{60}} = \frac{5\left(3 + \sqrt{5}\right)}{12}\left(2r_5 + r_6\right)^3 - \frac{\left(5 + \sqrt{5}\right)}{2}r_5^3 \text{ and}$$

$$A_{C_{60}} = 3r_5^2\sqrt{5^2 + 10\sqrt{5}} + 5\sqrt{3}\left(r_6^2 + r_5^2 + 4r_5r_6\right)$$
(15)

For $r_5 = r_6$ we obtain Eq (14). If $r_6 = 0$ ($r_5 = a/2$) the hexagons become equilateral triangles and for $r_5 = 0$ we just get a hollow icosahedral C_{12} cluster. For C_{20} (equal edge lengths) the vertices lie in the center of each face of an icosahedron, and the volume and surface area are easily obtained,

$$V_{C_{20}} = \frac{\left(15 + 7\sqrt{5}\right)}{4}r_e^3 \text{ and } A_{C_{20}} = 3r_e^2\sqrt{5^2 + 10\sqrt{5}}$$
(16)

How can we get the volume V and surface area A for any fullerene isomer? As fullerene cages are not guaranteed to have planar faces, their volume or surface area are only approximately defined. There are, however, a number of definitions according to which we can express both quantities. We could triangulate all faces by adding a barycenter $\vec{b}_j$ to each face with lines to each vertex of that face. We call the polyhedron obtained in this way a *triangulated face polyhedron*, TFP. For a fullerene, the graph representing the TFP is identical to the dual structure of its leap-frog transform. The total surface area A is obtained by summing over all areas A_i of the triangles obtained, which works even for faces where the vertices do not lie on a plane. Using Gauss' theorem (divergence theorem), the volume V is found by summing over the face normals,

$$V = \frac{1}{3}\sum_i A_i\left(\vec{p}_i \cdot \vec{n}_i\right)$$
(17)

where $\vec{p}_i$ is any point on face i, and A_i is the area of the face.

The different volumes and surfaces areas can be used for calculating some important measures for fullerenes, such as the *sphericity S* (how spherical a

fullerene is) and *convexity C* (how convex a fullerene is). The surface of a triangulated fullerene may not be convex. We can measure the non-convexity by comparing to the *convex hull* of the fullerene cage, which is the smallest convex polyhedron that contains all the points. The convex hull (CH) is uniquely defined, and there are several algorithms available, such as the incremental 3D convex hull algorithm.[130] A measure for convexity C is obtained from the proportion of 'empty space' between the non-convex polyhedron and the convex hull by comparing the volumes or surface areas, that is, $C_A = A/A_{CH}$ and $C_V = V/V_{CH}$.

The simplest measure of sphericity is the *isoperimetric quotient* q_{IPQ},[131] defined for a polyhedron as

$$q_{IPQ} = 36\pi\frac{V^2}{A^3} \text{ with } q_{IPQ} \in [0, 1]$$
$$\text{and } D_{IPQ} = \left(1 - q_{IPQ}\right)$$
(18)

where $q_{IPQ} = 1$ for an ideal sphere and D_{IPQ} is a measure of the deviation from an ideal spherical shape. D_{IPQ} is shown for several fullerenes in Figure 14.

We usually regard C_{20} - I_h and C_{60} - I_h as almost spherical because all vertices lie on a (covering) sphere. We may therefore analyze whether or not the vertices of a given fullerene lie on a sphere. For this, we define the *minimum covering sphere* as a sphere of minimum radius that encloses all vertices in the polyhedral embedding (J. J. Sylvester, 1857).[132,133] Mathematically, this translates into finding the solution to the problem[134,135]

$$R_{MCS} = \min_{\vec{c}_{MCS}}\max_i \left\|\vec{v}_i - \vec{c}_{MCS}\right\|,$$
(19)

where $\|\cdot\|$ denotes the Euclidian norm, $\vec{v}_i$ is the location of the vertex v_i in 3D space, and $\vec{c}_{MCS}$ is the center of the MCS with radius R and is usually close to the barycenter of the fullerene. The MCS is uniquely defined[134,135] and can be obtained using an efficient algorithm, such as the one proposed by Yıldırım.[136] The convex hull of a 3D embedding of a graph G is contained entirely within the MCS. For fullerenes with an ellipsoidal shape like C_{72} - D_{6d}, or with a cylindrical shape such as a nanotube[137] (see Figure 2), it is more appropriate to use a minimum covering ellipsoid or cylinder instead of a sphere. The ellipsoidal problem has been addressed recently, and is known as the *minimum volume axis-aligned ellipsoid problem* (MVAE).[138–141]

We can now define a number of useful measures for sphericity. The *MCS distortion* (normalized

FIGURE 14 | Various deformation parameters D (in percent) for a series of fullerenes selected according to stability. For larger fullerenes, Goldberg-Coxeter transformed structures of C_{20} were chosen. Geometries were obtained from DFT (up to C_{540}) or force field optimizations. IPQ: isoperimetric quotient; MCS: Minimum covering sphere; MDS: Minimum distance sphere; DTP: Diaz-Tendero parameter; FAP: Fowler asymmetry parameter; TEP: $(1 - \rho)$ from the topological efficiency parameter ρ.
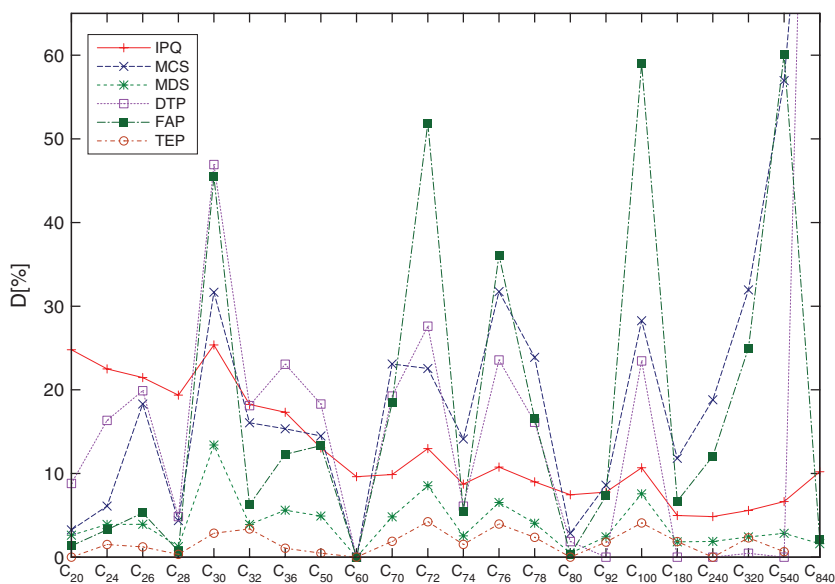
to the smallest C–C distance in the fullerene) is given by,

$$D_{\mathrm{MCS}} = \frac{1}{N r_{\min}} \sum_{i=1}^{N} \left(R_{\mathrm{MCS}} - \|\vec{p}_i - \vec{c}_{\mathrm{MCS}}\| \right) \quad (20)$$

The MCS definition for the distortion is biased to the case of few atoms sticking out on a sphere and another measure may therefore be more appropriate. We define the minimum distance sphere as

$$D_{\mathrm{MDS}} = \min_{c_{\mathrm{MDS}} \in \mathrm{CH}(S)} \frac{1}{N r_{\min}} \sum_i \left| R_{\mathrm{MDS}} - \left\|\vec{p}_i - \vec{c}_{\mathrm{MDS}}\right\| \right| \quad (21)$$

with

$$R_{\mathrm{MDS}} = \frac{1}{N} \sum_i \left\|\vec{p}_i - \vec{c}_{\mathrm{MDS}}\right\| \quad (22)$$

A similar definition that uses the mean deviation from the average distance taken from the barycentric point has been introduced by Nasu et al.[142]

Some other useful sphericity parameters are the Diaz-Tendero (DTP) parameter,[143,144]

$$q_{\mathrm{DTP}} = \sqrt{(a-b)^2 + (a-c)^2 + (b-c)^2}/a \quad (23)$$

where $a \geq b \geq c$ are the rotational constants, and the Fowler asymmetry parameter (FAP),

$$\lambda_{\mathrm{FAP}} = \sum_{i=1}^{N} \frac{(R_i - R_{\mathrm{av}})^2}{R_{\mathrm{av}}^2} \quad (24)$$

where R_i is the radial distance of atom i from the barycenter, and R_{av} is the average distance.[145] If all atoms lie on a sphere, we have $\lambda_{\mathrm{FAP}} = 0$.

Figure 14 shows a comparison of sphericity parameters for a number of stable fullerenes. As C_{20} is slightly deformed due to Jahn-Teller distortion, the vertices do not lie exactly on a sphere anymore, and $D_{\mathrm{MDS}} \neq 0$. In contrast, the purely topological efficiency parameter $(1 - \rho)$ (see discussion in the topological indicator section) is exactly zero for C_{20} (and for C_{60}, C_{80}, and C_{240}). For C_{60}, all vertices lie on a sphere and all deformation parameters are zero, except for the IPQ, which except for its simple definition is perhaps not the best measure for sphericity. All deformation parameters reveal the highly deformed fullerenes (spikes in Figure 14).

Toward the Solid State: Hilbert's Problem and Space Fillings

Solid C_{60} - I_h packs in a rotationally disordered face centered cubic (fcc) structure with a lattice constant of $a_{\mathrm{fcc}} = 14.17 \pm 0.01$ Å,[129,146] which according to Fischer et al. implies a close packing of spheres of a diameter of 10.02 Å.[146] C_{60} undergoes a phase transition below 255 K to a simple cubic (sc) structure, from which one can infer a lattice parameter of $a_{\mathrm{sc}} = 14.04 \pm 0.01$ Å.[147,148] The only other solid state fullerene obtained by experiment is that of C_{70} - D_{5h}, which adopts a closed packed structure of either hcp or fcc symmetry[138,149] with a fcc lattice constant of $a_{\mathrm{fcc}} = 14.96$ Å. In the solid state, the interactions between the fullerenes are of Van der Waals type. Note that the polarizability and therefore the Van der Waals coefficients grow linearly with increasing number of carbon atoms in the fullerene cage,[150] which should converge toward the graphene limit for the per-atom value. Experimentally, the solid state behavior of C_{60}

has been studied in great detail. One interesting fact is that the bulk moduli of C_{60} ($B = 6.8$ GPa for the simple cubic phase and 8.8 GPa for the fcc phase) and C_{70} (11 GPa for the rhombohedral phase) are quite small as applied pressure will just squeeze out the compressible Van der Waals space.[151−153] These bulk moduli are only twice as large compared to the rare gas solids,[154] and much smaller than that of diamond (442 GPa[155]). However, once the Van der Waals space is squeezed out and the fullerene cages touch, the bulk modulus increases substantially, as the fullerene cage is not easily compressible, similar to the high in-plane stiffness of graphite or graphene.[156] We mention that it requires high pressures above 20 GPa to turn C_{70} into graphite (using step-like shock-wave compression).[157] For overviews on solid-state properties of fullerenes, see Zettl and Cumings[153] or Fischer et al.[146]

From the experimental data of C_{60} - I_h, we can adjust the Van der Waals radius of the C_{60} cage such that the experimental lattice constant is obtained, that is, we use a hard sphere model for periodic packing (fcc is the closest packing available for hard spheres as proven by computer by Hales in 2000[158,159]). We can do this by using the MCS introduced in Eq (19), but we have to add the carbon Van der Waals radius ($r_{VdW}(C) = 1.415$ Å) to the MCS radius,

$$R_{VdW}(C_N) = R_{MCS}(C_N) + R_{VdW}(C) \qquad (25)$$

Figure 15 shows lattice constants for a number of fullerenes using this hard sphere model, which can be taken as an upper bound to experimental lattice constants. For the other experimentally known fullerene crystal structure, C_{70}, the fcc lattice constant a_{fcc} of 14.96 Å is in reasonable agreement with the hard-sphere value of 15.78 Å, considering the fact that the IPR C_{70} isomer is slightly prolate and distorted. The dependence of the a_{fcc} lattice constant on the vertex number can be expressed as $a_{fcc} = c\sqrt{N} + (4R_{VdW}(C))/\sqrt{2}$, where the shift follows from the geometry of the fcc cell and the $\sqrt{N}$-term represents the dependence of the fullerene radius on N. In the hard sphere model we have $a_{fcc} \sim R$, and the cage radius of the fullerene is $R \sim A^{1/2} \sim N^{1/2}$ (A being the surface area of the MCS).

For distorted fullerenes, the packing problem becomes far more complicated. For example, we could add the Van der Waals radius to every carbon atom and take the convex hull around this Van der Waals layer. We are then faced with close packing of complicated polyhedral structures, which is a difficult, unsolved problem. However, there exist algorithms for packing arbitrary polyhedra in finite spaces,[160,161] and it is possible that one could approximate properties
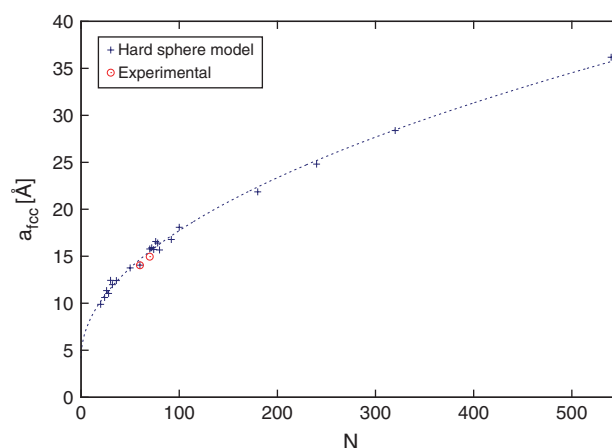

FIGURE 15 | fcc lattice constant a_{fcc} for a hard sphere model as a function of the number of carbon atoms N.

of the (periodic) close packing solution by making the finite cell large enough. For some fullerenes, ellipsoidal, or cylindrical covers are more appropriate as already mentioned.[141,162] The close packing of ellipsoids was recently investigated by Donev et al, who showed that the maximum packing density can exceed that of a close sphere packing.[163] Nevertheless, the question still remains how fullerenes of a certain topology pack in 3D space. This is related to one of Hilbert's fundamental problems: *How can one arrange most densely in space an infinite number of equal solids of given form, e.g., spheres, with given radii, that is, how can one so fit them together that the ratio of the filled to the unfilled space may be as great a possible?* A more rigorous mathematical proof (beside Hales' complete computer algorithm[158,159]) for fcc packing of hard spheres as the most dense packing is still missing, and packing any other deformed spheres remains an open area of research. One possible approximation is to expand the shape of a fullerene in terms of multipole deformations and study the 3D packing of such smooth topologies.

Topological and Chemical Indicators

Chemists can deduct many useful properties of a chemical system just by looking at its structure. For fullerenes, the distribution of the 12 pentagons on a surface, for example, a sphere, can tell us qualitatively how stable the fullerene is or how it would pack in the solid state. Moreover, the symmetry of the underlying structure determines many useful spectroscopic properties. It is perhaps a realistic goal to connect the graph theoretical properties of a fullerene directly with its physical properties by mapping the fullerene graph G into a number describing that property. In more general terms, we define a *topological indicator*

as a map τ_I from the graph G into a finite series of numbers,

$$\tau_I : G \mapsto \{x_1, \ldots, x_n\} \tag{26}$$

where the numbers x_i are called *topological indices* and can be chosen to be integers, rationals, or reals. A topological index is called a *chemical index* if it is related to a chemical (or physical) property. Topological indicators may be placed in the same category as crude chemical bonding models, except that they can be strictly defined in graph theoretical terms and sometimes have interesting mathematical properties. There is no restriction that the mapping between fullerene graphs and any topological indicator be one-to-one, and indeed, most of the commonly used topological indicators are the same for many different isomers. Of course, any chemical or physical property is ruled by its underlying electronic structure governed by the Schrödinger equation. However, solving the electronic structure problem for any large fullerene is a daunting task and therefore, topological indices that are easily obtained can be very useful as we shall see.

To give some (trivial) examples, we can list all the possible point groups for fullerenes and define $x_i = 0$ for the ideal point group not matched by the fullerene graph, and $x_i = 1$ if the point group is. The order of the ideal point group $|\mathcal{G}|$ as shown in Table 1 is also a topological index. Another example for a topological index is the 12 face spiral pentagon indices as described above.

The first topological index of chemical relevance was introduced by Wiener in 1947.[164] He defined a so-called path number (*Wiener index*) as the sum of the entries in the *topological distance matrix* d_{ij}, consisting of the length of the shortest path between every pair of vertices in the chemical graph representing the non-hydrogen atoms in the molecule,

$$W(G) = \frac{1}{2} \sum_{i,j \in \mathcal{V}} d_{ij} \tag{27}$$

where $d_{ii} = 0$. The Wiener index provided a good measure of compactness for acyclic alkanes and gave a reasonable correlation to boiling points.[164] The first application of the Wiener index to fullerenes came from Ori and co-workers, who obtained $W = 8340$ for C_{60}-I_h.[165] For fullerenes, low Wiener indices provide a measure of high compactness of the cage. This can be seen from the scaling law, which has been found to behave like $\mathcal{O}(N^{5/2})$ for 'spherical' fullerenes[166] and $\mathcal{O}(N^3)$ for fullerene nanotubes. For carbon nanotubes, analytical formulae in terms of polynomials in the vertex number are available, for

example, for the smallest D_{5h}/D_{5d} nanotubes we have $W(k) = 1/3(100k^3 + 1175k - 2010)$ with $N = 10k$ and $k \geq 5$,[167] and for the smallest D_{6h}/D_{6d} nanotubes we have $W(k) = 12(4k^3 + 69k - 136)$ with $N = 12k$ and $k \geq 7$.[168] It is conjectured that the Wiener index grows like $\mathcal{O}(N^{2+1/d})$, where d describes the dimensionality of the system (*the Wiener dimensionality*).[166] The almost cubic growth with increasing number of vertices can make the Wiener index unwieldy for larger fullerenes. Therefore, Ori and coworkers defined a *topological efficiency index* ρ, derived from the Wiener index[169,170]

$$\rho = 2 \frac{W(G)}{N W_{\min}} \quad \text{with} \quad W_{\min} = \min_i \left\{ \sum_{j \in \mathcal{V}} d(i,j) \right\} \tag{28}$$

which has the advantage that, unlike the Wiener index, it does not grow to large numbers. Small values of $\rho \geq 1$ indicate topologically efficient structures, for example, both C_{20}-I_h and C_{60}-I_h have $\rho = 1$.[168] It can be seen as a measure of sphericity that does not involve 3D Cartesian coordinates, as shown nicely in Figure 14. Vukičević et al. showed that among the 4478 isomers of C_{66}, the joint information of the Wiener index and the topological efficiency index correctly identifies the C_{66}-$C_{2v}(11)$ as the most stable molecule[169] (as detected experimentally in endohedral $Sc_2@C_{66}$[171]).

Many different topological indices have been introduced and studied since, mainly for the structural and statistical analysis of molecules, polyhedra, and graphs in general, often yielding interesting mathematical properties (for a list of topological indices see for example Ref 172). The distance matrix d_{ij} gives rise to a number of very useful topological indices including the topological radius R and diameter D,[173] Hosoya polynomials[174] and related Wiener indices, the Szeged index S_z,[175] and the Balaban index J,[29,176] to name but a few (for fullerenes one has $W \sim S_z$ and $W \sim -J$).[29,177] There are also a number of topological indices connected to the adjacency matrix (or Hückel matrix), for example Hückel orbital energies and related properties (occupation numbers, band gap,[31] spectral moments[178] etc.),[31] and the Estrada index.[179,180] For a more detailed discussion of topological indices see Refs 29, 89, 173, and 181.

Some of these topological indices can directly be related to the stability of the fullerene cage. For example, the *Fowler-Manolopoulos pentagon indices* $\{p_n | n = 0, \ldots, 5\}$ define the number of pentagons attached to n other pentagons (n is called the neighbor index),[31] that is, for IPR fullerenes we have $p_0 = 12$ and $p_n = 0$ for $n \geq 1$. For any fullerene, we of course must have $p_1 + \cdots + p_5 = 12$. *Fowler-Manolopoulos*

hexagon indices are similarly defined and useful for IPR fullerenes, that is, $\{h_i | i = 0, \ldots, 6\}$, where h_n defines the number of hexagons with neighbor index n. In an IPR fullerene every hexagon is adjacent to a minimum of three others and we can restrict the list of hexagon neighbor indices for example to (h_3, h_4, h_5, h_6).[31]

We may contract the neighbor indices to one useful topological index describing the stability of fullerenes.[31] The single *pentagon signature* P_1 is defined as

$$P_1 = \frac{1}{2} \sum_{k=1}^{5} k p_k \quad (29)$$

$\max(P_1) = 30$ (for C_{20} only), and for IPR fullerenes such as C_{60} we have $P_1 = 0$. For IPR fullerenes a more useful single topological index is defined through the hexagon signatures. The standard deviation σ_h of the hexagon neighbor index distribution is defined as

$$\sigma_h = \sqrt{\langle k^2 \rangle - \langle k \rangle^2} \quad (30)$$

where

$$\langle k^n \rangle = \frac{H_n}{H_0} \quad \text{with} \quad H_n = \sum_{k=0}^{6} k^n h_k \in \mathbb{N}$$

$$\text{and} \quad H_0 = \sum_{k=0}^{6} h_k = \frac{N}{2} - 10 \quad (31)$$

We call the topological index H_n the *n-th moment hexagon signature*. For general fullerene isomers, low P_1 values and high H_i values correlate with high thermodynamic stability.[31] It turns out, however, that H_1 stays constant for a given vertex count in IPR fullerenes, as this index is related to certain face patterns as we shall see. Fowler et al. advocated the use of the index σ_h instead, as low values of σ_h are better predictors for stability, and the strain is minimized when all hexagon neighbor indices are as similar as possible.[31] For example, for C_{60} we have $\{h_i\} = \{0, 0, 0, 20, 0, 0, 0\}$ giving $H_1 = 60$, $H_2 = 180$, and $\sigma_h = 0$. Fowler et al. devised the following scheme for estimating the internal order among fullerenes sorted by stability:[173] First order the isomers according to lowest P_1-value (each pentagon-pentagon fusion carries a penalty of about 20–25 kcal/mol). If multiple IPR fullerenes are present, that is, $P_1 = 0$, we order these first by largest H_2-value, and finally by lowest Wiener index W (which indicates high compactness of the fullerene cage). The result is an efficient but effective screening method to find the most stable fullerene isomers.
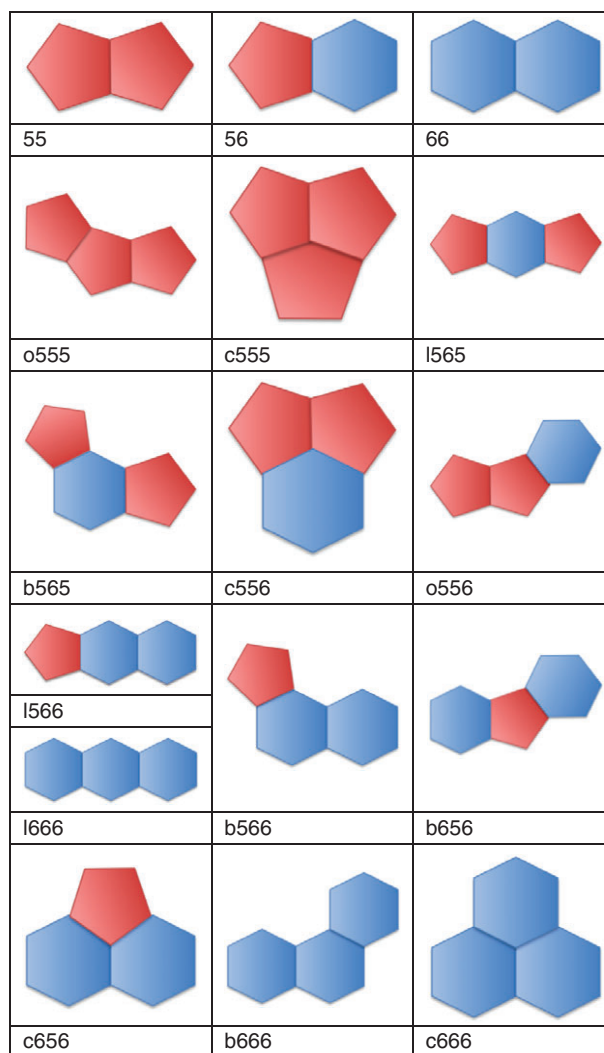

FIGURE 16 | The 15 basic shapes for the two- and three-ring (face) adjacencies on the surface of a fullerene; (*l*) denotes linear, (*b*) bent, (*o*) open, and (*c*) closed ring patterns (see Ref 183).

Ju et al. presented a relationship between the Fowler-Manolopoulos hexagon indices and a particular hexagon structure count to provide a graphical interpretation.[182] The complete list of different pentagon and hexagon combinations up to three connected faces are shown in Figure 16. Note that for connecting two or three faces we have

$$n_{55} + n_{56} + n_{66} = E = \frac{3N}{2} \quad \text{and}$$

$$n_{555} + n_{556} + n_{566} + n_{666} = \frac{11}{2}N - 30 \quad (32)$$

where the notation is described in Figure 16. For example n_{556} is the sum of all occurring ring patterns containing the combination of two pentagons and one

hexagon. Ju et al. showed that for the second moment hexagon signature one gets[182]

$$H_2^{\text{IPR}} = 2n_{66} + 6n_{c666} + 2\left(n_{l666} + n_{b666}\right)$$
$$= 2\left(n_{l666} + n_{b666}\right) + 9N - 480 \quad (33)$$

and

$$H_1^{\text{IPR}} = 2n_{66} = 3\left(N - 40\right) \quad (34)$$

Hence for IPR fullerenes, σ_h and H_2 are related through the simple equation

$$\sigma_h^{\text{IPR}} = (N - 20)^{-1}\left(2\left(N - 20\right)H_2 - 36\left(N - 40\right)^2\right)^{1/2} \quad (35)$$

and one requires only H_2 to discuss the stability of IPR fullerenes. Stevanović extended these relations to general fullerenes (IPR or not),[184]

$$H_1 = 3\left(N - 20\right) - n_{56} \quad (36)$$

and

$$H_2 = 18\left(N - 20\right) - \left(6n_{56} + 2n_{c666} + n_{l666} + n_{b666}\right) \quad (37)$$

This not only illustrates nicely the current development in the area of topological indices, it also suggests that the stability of fullerenes can be approximated by counting different face patterns.[183]

Indeed, Cioslowski et al.'s incremental scheme for the heat of formation ΔH_f^o for IPR fullerenes[33] uses 25 linearly independent face patterns (structural motifs) of up to 13 connected hexagons and pentagons to calculate the energy E_{FP}, including an additional curvature term E_{C},

$$\Delta H_f = E_{\text{FP}} + E_{\text{C}} = \sum_{i=1}^{25} m_i \varepsilon_i$$
$$- 8050.751\left(N - 30.050\right)^{-1} \left[\text{kcal/mol}\right] \quad (38)$$

where m_i stands for the total count of a specific face pattern (FP) that appears in the fullerene, ε_i is the FP energy contribution, and the second term in Eq (38) is the curvature term (C), which is repulsive for C_{20} and approaches zero for $N \to \infty$. For example, for $C_{60} \text{-} I_h$ we just have one pattern in Cioslowski et al.'s scheme consisting of a hexagon surrounded by 3 pentagons and 3 hexagons. There are 20 of these in C_{60}, and with $\varepsilon = 44.281$ kcal/mol, we obtain $\Delta H_f = 616.814$ kcal/mol for C_{60}.[33] This compares rather well with

the estimated NIST listed heat of formation for C_{60} (612 ± 25 kcal/mol), although this value should probably be corrected downwards to a value of 602.7 kcal/mol as recently pointed out by Karton et al. using high-level theoretical procedures.[185] The rms error for the standard enthalpies of formation for the 115 IPR isomers chosen was 4.0 kcal/mol compared to B3LYP/6-31G* calculations.

Alcami et al. devised a similar scheme for general fullerenes.[32] By analyzing the most stable structures from B3LYP-DFT calculations of C_{20} to C_{72}, and using only connections between four faces with varying number of pentagons with a total of 9 different motifs, an expression similar to Cioslowski et al. was used for E_{FP}, but without the curvature term E_{C}. This scheme gives $\Delta H_f = 654.0$ kcal/mol for $C_{60} \text{-} I_h$. For all fullerenes studied the rms error is 15.4 kcal/mol for the enthalpy of formation compared to DFT calculations, or 0.31 kcal/mol per carbon atom.

The question is: How well are topological indices suited to describe fullerene stability? Table 3 shows a comparison of stabilities for all C_{34} isomers obtained from DFT geometry optimizations (using the PBE functional[186] and a def2-SVP basis set for carbon[187]) in comparison with several topological indicators.[35] According to the pentagon signature, isomer $C_{34} \text{-} C_2(5)$ has the lowest P_1 value, but with a very small HOMO-LUMO gap obtained from Hückel theory. This is indeed the case as the DFT results show. Alcami et al.'s stability indicator correctly predicts the most stable ($P_1 = 14$) and the least stable isomer ($P_1 = 17$). For the four isomers with pentagon signature $P_1 = 15$, the two results (ΔE^{DFT} and ΔE^{A}) do not agree in their sequence (note that Alcami et al.'s scheme was not designed to distinguish between different isomers of a fixed vertex count). The different fullerene isomers are all very similar in surface area and volume. Concerning the HOMO-LUMO gap, the most stable isomer does not correspond to the one with the largest HOMO/LUMO gap. Moreover, these values are very sensitive to the method applied, and a better measure for the gap given by the singlet-triplet separation. The fullerenes with the smallest HOMO-LUMO gaps (isomers 2 and 6) prefer in fact the triplet ground state. The Hückel HOMO/LUMO gap on the other hand is only good for a qualitative discussion. We note that the two different fullerene isomers 3 and 5 have identical Wiener indices, and the isomer 6 with the smallest Wiener index is not the most stable isomer.

The first halma transform of C_{20} is C_{80} and therefore of I_h symmetry. There are seven IPR isomers out of a total of 31,924 isomers as possible candidates for the energetically most stable one. Table 4 shows

TABLE 3 | Stability and Topological Indicators for the Six Isomers of C_{34}

L_I	PG	P_1	ΔE^{DFT}	ΔE^A	$\Delta\varepsilon_{HL}^H$	$\Delta\varepsilon_{HL}^{DFT}$	ΔE_{ST}^{DFT}	A	V	W	N_{HC}	N_{PM}
1	C_2	17	74.93	13.5	0.069	0.424	0.0267	81.41	60.30	1978	28	212
2	C_s	15	28.10	4.2	0.120	0.150	−0.153	81.27	61.70	1975	58	219
2(T)	C_s	15	24.55	4.2	—	—	—	81.32	61.69	1975	58	219
3	C_s	15	31.48	4.0	0.368	0.406	0.0945	81.42	61.80	1973	52	196
4	C_2	15	15.19	5.5	0.343	0.619	0.2229	81.32	62.06	1976	33	229
5	C_2	14	0	0	0.006	0.480	0.1333	81.28	62.27	1973	42	204
6	C_{3v}	15	33.70	7.8	0	0.225	−0.094	81.42	61.79	1971	66	195
6(T)	C_{3v}	15	31.54	7.8	—	—	—	81.40	61.75	1971	66	195

L_I is the numbering scheme according to the lexicographically ordered face spiral pentagon indices, PG the ideal point group, P_1 the pentagon signature, energy differences (in kcal/mol) ΔE^{DFT} the DFT(PBE) energy difference to the most stable isomer (kcal/mol), ΔE^A the Alcami energy difference to the most stable isomer (kcal/mol), energy gaps (in eV) $\Delta\varepsilon_{HL}^H$ the Hückel HOMO-LUMO gap, $\Delta\varepsilon_{HL}^{DFT}$ the PBE HOMO-LUMO gap, ΔE_{ST}^{DFT} the singlet-triplet gap (in eV), A the surface area (Å^2), V the volume (Å^3), W the Wiener index (see Ref 188), N_{HC} the number of Hamiltonian cycles, and N_{PM} the number of perfect matchings. The symbol (T) for isomers 2 and 6 in the first column indicates that the triplet electronic state is taken instead of the singlet state.

TABLE 4 | Stability and Topological Indicators for the Seven IPR Isomers of C_{80}

L_I	PG	H_2	ΔE^{DFT}	ΔE^A	ΔE^C	ΔE^{HRE}	$\Delta\varepsilon_{HL}^H$	$\Delta\varepsilon_{HL}^{DFT}$	ΔE_{ST}^{DFT}	A	V	W	N_{HC}	N_{PM}
1	D_{5d}	500	0	0	4.34	2.12	0.220	0.355	0.168	203.70	255.16	17340	10450	270153
2	D_2	496	2.63	3.0	0.75	0.0	0.528	0.460	0.293	203.85	257.72	17352	10642	237585
3	C_{2v}	488	1.81	10.5	0.04	14.7	0.102	0.009	0.091	203.92	260.80	17412	9918	201623
4	D_3	492	7.03	7.5	7.17	6.70	0.408	0.098	−0.036	203.87	258.71	17368	9906	222588
4(T)	D_3	492	6.21	7.5	7.17	—	—	—	—	203.85	258.40	17368	9906	222588
5	C_{2v}	484	6.33	16.5	2.92	24.7	0.298	0.038	−0.090	203.99	262.48	17454	9004	182555
5(T)	C_{2v}	484	4.25	16.5	2.92	—	—	—	—	203.98	262.41	17454	9004	182555
6	D_{5h}	480	6.81	22.5	0	37.7	0	0.081	−0.002	204.01	263.50	17500	10970	169375
6(T)	D_{5h}	480	6.38	22.5	0	—	—	—	—	204.00	263.49	17500	10970	169375
7	I_h	480	17.49	30.0	14.2	63.4	0	0.115	−0.003	204.02	263.61	17600	10500	140625
7(T)	I_h	480	17.43	30.0	14.2	—	—	—	—	204.02	263.63	17600	10500	140625

L_I is the numbering scheme according to the lexicographically ordered IPR face spiral pentagon indices, PG the ideal point group, H_2 the second moment hexagon signature, energy differences (in kcal/mol) ΔE^{DFT} the DFT(PBE) energy difference to the most stable isomer, ΔE^A the Alcami energy difference to the most stable isomer, ΔE^C the Cioslowski energy difference to the most stable isomer, ΔE^{HRE} the Hückel resonance energy (taking the resonance value as $\beta = -60$ kcal/mol), energy gaps (in eV) $\Delta\varepsilon_{HL}^H$ the Hückel HOMO-LUMO gap, $\Delta\varepsilon_{HL}^{DFT}$ the PBE HOMO-LUMO gap, ΔE_{ST}^{DFT} the singlet-triplet gap (in eV), A the surface area (Å^2), V the volume (Å^3), W the Wiener index, N_{HC} the number of Hamiltonian cycles, and N_{PM} the number of perfect matchings. The symbol (T) indicates that the triplet electronic state is taken instead of the singlet state.

the properties of all IPR isomers of C_{80}. With larger fullerenes the band gap becomes very small (graphene is a semi-metal or zero-gap semiconductor[189]), and one has to check for states of higher spin multiplicity. For C_{80}, Hückel theory indicates an open-shell case for the isomers 6 and 7. In fact, the results show that four of the isomers have a triplet ground state, with the singlet and triplet states for C_{80} - I_h being quasi-degenerate. The DFT calculations further show that the most stable fullerene is not the high symmetry C_{80} - I_h isomer, but the first one in the IPR isomer list, which is of D_{5d} symmetry and has the largest H_2 value (previously, isomer 2 has been predicted to be the most stable isomer[190]). The results show that the first three isomers are very close in energy and it requires perhaps a more sophisticated electron correlation treatment

to sort out the sequence in stability. Isomer 1 also has the highest count in perfect matchings among all IPR isomers (although the non-IPR C_{60} - $D_{3d}(4)$ nanotube has a much higher perfect matching count of $N_{PM} = 524,250$). The volumes and surface areas are all very similar with the highest symmetry isomer C_{80} - I_h being largest.

The results shown here clearly demonstrate that the topological indicators help enormously to sort out the most stable isomers. The situation is often quite complicated as seen from the DFT calculations here, or for example from the work of other authors who compared stabilities within a list of isomers.[191–193] In the next section we introduce topological indicators that are connected to π-electron resonance structures (Kekulé structures) in fullerenes.

Kekulé Structures and Perfect Matchings, Clar and Fries Structures, and the Pauling Bond Order

Every chemist learns how to draw double bonds into an aromatic system called a Kekulé (or resonance) structure, sometimes also called a benzenoid graph.[194] For benzene there are only two possible Kekulé structures with three double bonds as we all know, but for C_{60} there are as many as 12,500 Kekulé structures with 30 double bonds (a fullerene has exactly $n_{DB} = N/2$ double bonds), of which only 158 are symmetry distinct, that is, non-isomorphic.[195–197] A *Kekulé structure* is the same as a *perfect matching* in the chemical graph $G = (\mathcal{V}, \mathcal{E})$, where the edges of the matching correspond to double bonds. We write $\mathcal{K}(G)$ for the set of all perfect matchings of the graph, and the number of different Kekulé structures $K = |\mathcal{K}(G)|$ is called the *Kekulé number*. In graph theory, a perfect matching is a selection of edges such that every vertex of the graph G is part of exactly one edge in the matching. The edges of the matching correspond to the double bonds.

Chemists know from basic Hückel theory that for two different benzenoid graphs B_1 and B_2, $K(B_1) > K(B_2)$ implies that B_1 is more stable than B_2 because of resonance stabilization. Schmalz et al. calculated the Kekulé number for several small fullerenes up to C_{84}.[50] Their work showed that for C_{60}, the least stable isomer C_{60}-D_{5h}(1) has $K = 16,501$, while for the most stable isomer C_{60}-I_h(1812) we have $K = 12,500$.[50] In fact, Austin et al. showed that 20 isomers of C_{60} have a higher Kekulé numbers than C_{60}-I_h.[198] The Kekulé number is therefore not a good indicator for fullerene stability,[198] but useful for rationalizing the different bond lengths in fullerenes as we shall see.

All cubic graphs have exponentially many perfect matchings and hence exponentially many Kekulé structures.[199] While the theoretical lower bounds proved in Refs 113, 199 have small exponents, the actual exponential behavior kicks in rapidly, as seen in Figure 17: The mean number of perfect matchings for a C_N isomer is approximately $20 \cdot 2^{(N-20)/4}$. In general, calculating the number of perfect matchings for graphs is intractable,[i] but for planar graphs (such as fullerenes) the Kekulé number can be computed in $\mathcal{O}(N^3)$ time using the Pfaffian matrix (the Fisher-Kasteleyn-Temperley algorithm).[200]

Pauling, Brockway, and Beach introduced bond orders derived from Kekulé structures in order to rationalize the differences in the C–C bond lengths encountered for polycyclic aromatic compounds.[201] The *Pauling bond order* (PBO) P_{ij} of an edge $v_i - v_j$ is defined as the sum over all appearances of double
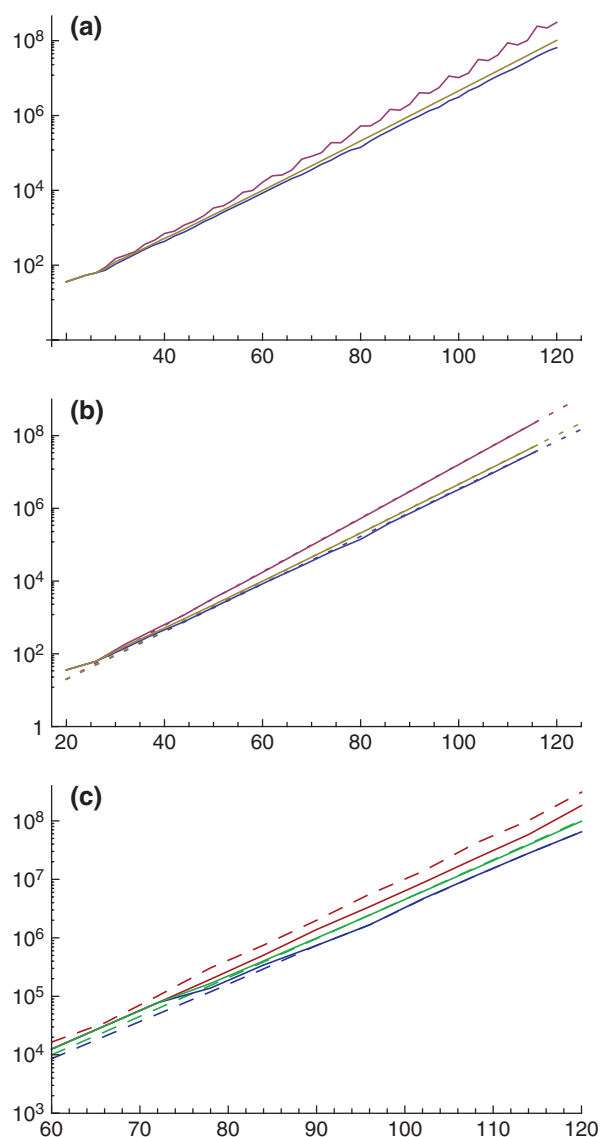

FIGURE 17 | Minimum, median, and maximum perfect matching count for all isomers of C_N up to C_{120}. (a) When looking at the plot for all N, we notice three distinct series depending on the value of $N \bmod 6$. (b) For each of the three series, both the maximum and minimum counts follow a simple exponential function (shown as dashed lines). Here, the 'peak series' at $N \bmod 6 = 2$ is shown. (c) The bounds for the IPR isomers (solid curves) are shown together with the bound for all isomers (dashed curves) for the series $N \bmod 6 = 0$. The other two series behave similarly.

bonds in perfects matchings

$$P_{ij} = \frac{1}{K} \sum_{M \in \mathcal{K}(G)} \beta_{ij} \qquad (39)$$

where $\beta_{ij} = 1$ if the edge $v_i - v_j$ has a double bond in the perfect matching M, otherwise $\beta_{ij} = 0$. This gives $0 \leq P_{ij} \leq 1$, with 0 being a pure C–C single bond and 1
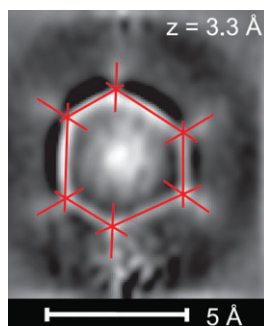
FIGURE 18 | Atomic force microscopy (AFM) image for C_{60} by Gross and co-workers[204] at a tip height of $z = 3.3$ Å showing the different bond orders of individual carbon-carbon bonds in a hexagon. (Copyright © 2012, American Association for the Advancement of Science)

a pure C=C double bond. In C_{60}-I_h there are two different type of bonds and therefore two different PBOs, depending if the edge shares two hexagons ($P_{hh} = 11/25 = 0.44$) or a hexagon and a pentagon ($P_{hp} = 7/25 = 0.28$).[202] Note that the *Hückel bond orders* derived from the eigenvectors of the adjacency matrix are generally larger with $P_{hh} = 0.6010$ and $P_{hp} = 0.4758$ for C_{60}-I_h.[203]

Narita et al. derived a linear relationship between the PBO and the bond distance in a fullerene obtained from X-ray diffraction,[202]

$$r_{ij}[\text{Å}] = 1.554 - 0.399 P_{ij} \tag{40}$$

Figure 18 shows an AFM picture of one of the symmetry equivalent hexagons in C_{60} clearly showing the two different types of bonds. The measured bond lengths are $r_{hh} = 1.38(2)$ Å and $r_{hp} = 1.454(12)$ Å,[204] in excellent agreement with the values obtained from Eq (40) ($r_{hh} = 1.378$ Å and $r_{hp} = 1.442$ Å).

Kekulé structures containing benzenoid moieties are of special interest. These are the Fries and Clar structures. *Fries structures* are Kekulé structures with maximum number of benzenoid hexagons. The *Fries number Fries(G)* of a benzenoid graph is the maximum number of benzenoid hexagons over all of its Kekulé structures, and a Fries structure is a perfect matching that realizes this maximum (there could be many). Similarly, the *Clar number Clar(G)* is the largest number of independent sets of benzenoid faces (separated from each other) over all Kekulé structures, and a *Clar structure* is a perfect matching that realizes this (there could be many). It is clear that a Clar structure localizes benzenoid structures in fullerenes. For C_{60}-I_h we have $Fries(G) = 20$ and $Clar(G) = 8$, and an example for a Fries and Clar structure of C_{60}-I_h is shown in Figure 19. One might naively assume that a set of Clar structures form a subset of Fries structures, but this is generally not the case for fullerenes.[205]
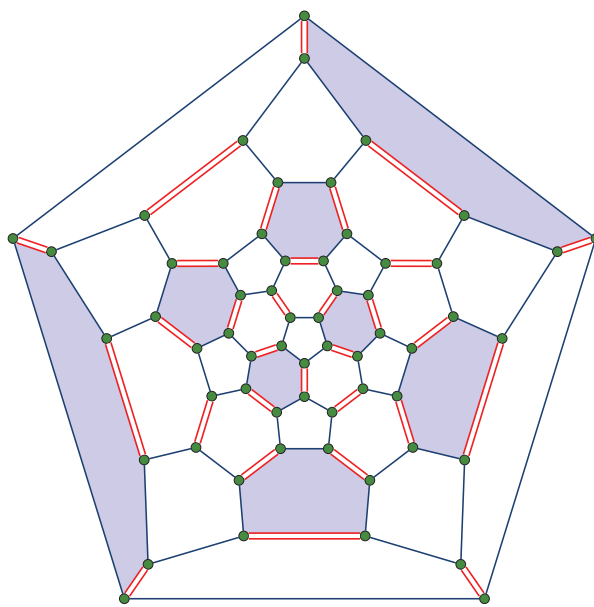

FIGURE 19 | One of the Fries structures of C_{60}, and superimposed the structure with highest Clar number ($Clar(C_{60}) = 8$). Double bonds are shown in red and isolated aromatic hexagons are shaded in.

We expect maximum stability for fullerenes with the highest Clar number. For example, C_{60}-I_h is unique among all other isomers in that it has a Fries structure where all hexagons contain three double bonds and all pentagons none. This is also seen as a reason for the unique stability of C_{60}. However, finding the Clar number is not a trivial problem as it is computationally NP-hard.[206] Ye and Zhang recently showed that for C_{60} there are exactly 18 fullerenes with maximal Clar number of 8.[207] Some of them contain as many as 6 fused pentagons. Hence the Clar number alone is not a good measure for stability. However, out of the 18 fullerenes with Clar number 8, C_{60} has the largest Kekulé count.[208] Fowler showed that leapfrog transforms of fullerenes not only are closed shell, but also have the maximum proportion of benzenoid hexagons.[209]

Figure 17(c) shows that the expected number of perfect matchings is no different for IPR fullerenes than it is for all fullerenes, except for small fullerenes for which it is larger than average. However, the maximum number is always significantly lower for IPR fullerenes. One could assume that the larger the Kekulé number is the more Clar sextets can be found and the more stable the fullerene is. While this has not been explored in detail, Table 4 shows that for C_{80} the most stable D_{5h} isomer has the lowest perfect matching count. There are, however, some good lower and upper bounds of these topological indices known. Došlić showed that the number of Kekulé structures grows exponentially with a lower bound of $2^{N/8}$.[210]

This is not a very tight bound, however, as for C_{60} it predicts at least 181 Kekulé structures, and there are as many as 12,500. The upper bound for Fries numbers is well known, $Fries(G) \leq N/3$, which is seen to be the graphenic limit. Fries structures with a maximum $N/3$ Fries number are called *complete Fries structures*[211] or *perfect Clar structures*. This happens exactly for Clar structures that use every vertex. In that case, the Clar and the Fries structure is the same, and corresponds to a 'soccer ball coloring' of the faces. An interesting result comes from Pisanski who proved in a paper with Fowler that the fullerenes with maximum Fries number $N/3$ are exactly the class of leapfrog fullerenes.[212] Given a leapfrog, we can find a perfect Clar structure, and given a perfect Clar structure, we can derive an inverse leapfrog transformation. This gives an easy way to test whether a particular isomer admits a perfect Clar structure: simply test whether the inverse leapfrog operation is successful. An upper bound for Clar numbers has been obtained by Zhang and Ye, $Clar(G) \leq (N/6 - 2)$.[213] Both IPR fullerenes, C_{60}-I_h, and C_{70}-D_{5h} with $Clar(C_{70}) = 9$ achieve this upper bound. Such fullerenes are called *extremal fullerenes*.[213]

Finally we mention that the Kekulé structures can be used to determine the resonance stability of fullerenes. To start with a very simple model, Randić et al. took the Kekulé structures of fullerenes ranging from C_{20} to C_{72}, and calculated the *π-content* P_π of hexagons and pentagons, which is obtained by summing all the Pauling bond orders in a specific ring.[197] For C_{60}-I_h this gives $P_\pi^h = 3P_{hp} + 3P_{hh} = 54/25 = 2.16$ for a hexagon, and $P_\pi^p = 5P_{hp} = 35/25 = 1.40$. High hexagon π-count together with low pentagon π-count gives stability to a fullerene. High hexagon π-count increases the aromaticity in the system (for more details see Ref 197). Klein et al. applied Herndon's resonance theory[214,215] using counts of $2m$-resonance cycles to obtain the resonance energy.[195] They correctly pointed out that the reduced p_π-orbital overlap in strongly curved fullerenes will reduce the resonance energy and has to be taken into account.[195] Here we should mention again that obtaining all Kekulé structures for a fullerene is an exponential problem, and it is more advantageous to apply methods that scale polynomially in time, such as Hückel or more sophisticated (semi-empirical) theories.

Hamiltonian Cycles, IUPAC Rules, and Naming Fullerene

For naming an alkene, the IUPAC rules state that one has to find the longest continuing carbon chain containing as many double bonds as possible. For a cyclic system one chooses the longest cyclic chain, and if there are multiple longest cycles, one must choose the one that maximizes the number of double bonds along the chain. This is related to finding a *Hamilton cycle*, which is a closed path in a graph that visits every vertex exactly once. If at least one such cycle exists, we say that the graph is *Hamiltonian*. In this case, the Hamilton cycles are the longest carbon chains, and the optimal one must be chosen among these.

It is an open problem whether every fullerene has a Hamilton cycle.[j] In practice, however, we find that fullerenes are not only Hamiltonian, but admit exponentially many Hamilton cycles. The mean number of Hamilton cycles taken over all C_N-isomers grows approximately as $8 \cdot 2^{(N-20)/5.8}$ for $N \mod 4 = 0$ and as $12 \cdot 2^{(N-20)/6}$ for $N \mod 4 = 2$ (Schwerdtfeger et al., unpublished manuscript). Because of this, naming fullerenes according to the IUPAC alkene rules is a computationally heavy task: we must search through all the exponentially many Hamiltonian cycles (main rings) to find the one in which the secondary bridges are labeled in the lexicographically smallest way. This is computationally feasible only for small fullerenes such as the ones shown in Figure 20.

In addition to being infeasible to calculate, as N grows, the name resulting for a fullerene from the IUPAC alkene rules rapidly becomes long and unmanageable. Even for a relatively small fullerene such as C_{60}-I_h, the name[k] is already unreadable, and the name length keeps growing with the fullerene size.[216] The IUPAC alkene name for fullerenes is now seen mostly as a curiosity—and a good example of how a well meant rule has its limits.

IUPAC employs an alternative naming scheme for fullerenes: C_N-PG[5, 6]fullerene, where PG stands for the (ideal) point group, and [5, 6] denotes a polyhedral cage with only pentagon and hexagon faces. For example, the IPR C_{60} fullerene has the official IUPAC name C_{60}-I_h[5, 6]fullerene. While computing the name of a fullerene according to this scheme is easy and efficient, and contrary to the alkene naming scheme is short and easy to understand, we find that this scheme is not much better than the IUPAC alkene nomenclature. On the one hand it is unnecessarily long: 'fullerene' implies '[5, 6]', and vice versa. On the other hand, it does not uniquely specify a fullerene, since many isomers share the same vertex count and symmetry. For example, while C_{120}-T_d[5, 6]fullerene happens to be unique, C_{120}-C_2[5, 6]fullerene refers to 10,787 different fullerene isomers, and C_{120}-C_1[5, 6]fullerene refers to no less than 1,660,007 different molecules. We therefore advocate the use of one of the following two names to uniquely specify fullerenes, based
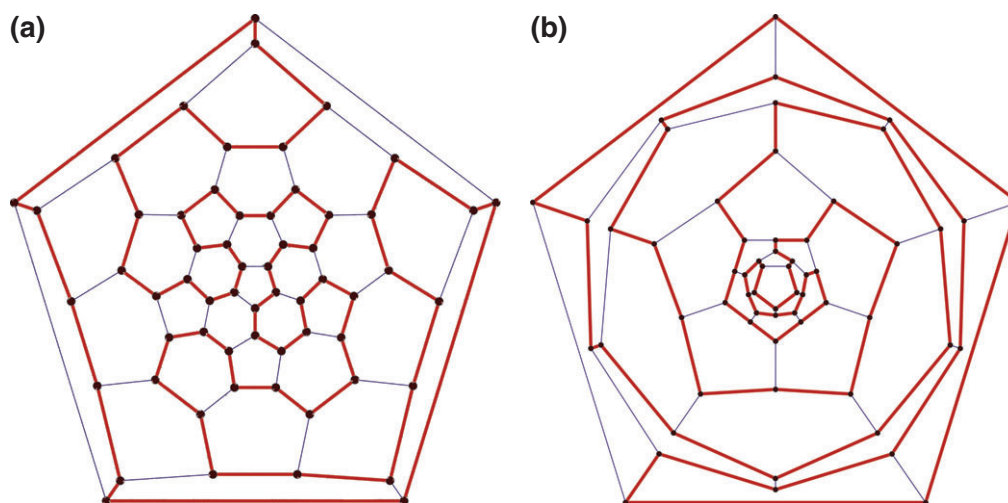
FIGURE 20 | One of the Hamiltonian cycles out of the many for (a) C_{60}-I_h ($N_{HC} = 1090$), and (b) the C_{60}-D_{5h} carbon nanotube ($N_{HC} = 3040$).

on the (generalized) canonical face spiral pentagon indices (FSPI), see the chapter on face spirals above. Both schemes uniquely and compactly identify a specific fullerene molecule.

1. For moderate values of N, we can specify the fullerene by its canonical index, which is the lexicographic number of its FSPI among the isomers. For example, the IPR C_{60} molecule can be written as C_{60}-I_h(1812) or C_{60}-I_h(IPR−1), as it is the last fullerene of the 1812 C_{60} isomers in the lexicographically ordered FSPI list.

2. For large C_N, for which it is not feasible to compile databases for all isomers, we annotate instead with the FSPI. For the vast majority of fullerenes, this is a list of 12 small integers. For the extremely rare cases where jumps are necessary (there are only two non-spiral fullerenes out of the 2.6×10^{12} fullerenes up to C_{400}), two extra integers are required per jump. No currently known case requires more than one jump. With this scheme, C_{60}-I_h(IPR−1) is written C_{60}-$I_h\{1, 7, 9, 11, 13, 15, 18, 20, 22, 24, 26, 32\}$, and the unspiralable C_{380} is written C_{380}-$T\{110, 2; 45, 70, 71, 82, 83, 110, 119, 120, 144, 184, 185, 192\}$. In the latter example, the two numbers before the semicolon denote a cyclic shift of length 2 before adding face number 110.[59]

The canonical FSPI notation is especially advantageous for more reasons than being compact and complete without needing to refer to a precomputed database. The procedure to construct a fullerene graph from the FSPI (the 'windup' operation) is geometrically intuitive—visualized like peeling an orange—and the algorithm is so simple that it can be performed with pen and paper. Thus, one can even reconstruct fullerenes of moderate sizes from the FSPI by hand, without the help of a computer.

The algorithm for the windup operation is $\mathcal{O}(N)$, and the inverse operation, *unwind*, takes $\mathcal{O}(N)$ expected time to find a single generalized spiral, and $\mathcal{O}(N^2)$ to find the canonical one.[59] The canonical FSPI constitutes a canonical labeling of fullerene graphs up to isomorphism. Hence one can check whether two fullerene graphs are isomorphic simply by testing whether they have the same canonical FSPI, and the canonical FSPI gives us a unique graph representative of each isomorphism class via the windup procedure. As discussed later, the FSPI representation makes it easy to directly compute the ideal symmetry group of the fullerene. Because the generalized face spiral algorithm is complete for all connected planar cubic graphs, a compressed form of the face spiral similar to the FSPI can be used in general for fulleroids, to be introduced in the last chapter.

Thermodynamic Stability and the Graphene Limit

The spherical shape of C_{60}-I_h with no adjacent pentagons is seen as the main reason for its unusual stability,[217] which underlines the importance of Kroto's isolated pentagon rule (IPR).[18] For example, Nagase and co-workers investigated the stability of potential candidates for the lowest energy structure of C_{74}, with the sole IPR D_{3h} isomer being 16 kcal/mol lower in energy than the C_2 isomer containing two fused pentagons.[218] It is therefore convenient to compare the stability of a fullerene to

C_{60}-I_h (relative fullerene stability, RFS) by using the isodesmic reaction $C_{60}/60 \to C_N/N$,

$$\Delta E^{RFS}(N) = \frac{1}{N} E[C_N] - \frac{1}{60} E[C_{60} - I_h] \quad (41)$$

where $E[C_N]$ is the total energy for a C_N fullerene. For $N \to \infty$ we obtain the graphene limit, which can be estimated to be approximately $\Delta E^{RFS}(\infty) = -9$ kcal/mol.

As $E \sim N$, E/N approaches a constant value for infinite systems, for example, the graphene limit if the pentagons are as separated as possible from each other, so that the polyhedral surface is mainly constituted of flat graphene sheets. Alternatively, for nanotube fullerenes with pentagon caps, the infinite particle limit is just the corresponding infinite nanotube. For the graphene limit, the next dominant term in a $1/N$ expansion will be the surface tension or curvature term, which is $\sim N^{-1}$ as for example used by Cioslowski et al.,[33] see Eq (38) (although a $N^{-1/2}$ law has been also suggested before[59]). Indeed, as Figure 21 shows, the stability follows approximately a linear behavior in our $1/N$ fit (we set $\Delta E_{RFS} = 0$ for $N = 60$),

$$\Delta E^{RFS}(N) = 527.4 N^{-1} - 8.79 \quad (\text{kcal/mol}) \quad (42)$$

that is fullerenes become more energetically stable with increasing vertex number N. It was already shown experimentally that C_{70} is more electronically stable than C_{60}.[219] Alcami et al.'s scheme predicts the correct graphene limit ($N \to \infty$), and Cioslowski's scheme performs well for medium sized IPR fullerenes, but has an incorrect convergence behavior toward the graphene limit.[32,33] C_{20} is the smallest member of the fullerene family, and as seen from Figure 21 also the least electronically stable one. It has been detected in

2000 by Prinzbach[16] (see also Ref 220), and a current review on the state of affair concerning C_{20} is given by Fei et al.[221]

It becomes more and more difficult to extract the most stable isomers from the huge isomer space as the size of the fullerene increases. Besides using topological indicators, Hückel theory can be used to determine the resonance stability of a fullerene. It requires diagonalization of the adjacency matrix A_{ij} (the Hückel matrix is defined as $H_{ij} = \alpha \delta_{ij} + \beta A_{ij}$, where α is the Coulomb and β the resonance integral, and δ_{ij} is the unit matrix), and the occupied Hückel orbitals determine the *Hückel resonance stability* (HRS) of a fullerene (in units of β),

$$\Delta E^{HRS}(N) = E_\pi - N$$

$$\text{with} \quad E_\pi = \sum_{i=1}^{occ} n_i \varepsilon_i \quad (\varepsilon_i \in [-3, +3]) \quad (43)$$

where $n_i = 0, 1, 2$ are the occupation numbers, ε_i the orbital energy for Hückel orbital i, and the last term comes from subtracting the non-resonant ethene value (single double bond). This gives $E_{HRS} = 33.161\beta$ for C_{60}. Per π-electron this gives a resonance energy of 0.5527β much higher compared to benzene with exactly $\beta/3$. This should indicate that C_{60} is more aromatic than benzene, which has been a matter of some debate in the past (see the review by Bühl and Hirsch[223]). The problem is that the π-overlap in non-planar systems is not ideal and there is substantial mixing (hybridization) with the p_σ orbitals of carbon, thus questioning the σ-π-separability in Hückel theory. Hence there should be a correction accounting for the curvature at each carbon atom. Such curvature corrections, for example through using the π-orbital axis vector method (POAV), have been considered before

FIGURE 21 | The stability of fullerenes C_N in comparison to C_{60} obtained from density functional calculations up to the graphene limit ($N \to \infty$). Topological stability indices from resonance energies[222] (TRE using $\beta = -216$ kcal/mol) or ring patterns by Alcami[32] and Cioslowski[33] are also shown. The graphene limit is estimated from the heat of formation of C_{60}.[185]
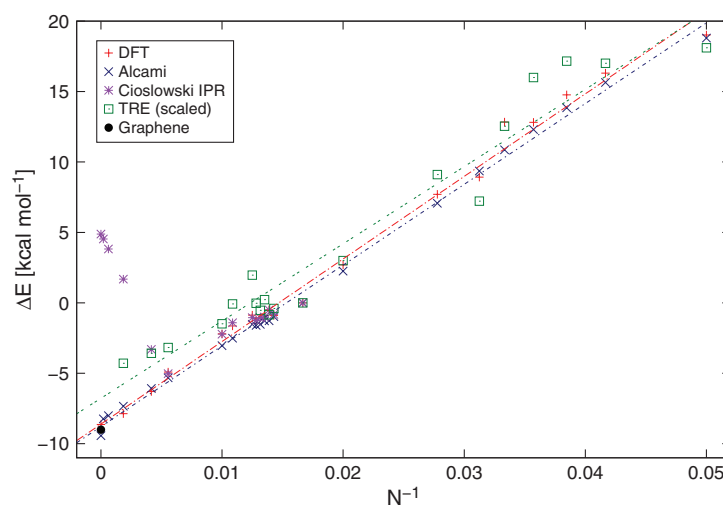
with some success,[224,225] and the different approaches are discussed in detail by Bakowies and Thiel.[226] For example, Haddon et al. showed that C_{240} is significantly more stable than C_{60},[225] which is indeed the case as Figure 21 shows. Clearly, as the fullerene system becomes larger, the curvature term becomes smaller. Moreover, for similar shaped fullerenes the Hückel resonance energy might still be a good approximation. Indeed, as Table 4 for C_{80} shows, the first two isomers are the most stable ones predicted by the simple Hückel resonance energy term in agreement with DFT calculations, and isomer 7 is the least stable one. The Hückel method only requires a diagonalization of the adjacency matrix, and for obtaining bond orders and resonance energies it is computationally more efficient than sorting out Kekulé structures.

We mention that the Hückel spectrum $\{\varepsilon_i\}$ for fullerenes shows some interesting mathematical properties.[227,228] The largest eigenvalue (which translates into the lowest occupied level as the resonance integral β is negative) in a fullerene is always $\varepsilon_{max} = +3$. The smallest eigenvalue (highest unoccupied level) is largest for C_{20} with $\varepsilon_{min} = -\sqrt{5}$, and for the IPR isomers C_{60} we have $\varepsilon_{min} = -\left(1+\sqrt{5}\right)^2/4$. As a geometric consequence, the famous golden ratio $\left(1+\sqrt{5}\right)/2$ appears here as it does in the volume and surface area calculations discussed above. We also mention that in general, different graphs can have the same Hückel spectrum,[229] and this is the case also for fullerenes: the eigenvalues do not uniquely determine the fullerene graph.[108]

It is well known that the Hückel scheme for canonical resonance structures is of rather limited use, and Aihara[230] and Gutman et al.[231] therefore introduced a different reference system by defining the topological resonance energy (TRE) for a graph G as

$$\Delta E^{TRE}(G) = E^\pi(G) - E^{MP}(G) \qquad (44)$$

where the reference energy $E^{MP}(G)$ is the sum of all roots given by the *matching polynomial*, which for a fullerene is

$$P^{MP}(G) = \sum_{k=0}^{N/2} (-1)^k c(G,k) x^{N-2k} \quad \left(c^{MP}(G,k) \in \mathbb{Z}\right) \qquad (45)$$

Here the polynomial coefficients $c(G,k)$ define the number of ways of choosing k non-adjacent edges from the graph G. Balasubramanian gave polynomial coefficients $c(G,k)$ for a number of fullerenes up to C_{50},[232] Babić determined the

coefficients for C_{70},[216] and Salvador for C_{60} and C_{70} to C_{100}.[233] The first few polynomial coefficients are known as they are independent of the isomers for a specific vertex count, that is, $c(G,0) = 1$, $c(G,1) = -3N/2$, $c(G,2) = 3N(3N-10)/8$, $c(G,3) = -(9N^3 - 90N^2 + 232N)/16$.[232] The last coefficient $c(G, N/2)$ is just the number of perfect matchings in the graph. The computation of these coefficients soon becomes computationally intractable.[233] Babić et al. found, however, a good correlation between E^{MP} and E^π values for fullerenes, and the E^π value suffices to calculate the topological resonance energy approximately as (in units of β),[222]

$$\Delta E^{TRE} = 1.024296 E^\pi - 1.512148N \qquad (46)$$

In order to give reasonable results for the isodesmic reaction energy (Eq 41), a rather low value of $\beta = -216$ kcal/mol has to be applied. This scaled TRE plot is shown in Figure 21, which is in reasonable agreement with the results obtained from DFT calculations.

The five or six Pauling bond orders in a pentagon or hexagon respectively can be added to give the Pauling ring bond order.[234] For C_{60}-I_h this gives 1.40 ($5 \times 11/25$) for a pentagon and 2.16 ($3 \times 11/25 + 3 \times 7/25$) for a hexagon compared to 3.00 for benzene. According to Randić this suggests only moderate aromaticity for C_{60}-I_h.[234] We are not going into the controversy of aromaticity of fullerenes,[235] but refer to a recent paper by Schleyer and co-workers,[236] who find that both C_{20}-I_h and C_{60}-I_h are not spherically π aromatic[237] but spherically π anti-aromatic, which for C_{60} explains the large heat of formation. In this respect it is interesting that Schleyer and co-workers conclude that fullerenes are not highly stable molecules,[236] which perhaps is in line with the data shown in Figure 21 showing no 'magic' stability for C_{60} compared to the other fullerenes. We finally mention that fullerene cage abundance is not only guided by thermodynamics, but mostly by kinetic stability. For example, the relative isomer abundance of fullerenes and carbon nanotubes correlates well with kinetic stability.[238]

Electronic Aspects to Structure and Stability

So far we have discussed topological aspects to determine the structure and stability of fullerenes and basic Hückel theory gives us a first insight into the electronic structure.[239] For example, Fowler and co-workers have shown that leapfrog fullerenes adopt a closed-shell structure,[212,240,241] and have equal numbers of positive and negative eigenvalues.[242]

For a more detailed discussion on this subject see Ref 243. However, as we have already seen, more detailed quantum chemical calculations are required to describe the bonding in fullerenes accurately (see also the work by Thiel and co-workers[244–246]). For example, the IPR isomer C_{80}-C_{2v}(5) shown in Table 4 prefers a triplet ground state (at the DFT-PBE level of theory) contrary to Hückel theory, which predicts a singlet state. This is perhaps not surprising as already Hückel theory predicts a small HOMO/LUMO gap. As the band gap closes further with an increasing number of vertices (see for example the recent paper by Noël et al.[247]), we cannot expect anymore to predict the correct spin ground state from simple topological arguments. Moreover, the system becomes more multi-reference in nature, making even a quantum theoretical treatment difficult. As an example, C_{50}-D_{5h}(271) was investigated by Lu et al. who showed that two singlet states with different HOMO symmetries are quasi-degenerate.[248]

In addition, some fullerenes may undergo first- or second-order Jahn-Teller (JT) distortions (which could, however, be very small and almost undetectable for larger fullerenes), that is, they can distort to subgroups of the ideal point group symmetry given by the fullerene topology.[249,250] For example, C_{20} is well known to distort away from the ideal I_h symmetry, which has led to much discussion and debate over the correct electronic ground state.[251] The JT distortion in C_{20} is a consequence of two electrons being distributed over four energetically degenerate g_u-orbitals, resulting in a rather complicated topology of the JT energy hypersurface.[248,250,252–254] JT distortions for highly symmetric open- or closed-shell fullerenes may require a multi-reference treatment. It is therefore often difficult to predict the correct electronic ground state and corresponding physical point group symmetry of a fullerene.

The Gas Phase Formation of Fullerenes

Since the discovery of fullerenes almost 30 years ago, there has been considerable activity, both from the experimental and theoretical side, to gain a detailed understanding of fullerene formation in the gas phase. However, the formation mechanism and especially the high yield of C_{60}-I_h and C_{70}-D_{5h} remains elusive and somewhat controversial.

Fullerenes can be produced by (a) evaporating a carbon target (graphite, amorphous carbon, fullerenes), optionally with addition of metal oxides with a laser,[5] (b) an electric arc between carbon electrodes,[9] or (c) by partial combustion of carbon rich organic compounds.[255] Each of these methods can be

adjusted by several experimental parameters (gas pressure, carrier gas, rod feeding rate, amount of oxygen, etc., and therefore indirectly the carbon vapor concentration, expansion rate, annealing time, etc.). Furthermore, fullerenes are found in space,[14] at meteor impact sites, after lightnings and bush-fires, and soot from household candles.[99] These conditions are similar in that carbon vapor is formed at very high temperatures with a deficit of possible reactants like oxygen or hydrogen. The distribution of yielded fullerene cage sizes depends on the production method and the above-mentioned experimental parameters; however, C_{60}-I_h and C_{70}-D_{5h} are always among the most abundant species.

A large number of formation mechanisms have been proposed.[99] First, inspired by their resemblance to graphene sheets or nanotubes, it was suggested that graphene curls or nanotubes break apart to form fullerene cages, followed by various bottom-up strategies that suggest the successive addition of faces (party line[256,257], pentagon road[257]) or polyyne rings (ring stacking[258,259]) before the cage is closed, the folding of chains to form a cage (ring fusion zipper[260]), or the growth of already existing cages (fullerene road[261], closed network growth[98]), and many others. The currently most widely accepted mechanism comes from Irle, Zheng, Wang, and Morokuma, and is called the 'shrinking hot giant road'.[99] It is based on the concept of self organizing structures under non-equilibrium conditions, backed by extensive QM/MD simulations.

This mechanism can be divided into five phases: First, linear polyyne chains and cycles form. In the second stage (nucleation), entangled carbon chains rehybridize and form faces. It is to be noted, that pentagons and hexagons are close in energy at the given temperatures,[99] however, smaller and larger faces are formed as well. Third, more carbon dimers attach to the side chains of an existing nucleus (growth), allowing for the formation of additional faces. Fourth, after the formation of sufficiently many faces of sizes <6, the cage may close spontaneously (cage closure), leaving a carbon cage with face sizes not restricted to 5 and 6 and with polyyne side chains attached to it. The final step is the ejection of carbon dimers off side chains and the cage in combination with rapid isomerization of the cage structure resulting in a fullerene without side chains and faces of sizes 5 and 6 only. Fullerenes can not only shrink but also grow in steps of C_2,[95,98,262] and the existence of C_2 and C_3 fragments is backed by spectroscopy.[263] The addition and ejection of small carbon fragments (especially C_2) to and from forming fullerene cages is a fast equilibrium. While the non-cage carbon concentration is high addition prevails; as the carbon vapor

expands ejection begins to dominate.[95] The first four steps are exothermic, while the last step is endothermic but increases the overall entropy.

As shown in Figure 21, large fullerenes are more electronically stable than small ones, with graphene having a lower energy than any fullerene. In an equilibrium one would therefore anticipate the formation of graphene—the formation of strained cages and especially the high yield of C_{60}-I_h and C_{70}-D_{5h} require further explanation. The experimental conditions of the cooling and expanding carbon vapor are, however, far from an equilibrium, and the whole formation must be understood as a process of self-organization that is governed by kinetics more so than thermodynamics. Once fullerenes have formed they are subject to restricted equilibration only. Curl et al. have shown numerically that exchange of carbon dimers between existing cages is sufficient to explain the high yield of C_{60}-I_h and C_{70}-D_{5h} as well as a broad distribution of larger cages.[264] They show, that the driving forces for the C_2 exchange are the energy difference between C_N and $C_{N\pm2}$ and the high stability of C_{60}-I_h and C_{70}-D_{5h} relative to their isomers rather than entropy; even at 4000 K entropic effects are not strong enough to explain the existence of small cages.[264]

The experimental observation of endohedral metallofullerenes supports a top-down formation mechanism in two ways: As any enclosed fragments need to enter the cage before it is closed, fullerenes containing fragments that use up most of the space available in the carbon cage must either be formed top down or their existence implies the breaking and reformation of carbon bonds to open and close the cage after it was formed. Secondly, enclosed metal fragments may stabilize otherwise unstable fullerenes: Zhang et al.[265] report the finding of non-IPR $M_2C_2@C_{84}$(51383), which they interpret to be a missing link in the top-down road, and which would have ejected further C_2 fragments without the stabilizing metal carbide.

How Much Space Is Inside a Fullerene? Endohedral Fullerenes and Buckyonions

We consider only topological aspects here as there are several reviews on the chemistry of endohedral fullerenes available.[22,266,267] We only note that endohedral enclosure can change the stability between different isomers.[268] For example, $Tb_3N@C_{84}$ has been isolated and shows one fused pentagon pair.[269] Rodríguez-Fortea et al. argued that if the enclosed metal atom or cluster donates electrons to the fullerene cage, the negative charge resides mostly at the pentagons.[270] As this creates a Coulomb repulsion between the pentagons, one can introduce the inverse pentagon separation index (IPSI),

$$IPSI = \sum_{i=1}^{12} \sum_{j>i}^{12} R_{ij}^{-1} \qquad (47)$$

with R_{ij} being the Euclidian distance between the pentagons (although the topological distance might be used instead). Small IPSI-values are preferred[270] as these correspond to a small Coulomb repulsion.

It is clear that the cavity in the fullerene cage should be large enough to encapsulate atoms, molecules, or even smaller fullerenes.[22,271–282] The size of the cavity can be estimated from fitting shapes such as spheres or ellipsoids inside a fullerene cage as discussed above.

Conversely to the minimum covering sphere problem (MCS), we wish to find the largest sphere that is fully contained *within* the polyhedron. This is called the *maximal inscribed sphere* (MIS), or simply *inscribed sphere*, and its radius for a given polyhedron P is

$$R_{MIS} = \max_{\vec{c}_{MIS}} \min_{\vec{x} \in P} \| \vec{x} - \vec{c}_{MIS} \| \qquad (48)$$

where $\vec{c}_{MIS}$ is constrained to the points interior to P. In the case of convex polyhedra, the MIS is unique, and can be computed directly by finding the Chebyshev centre of the polyhedron.[283] The inscribed radius is then determined by a linear programming problem. However, in the non-convex case, the MIS is no longer unique: Consider two overlapping circles in 2D space with the points lying on these circles. We now have two equivalent possibilities for placing our inner circle. The same argument holds for peanut-shaped fulleroids, which are introduced in the last chapter. Hence, in the non-convex case, we only search for *one* of the possibly many largest spheres contained entirely inside the polyhedron, giving us a numerical optimization problem.

Once the MIS has been obtained, we can estimate whether an atom or molecule fits inside the fullerene without coming close to the repulsive wall of the fullerene cage. For example, the space available inside C_{60}-I_h is roughly $R_{MIS}(C_{60}) - R_{VdW}(C) \approx 3.550 - 1.415$ Å $= 2.135$ Å. If we compare this to the Van der Waals radii for the rare gas atoms, which are 1.40 Å for He, 1.54 Å for Ne, 1.88 Å for Ar, 2.02 Å for Kr, and 2.16 Å for Xe,[284] we see that they all fit into C_{60}-I_h as experimentally already verified[285–291] (even for the borderline case of Xe as theoretical investigations show[292–294]). Even molecules like water fit into C_{60}.[295,296] If we take C_{20} as a endohedral host molecule

we arrive at a different picture as $R_{MIS}(C_{20})$ $- R_{VdW}(C) = 2.040 - 1.415 Å = 0.635 Å$, and even He does not fit anymore into the C_{20} cage.[297,298] We note the important role of dispersion interactions in endohedral fullerenes.[299] Further, C_{60} is a very stiff molecule,[300] and the cage cannot so easily be expanded by endohedral atoms or molecules. In other words, the endohedral system can become repulsive very soon if the size of the endohedral atom or molecule becomes too large.[301]

As a further example we consider *hyperfullerenes* (also called *buckyonions*),[271,272,274,302] that is, fullerenes which contain smaller fullerenes inside their cage. They have already been detected and studied by theoretical methods.[271,272,274,277–280] In a similar way to the rare gas estimates, we can derive approximately the following (conservative) condition for a non-repulsive enclosing hyperfullerene,

$$\Delta R_{N,M} = R_{MIS}\left(C_{N>M}\right) - R_{MCS}\left(C_M\right) - 2R_{VdW}(C) > 0 \quad (49)$$

This only holds for ideal spherical systems, but can be seen as a lower limit for the guest C_M fullerene. For $C_{20}@C_{60}$ we get $\Delta R_{60,20} = (3.553 - 2.084 - 2 \times 1.415)$ Å $= -1.361$ Å and it is therefore predicted to be thermodynamically very unstable. Indeed, DFT(B3LYP) calculations predict $C_{20}@C_{60} \rightarrow C_{20} + C_{60} - 1230$ kcal/mol (−15 kcal/mol per carbon atom), the high energy required to expand the C_{60} cage. In fact, analyzing $C_{20}@C_{60}$ we find that the carbon atoms of C_{20} close bonds with the carbon of the C_{60} cage, that is, the structure should be considered as a carbon cluster rather than a hyperfullerene. Moreover, the volume of $C_{20}@C_{60}$ increases by 22% compared to C_{60}. In contrast, C_{60} fits nicely into C_{240}, and C_{240} just into C_{540} in agreement with the analysis of Bates and Scuseria (see Figure 22).[303] Here we get $\Delta R_{240,60} = 0.583 Å$ and $\Delta R_{540,240} = 0.066 Å$.

The buckyonions, which have been considered in the past, are all Goldberg-Coxeter transforms of C_{20} and have the most spherical appearance as they are of icosahedral symmetry. It has been suggested that the rather high sphericity observed for buckyonions in experiments in contrast to the faceted polyhedral structure predicted (see Figure 22) is due to C_2 removal in a [c5666] fragment consisting of 1 pentagon and 3 hexagons (notation of Figure 16 is used here) introducing one heptagon and an additional pentagon, that is, [l575].[303] As heptagons introduce local negative Gaussian curvature (see discussion below), the fragment flattens out and the buckyonion becomes more spherical in shape.[303]
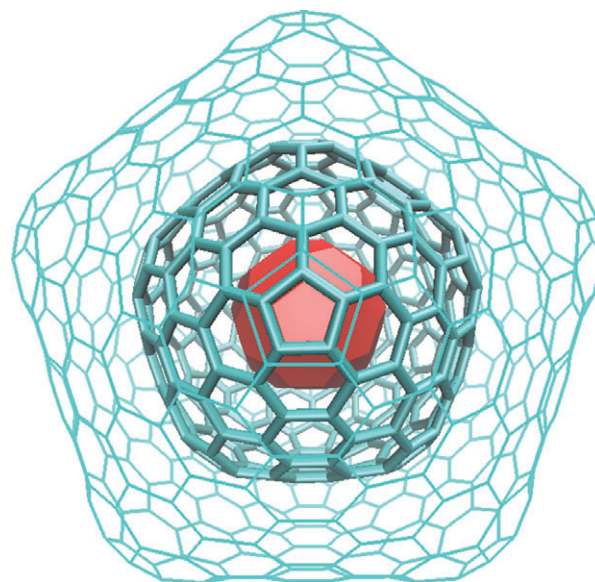

FIGURE 22 | The buckyonion structure $C_{60}@C_{240}@C_{540}$.

For the buckonions one can establish a simple relationship between the number of vertices $N > M$ of the buckyonions $C_M@C_N$. As $R \sim \sqrt{N}$ (R being the radius of the cage), an analysis of $GC_{k,l}$-transforms of fullerenes up to $k = 6$ shows that $R_{MIS} \approx 0.424\sqrt{M}$ Å. This gives a very simple estimate from Eq (49) for such fullerenes,

$$\sqrt{N} \gtrsim 6.68 + \sqrt{M} \quad (N > M) \quad (50)$$

and we see that this is fulfilled for the cases already discussed, and for the largest buckyonion $C_{60}@C_{240}@C_{540}@C_{960}@C_{1500}$ considered by Bates and Scuseria.[303] In fact, Casella et al. recently showed by using dispersion corrected DFT that the formation of $C_{60}@C_{180}$ from the two fullerenes is endothermic while $C_{60}@C_{240}$ is exothermic, and in the latter case only because dispersion interactions have been accounted for.[304] We finally note that (possibly damaged) buckyonions are the main product in most gas phase fullerene generation procedures.[262]

Weird Fulleroidal Shapes: Generalizing Fullerene Structures

Finally, what happens if we relax the rules a little bit, and allow for other types of three-valent (sp²) carbon frameworks? There are many generalizations that lead to structures of beautiful shapes that have both elegant mathematical theory and physical realizations: allowing for polygons with faces different from pentagons and hexagons; for surfaces other than a sphere (genus 0), such as a *torus* (genus 1), a *Klein bottle* or a *double*

torus (genus 2); negatively curved *Mackay-Terrones* or *Vanderbilt-Tersoff* surfaces; etc.[121,242,305–309]

We will discuss mainly two types of carbon frameworks: fulleroids, which are fullerene-like structures, and Schwarzites, which are periodic negative-curvature surfaces. Different authors employ a wide range of working definitions for fulleroids. We advocate the following definition, generalizing fullerenes: A *fulleroid* graph is a three-connected trivalent polyhedral graph. The definition is identical to that of fullerenes, except that there is no restriction on face sizes. Hence, a fullerene is a fulleroid with only pentagon and hexagon faces. We further generalize to *genus-n fulleroids*, abbreviated G_n-fulleroids, defined as the three-connected trivalent genus-*n* graphs.

What kind of fulleroids are allowed? Can we tile a sphere or a torus with heptagons only (the answer is no), or with only pentagons and heptagons? (the answer is yes, with the right number.) And how can we construct such fulleroids?[310] In order to answer these questions, we need to generalize Euler's equation to the *Euler-Poincaré polyhedral formula* for orientable[l] surfaces,

$$N - E + F = 2(1 - g) = \chi \qquad (51)$$

where g is the genus of the graph,[m] and the corresponding value χ is called the *Euler characteristic*.[39] The Klein bottle is a non-orientable surface (like the Möbius strip), and the corresponding (non-orientable) genus is $g' = 2$ with an Euler characteristic of $\chi = 0$ (here we take $\chi = 2 - g'$ instead).

What happens when we allow vertex degrees $r > 3$? Consider a possibly irregular genus-*n* graph with N vertices. Let N_r be the number of vertices with degree r, and F_n be the number of *n*-gonal faces. Then we trivially have

$$F = \sum_n F_n, \quad N = \sum_r N_r, \quad \text{and} \quad 2E = \sum_n nF_n = \sum_r rN_r \qquad (52)$$

Combining this with the Euler-Poincaré polyhedral formula, we obtain

$$2\sum_{r \geq 3}(3 - r)N_r + \sum_{n \geq 3}(6 - n)F_n = 12(1 - g) = 6\chi \qquad (53)$$

If we only allow for three-valent graphs (fulleroids), the first term on the left hand side of Eq (53) conveniently vanishes (hence their special place in graph theory). This gives,[311]

$$3F_3 + 2F_4 + F_5 + \sum_{n \geq 7}(6 - n)F_n = 12(1 - g) = 6\chi \qquad (54)$$

From this equation we make a number of observations. a) We can play with as many hexagons as we want to build fullerenes or fulleroids, but the number of *n*-gons with $n \neq 6$ is limited by Eq (54) or (53). b) While both equations allow for a large variety of face combinations, certain combinations are not allowed. The hand-shaking lemma (last formula in Eq (52)) allows only for an even number of vertices. We already know that there exist no polyhedral structures of the type $C_{22}[5,6]$. To give another example, for $C_N[5,7]$ polyhedra with pentagons and heptagons only (no hexagons) one requires at least two heptagons since, analogous to C_{22}, the combination of 13 pentagons and one heptagon is not valid despite being allowed by Euler's formula. Because of this, the smallest [5,7]-fulleroid is C_{28}-D_{7d} with 14 pentagons and 2 heptagons, as shown in Figure 23.[n] Structures containing only one heptagon are not forbidden, however, but requires introducing hexagons to form $C_N[5,6,7]$-structures. These can be obtained by replacing a [c5666] fragment by [l575],[303] and can even be energetically favorable. For example, Fowler and co-workers showed that C_{62} consisting of one heptagon, 13 pentagon, and 19 hexagon faces is of lower energy than all the 2385 regular fullerene
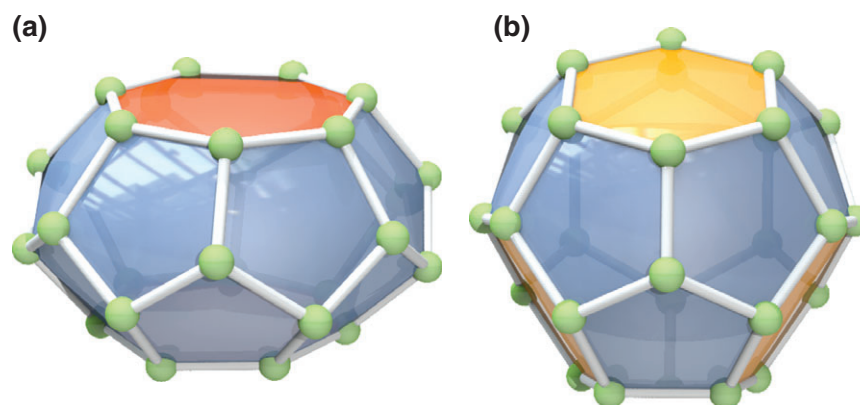

(a)   **(b)**

FIGURE 23 | $C_{28}[5,7]$-D_{7d}, the smallest fulleroid with heptagon extension, compared to the most stable (by $\Delta E = -102$ kcal/mol) C_{28}-$T_d[5,6]$ fullerene isomer.

isomers of C_{62}.[312] c) For cubic planar graphs with only one type of face we get $F_3 = 4$ (tetrahedron), $F_4 = 6$ (cube), and $F_5 = 12$ (dodecahedron), which are the three three-valent polyhedra of the five *Platonic Solids*, the other two, the octahedron and icosahedron, require $r = 4$ and $r = 5$, respectively, in Eq (53); d) If we allow for two different *n*-gons, we arrive at the 13 *Archimedean solids* including our famous buckyball C_{60}-I_h. e) Of course, we can tile a surface with triangles and the duals of fulleroids are prime examples, but in order to do this beside the tetrahedron, we must allow for different valencies of the vertices. f) We can tile a toroid ($g = 1$) with hexagons only, consistent with Eq (54), see Figure 24. The torus is the only closed, orientable surface that can be tiled exclusively with hexagons. However, the plane, which is not closed, can be tiled with hexagons as well (graphene), as can the Klein-bottle (which is not orientable). Introducing pentagons into a toroid requires higher *n*-gons such as heptagons, since its total Gaussian curvature must be $2\pi(2 - 2 \cdot 1) = 0$. The Euler-Poincaré's formula allows to introduce pentagons into toroids if we introduce an equal number of heptagons, for example, we can tile a torus exclusively with pentagons and heptagons. Such 'defects' are well known in carbon nanotubes,[313] which can be realized as infinite toroids with $g = 1$ and $\chi = 0$. Tiling in a pattern with alternating pentagons and heptagons yields a toroidal arrangement of azulenes, called azuloids.[314]

A few examples should be mentioned here. The smaller fullerenes ($N < 60$) are not very stable compared to C_{60} because of the energy penalty one has to pay for fusing pentagons. As a result, structures deviating from the classical fullerenes can be more stable energetically or lie close by. For example, for C_{26}, An et al. found six low lying isomers with the lowest structure being the fullerene C_{26}-D_{3h}[5,6], but only 3 kcal/mol lower in energy than the C_{26}-C_s[4,5,6], a fulleroid that contains one square.[315] Some combinations with heptagons

are, however, disfavored energetically. For example, a Stone-Wales transformation^o of four connected hexagons to two pentagons and two heptagons in C_{540}-D_{2h} costs 260 kcal/mol.[317]

Turning to toroidal fulleroids (also called *toroids*) with $g = 1$ and $\chi = 0$, there are different techniques to construct such structures using either combinatorial or geometric approaches.[318–320] Like in the nano-tubes, the hexagons can be oriented in different ways around the torus ring. For example, Figure 24(a) shows hexagons with 1/3 of the edges aligned tangential to the toroidal direction. We could also chose the hexagons to be aligned with 1/3 of the edges perpendicular to the toroidal direction (Figure 24(b)), and similar to nanotubes there are also chiral alignments depending on the chirality vector. Kirby and Pisanski showed how 2D graph drawings of toroids can be obtained.[314] Borštnik and Lukman[321] as well as Diudea and Kirby[322] considered the structure and stability of such toroids using simple molecular mechanics. Faghani analyzed the symmetry of toroidal fulleroids.[126] Kang analyzed the band gap in such toroids by graph theoretical means.[323] Deza et al. pointed out that leapfrog toroids and Klein-bottles have equal numbers of positive and negative eigenvalues, but with 4 and 2 eigenvalues being zero respectively.[242] Interestingly, the leapfrog transformation performed on toroids (such as the one shown in Figure 24) results in an open shell toroid.[324]

As discussed earlier, the positive curvature in fullerenes originate from the pentagons, because sheets of hexagons like to be planar. Introducing heptagons or even octagons into a fullerene requires additional faces of size less than 6 to outweigh them, and results in a highly non-convex structure with often strong negative local Gaussian curvature,[325] introducing a saddle-type topology to the structure. Two examples of such fulleroids are shown in Figure 25. In this figure, every patch consisting of a pentagon surrounded by hexagons is replaced by six pentagons surrounded by
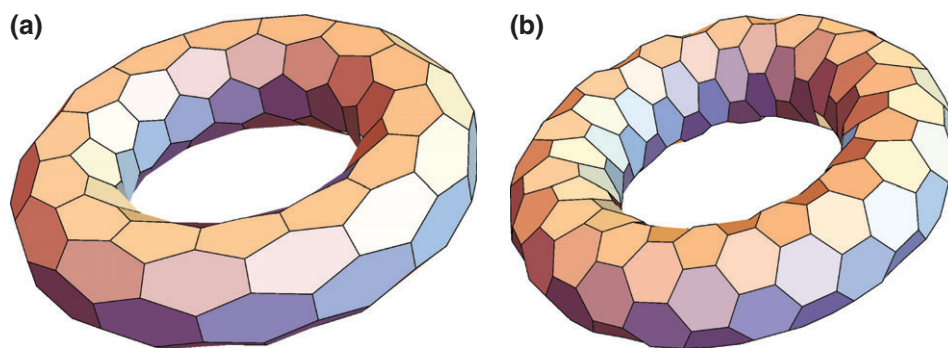
(a)   **(b)**

FIGURE 24 | Torus consisting of hexagons only with 1/3 of the edges tangential (a) and perpendicular (b) to the toroidal direction.
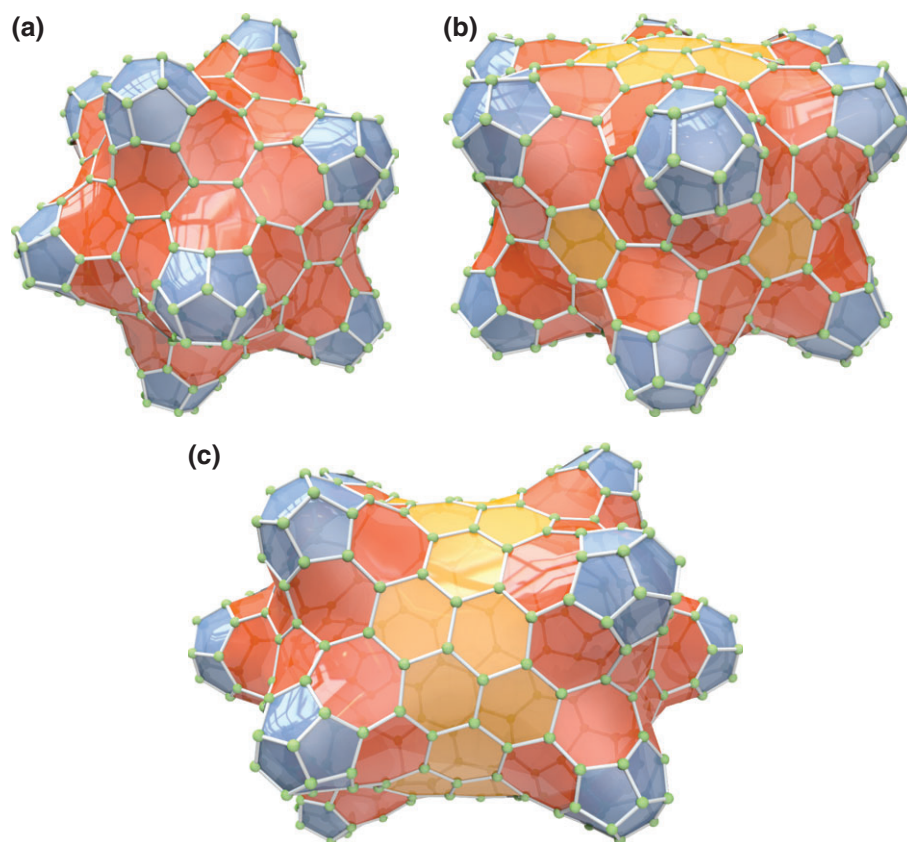
FIGURE 25 | Spiky fulleroids with negative curvature containing heptagons derived from fullerenes through patch replacement. (a) C_{260}-I[5, 7] fulleroid derived from C_{140}-I. (b) C_{300}-D_{6h}[5, 6, 7] derived from C_{180}-D_{6h}. (c) C_{310}-D_{5h}[5, 6, 7] derived from C_{190}-D_{5h}.
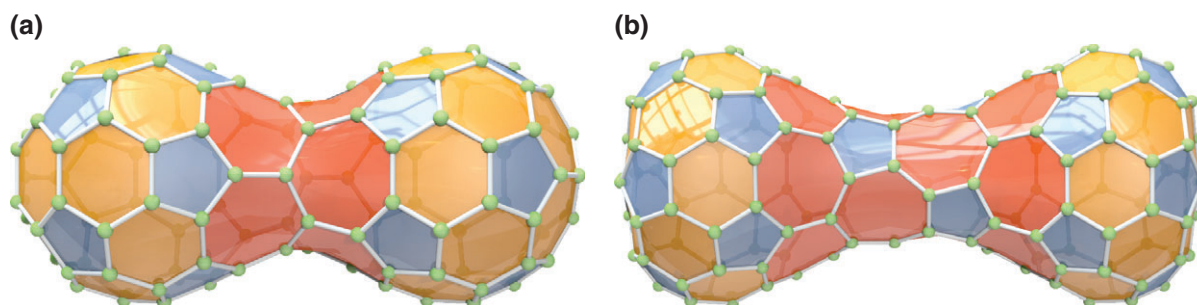

FIGURE 26 | Peanut shaped fulleroids. (a) C_{120}-D_{5d}[5, 6, 7] with 10 heptagons and 22 pentagons. (b) C_{168}-D_{3d}[5, 6, 7] with 18 heptagons and 30 pentagons.

five heptagons, for three different fullerenes, yielding characteristic 'spiky' fulleroids. In Figure 26, heptagons are introduced in a fashion that leads to peanut shaped fulleroids,[326] and in fact, many types of interesting shapes can be constructed.

More interesting fulleroid shapes can be found in a recent paper by Diudea et al.[327] Negatively curved fulleroids of higher genus (so-called perforated fullerenes) have been explored by Terrones and Terrones,[328] who studied their electronic structures.[329] Under specific conditions fullerenes can be combined

by coalescence, forming larger carbon structures such as deformed nano-tubes or nano-peapods.[330] For an overview of such carbon nano-peapods see Ref 331.

Structures of negatively curved graphitic carbon, which can be periodically extended to a lattice, have been proposed in 1991 by Mckay and Terrones,[305] and subsequently explored by experiment.[332–335] These so-called 'spongy' carbon frameworks or *Schwarzites* are named in honor of the mathematician Hermann Schwarz (1843–1921), who investigated minimal surfaces with zero mean Gaussian
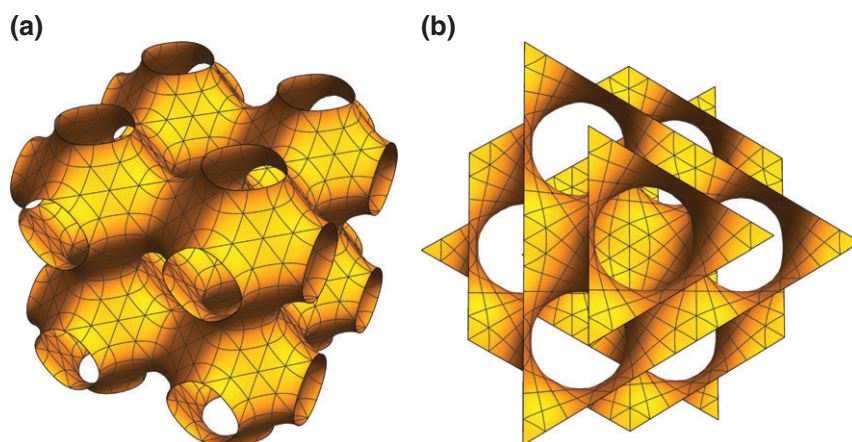
(a)   **(b)**

FIGURE 27 | Periodic P-type (a) and D-type (b) Schwarzite surfaces.

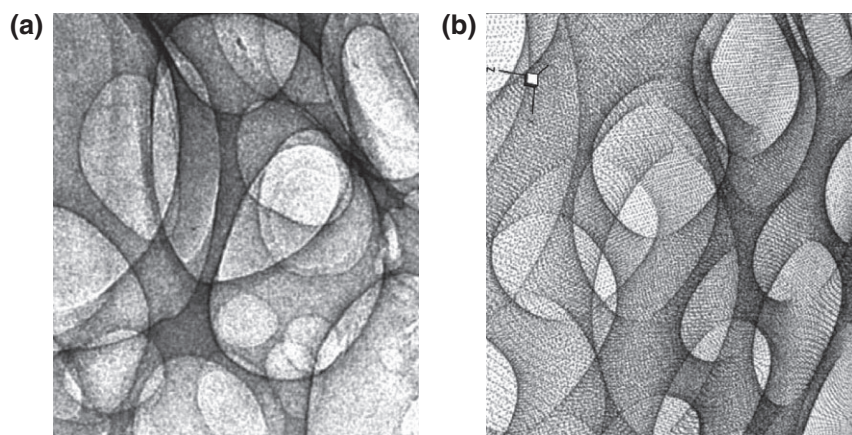**(a)**   **(b)**

FIGURE 28 | Comparison between a small portion of a TEM image of a P-type Schwarzite and the surface described by Eq (55) projected onto a plane normal to the *z*-direction (see Ref 333 for details). (Copyright © 2013 AIP Publishing LLC)

curvature.[336] Schwarzites are structures containing (beside hexagons) heptagons and/or octagons and are of genus $g \geq 3$. These Schwarzites can be periodically continued through so-called junctions as shown in Figure 27 for the case $g = 3$ (Figure 27(a)). The two structures in Figure 27 are termed P-type and D-type, and can be approximately represented by the simple formulae derived from the Weierstrass-Enneper parameterization for minimal surfaces,[337]

$$\cos(x) + \cos(y) + \cos(z) = 0 \quad (P - type) \quad (55)$$

$$\sin(x)\sin(y)\sin(z) + \sin(x)\cos(y)\cos(z)$$
$$+ \cos(x)\sin(y)\cos(z)$$
$$+ \cos(x)\cos(y)\sin(z) = 0 \quad (D - type) \quad (56)$$

Relevant reviews on such minimal surface carbon networks have been given by Terrones and Mackay[311] and by Terrones and Terrones.[338]

Lenosky et al. have performed local density functional calculations for two different $g = 3$ periodic Schwarzite structures with 216 atoms and a tessellation of hexagons and 24 heptagons within the unit

cell.[339] The vertices on such surfaces can be obtained through the Weierstrass representation.[340,341] These calculations reveal a higher thermodynamic stability compared to C_{60}, but not surprisingly lower compared to the graphene sheet (or graphite). D-type Schwarzites have the structure of a 'diamond shaped' lattice so that the unit cell can be split into two identical elements having 12 heptagons each, whereas P-type Schwarzites have the structure of a simple cubic lattice (see Figure 27). In principle, Schwarzites can be associated to any kind of lattice, either periodic or amorphous, the latter are realized in so-called random Schwarzites observed experimentally.[332–335] Such random Schwarzites show rather nice transmission electron microscope (TEM) images (Figure 28) rather different to periodic Schwarzites. A recent comprehensive review over experimental and theoretical studies on Schwarzites has been given by Benedek et al.[335]

Finally, we consider non-cubic (*n*-valent) polyhedral structures. In chemistry this is realized by using elements from the periodic table which can share more (or less) than three bonds with its neighbors. Prime examples are all-boron 'fullerenes',[342] gaudiene C_{72}-O_h (with two- and three-valent carbon as analogs
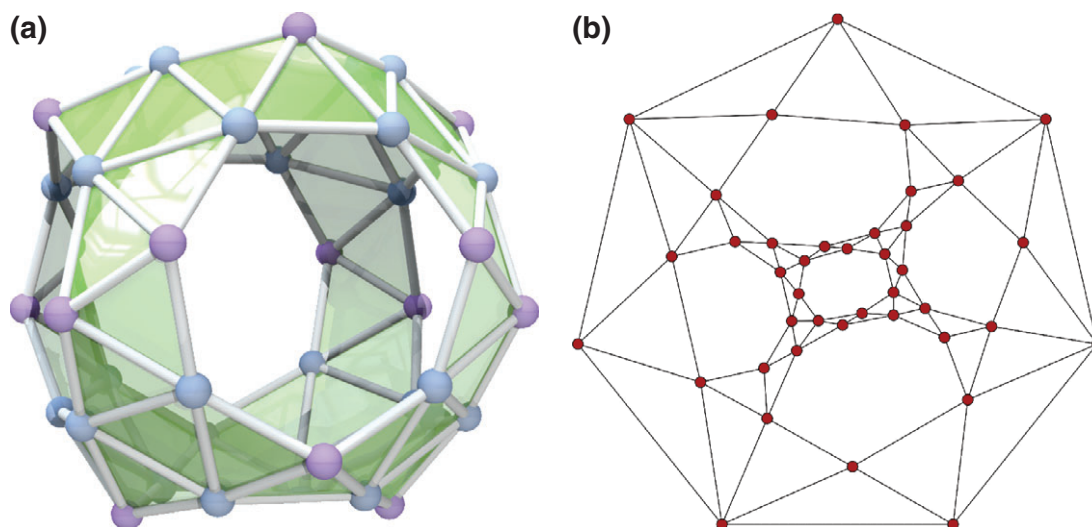
(a)

(b)

FIGURE 29 | All boron fullerene B_{40} (adapted from Ref 350). (a) 3D structure; (b) 2D graph.

to graphyne),[343,344] and golden 'fullerenes'[345−348] (we shall call these structures polyhedral molecules rather than fullerenes). For example, Au_{32} and Au_{72} are a triangulated surfaces of icosahedral symmetry.[346−348] It is well known that small gold clusters adopt 2D structures with the most coordinated gold atom having a valency of six.[349] Extended to infinity, this gives the dual structure of a graphene sheet, that is a triangulation of the plane with vertices of degree six (see Figure 9). In complete analogy to the fullerenes, golden 'fullerenes' are the duals of fullerene structures, for example, Au_{32}-I_h is the dual of C_{60}-I_h, Au_{42}-I is the dual of C_{80}-I, and Au_{72}-I is the dual of C_{140}-I (the Goldberg-Coxeter transform of C_{20} with $k = 2$ and $l = 1$). We may ask how many possible isomers are there for Au_{72}? Since the mapping from the fullerene isomer space into the dual space is bijective, there are as many isomers for Au_{72} as there are for C_{140}, and there are 7,341,204 of these. The stability of these structures have not been explored yet! A smaller dual-type golden fullerene structure, Au_{16}^{-}, has been observed spectroscopically by Bulusu et al.[345] Here the fullerene analog is C_{28}, where we have only two isomers, of T_d and D_2 symmetry. Only the Au_{16}^{-}-T_d structure has been investigated presently.

As a second example, the all-boron B_{40} fullerene has been identified by photoelectron spectroscopy only very recently by Wang and co-workers (as the anionic species B_{40}^{-}),[350] consisting of 4 heptagons, 2 hexagons, and 48 triangles (see Figure 29). In this intriguing new polyhedral structure the vertices are of degrees 4 and 5. To be more precise, we have $F_3 = 48$, $F_6 = 2$, $F_7 = 4$, $N_4 = 16$, $N_5 = 24$ for B_{40}, which gives according to Eq (52) $E = 92$ for the number of edges.

CONCLUSIONS

To review the many developments in the topology and graph theory of fullerenes or fulleroids would be a monumental task. We have only outlined a few important concepts in order to give the reader a good introduction into this exciting field. There is certainly the need of a more comprehensive review or book. Nevertheless, we hope to have shown that the interplay between mathematics and structural chemistry is both interesting, rich and well alive. As more sophisticated method in the synthesis of carbon and other materials become available, we hope that some of the exotic, but very beautiful, structures become accessible with many useful applications in chemistry and materials science.

NOTES

[a] If we grow Goldberg-Coxeter transforms of C_{20} to infinity we obtain spherical graphene sheets connected by 12 pentagons. For definitions see below.

[b] An interesting side aspect is that fullerene-like shapes are realized also in viral shapes.[20]

[c] Most of the useful graph theoretical and topological aspects discussed here are implemented into a Fortran/C++ program called *Fullerene*, an open-source code freely available at the Massey University website.[35]

[d] The embedding is unique in the following sense: All the planar embeddings of a three-connected graph are topologically equivalent, which means that they can be continuously deformed into each other without crossing any edges. Consequently, every planar embedding of such a graph defines the same set of faces. The converse it true as well: only three-connected graphs have this property.

e Fulleroids are cubic graph fullerene-like structures where we allow also for other polygons than pentagons or hexagons.

f In the mathematical sense that they are dense in this set, i.e. any smooth non-negative curvature genus 0 surface is the limit of a sequence of genus 0 triangulations with vertex degree six and less.

g The interested reader is directed to the Gauss-Bonnet theorem, which generalizes Euler's theorem to arbitrary Riemann surfaces. In the discrete case they are the same, except that Gauss-Bonnet is stated in terms of the Gaussian curvature. From this identification, we can see that every n-gon, or vertex of degree n in the dual, contributes the angle $2\pi(6-n)/6$ to the Gaussian curvature, which must sum to $2\pi(2-2g)$, where g is the surface's genus.

h When there are multiple exponentially crowded centers, the Tutte-embedding is still guaranteed planar, but the mapping to the sphere can have crossings. In practice, however, it turns out to not matter.

i Counting perfect matchings for general graphs is #P-complete. #P is the complexity class of counting solutions for decision problems in NP. While only exponential algorithms exist both for NP-complete and #P-complete problems, in practice #P-complete problems are dramatically harder than NP-complete.

j It is known that not all connected cubic planar graphs are Hamiltonian, and that it is an NP-complete problem to determine whether any one cubic planar graph admits a Hamilton cycle. However, it is a long standing but yet unproven conjecture that *fullerene* graphs, a small subset of the cubic planar graphs, are all Hamiltonian. It has been verified by Brinkmann, Goedgebeur, and McKay for all 2.4×10^{11} fullerene isomers up to C_{316}.[75] In Schwerdtfeger et al. (unpublished manuscript), we investigate in detail the Hamiltonian cycle counts admitted by fullerene graphs.

k hentriacontacyclo[$29.29.0.0^{2,14}.0^{3,12}.0^{4,59}.0^{5,10}.0^{6,58}$ $.0^{7,55}.0^{8,53}.0^{9,21}.0^{11,20}.0^{13,18}.0^{15,30}.0^{16,28}.0^{17,25}.0^{19,24}$ $.0^{22,52}.0^{23,50}.0^{26,49}.0^{27,47}.0^{29,45}.0^{32,44}.0^{33,60}.0^{34,57}$ $.0^{35,43}.0^{36,56}.0^{37,41}.0^{38,54}.0^{39,51}.0^{40,48}.0^{42,46}$]hexaconta$-1, 3, (10), 6, 8, 11, 13(18), 14, 16, 19, 21, 23, 25, 27, 29(45), 30, 32(44), 33, 35(43), 36, 38(54), 39 (51), 40(48), 41, 46, 49, 52, 55, 57, 59 -$triacontaene.

l Orientability is a property of a surface in Euclidean space describing whether it is possible to make a consistent choice of a surface normal vector at every point.

m The genus of a connected and orientable surface is the maximum number of possible cuttings along non-intersecting closed simple curves such that the surface is still connected.

n Fulleroids may in general have point group symmetries not admissible to the regular fullerenes.

o There are many other operations which can be performed on polyhedra resulting in transformed fullerenes or fulleroids, see the review by Vizitiu and Diudea.[316]

ACKNOWLEDGMENTS

REFERENCES

1. Ōsawa E. Superaromaticity. *Kagaku (Chem)* 1970, 25:854–863.

2. Ōsawa E, Kroto HW, Fowler PW, Wasserman E. The evolution of the football structure for the C_{60} molecule: a retrospective [and discussion]. *Phil Trans R Soc Lond A* 1993, 343:1–8. doi: 10.1098/rsta.1993.0035.

3. Bochvar DA, Gal'pern EG. Electronic structure of the molecules C_{20} and C_{60}. *Proc Acad Sci SSSR* 1973, 209:239–241.

4. Stankevich I, Nikerov M, Bochvar D. Structural chemistry of crystalline carbon: geometry, stability, electronic spectrum. *Russ Chem Rev* 1984, 53:640–655. doi: 10.1070/RC1984v053n07ABEH003084.

5. Kroto HW, Heath JR, O'Brien SC, Curl RF, Smalley RE. C_{60}: Buckminsterfullerene. *Nature* 1985, 318:162–163. doi: 10.1038/318162a0.

6. Kroto HW. C_{60}: Buckminsterfullerene, the celestial sphere that fell to earth. *Angew Chem Int Ed* 1992, 31:111–129. doi: 10.1002/anie.199201113.

7. Hare JP, Kroto HW. A postbuckminsterfullerene view of carbon in the galaxy. *Acc Chem Res* 1992, 25:106–112. doi: 10.1021/ar00015a002.

8. Kroto H. Symmetry, space, stars, and C_{60} (Nobel lecture). *Angew Chem Int Ed* 1997, 36:1578–1593. doi: 10.1002/anie.199715781.

9. Krätschmer W, Lamb LD, Fostiropoulos K, Huffman DR. Solid C_{60}: a new form of carbon. *Nature* 1990, 347:354–358. doi: 10.1038/347354a0.

10. Mattauch J, Ewald H, Hahn O, Strassmann F. Hat ein Caesium-Isotop langer Halbwertszeit existiert? Ein Beitrag zur Deutung ungewöhnlicher Linien in der Massenspektrographie. *Z Physik* 1943, 120:598–617.

11. Iijima S. Direct observation of the tetrahedral bonding in graphitized carbon black by high resolution electron microscopy. *J Cryst Growth* 1980, 50:675–683. doi: 10.1016/0022-0248(80)90013-5.

12. Buseck PR, Tsipursky SJ, Hettich R. Fullerenes from the geological environment. *Science* 1992, 257:215–217. doi: 10.1126/science.257.5067.215.

13. Cami J, Bernard-Salas J, Peeters E, Malek SE. Detection of C_{60} and C_{70} in a young planetary nebula. *Science* 2010, 329:1180–1182. doi: 10.1126/science.1192035.

14. Berné O, Tielens AGGM. Formation of buckminsterfullerene (C_{60}) in interstellar space. *Proc Natl Acad Sci U S A* 2012, 109:401–406. doi: 10.1073/pnas.1114207108.

15. Schultz HP. Topological organic chemistry. polyhedranes and prismanes. *J Org Chem* 1965, 30:1361–1364. doi: 10.1021/jo01016a005.

16. Prinzbach H, Weiler A, Landenberger P, Wahl F, Worth J, Scott LT, Gelmont M, Olevano D, v Issendorff B. Gas-phase production and photoelectron spectroscopy of the smallest fullerene C_{20}. *Nature* 2000, 407:60–63. doi: 10.1038/35024037.

17. Sutton D. *Platonic and Archimedean Solids*. New York: Wooden Books; 2002.

18. Kroto HW. The stability of the fullerenes C_n, with n = 24, 28, 32, 36, 50, 60 and 70. *Nature* 1987, 329:529–531. doi: 10.1038/329529a0.

19. Thurston WP. Shapes of polyhedra and triangulations of the sphere. *Geo Topol Mono* 1998, 1:511–549.

20. Zhao G, Perilla JR, Yufenyuy EL, Meng X, Chen B, Ning J, Ahn J, Gronenborn AM, Schulten K, Aiken C, et al. Mature HIV-1 capsid structure by cryo-electron microscopy and all-atom molecular dynamics. *Nature* 2013, 497:643–646. doi: 10.1038/nature12162.

21. Tagmatarchis N, Okada K, Tomiyama T, Yoshida T, Kobayashi Y, Shinohara H. A catalytic synthesis and structural characterization of a new [84]fullerene isomer. *Chem Commun* 2001, 1366–1367. doi: 10.1039/B103679N.

22. Popov AA, Yang S, Dunsch L. Endohedral fullerenes. *Chem Rev* 2013, 113:5989–6113. doi: 10.1021/cr300297r.

23. Yamada M, Akasaka T, Nagase S. Carbene additions to fullerenes. *Chem Rev* 2013, 113:7209–7264. doi: 10.1021/cr3004955.

24. Franco JU, Hammons JC, Rios D, Olmstead MM. New tetraazaannulene hosts for fullerenes. *Inorg Chem* 2010, 49:5120–5125. doi: 10.1021/ic1002513.

25. York APE. Inorganic fullerenes, onions, and tubes. *J Chem Educ* 2004, 81:673. doi: 10.1021/ed081p673.

26. Scott LT, Boorum MM, McMahon BJ, Hagen S, Mack J, Blank J, Wegner H, de Meijere A. A rational chemical synthesis of C_{60}. *Science* 2002, 295:1500–1503. doi: 10.1126/science.1068427.

27. Kabdulov M, Jansen M, Amsharov KY. Bottom-up C_{60} fullerene construction from a fluorinated $C_{60}H_{21}F_9$ precursor by laser-induced tandem cyclization. *Chem Eur J* 2013, 19:17262–17266. doi: 10.1002/chem.201303838.

28. Cioslowski J. *Electronic Structure Calculations on Fullerenes and Their Derivatives*. New York: Wooden Books; 1995.

29. Balaban AT, Liu X, Klein DJ, Babić D, Schmalz TG, Seitz WA, Randic M. Graph invariants for fullerenes. *J Chem Inf Comput Sci* 1995, 35:396–404. doi: 10.1021/ci00025a007.

30. Zhu HY, Klein DJ. Graph-geometric invariants for molecular structures. *J Chem Inf Comput Sci* 1996, 36:1067–1075. doi: 10.1021/ci960025a.

31. Fowler PW, Manolopoulos DE. *An Atlas of Fullerenes*. 2nd ed. Mineola, NY: Dover Publications Inc.; 2006.

32. Alcamí M, Sánchez G, Díaz-Tendero S, Wang Y, Martín F. Structural patterns in fullerenes showing adjacent pentagons: C_{20} to C_{72}. *J Nanosci Nanotechnol* 2007, 7:1329–1338. doi: 10.1166/jnn.2007.311.

33. Cioslowski J, Rao N, Moncrieff D. Standard enthalpies of formation of fullerenes and their dependence on structural motifs. *J Am Chem Soc* 2000, 122:8265–8270. doi: 10.1021/ja001109+.

34. Brinkmann G, Goedgebeur J, Mélot H, Coolsaet K. House of graphs: a database of interesting graphs. *Discrete Appl Math* 2013, 161:311–314.

35. Schwerdtfeger P, Wirz L, Avery J. Program fullerene: a software package for constructing and analyzing structures of regular fullerenes. *J Comput Chem* 2013, 34:1508–1526. doi: 10.1002/jcc.23278.

36. Fowler PW. Fullerene stability and structure. *Contemp Phys* 1996, 37:235–247. doi: 10.1080/00107519608217530.

37. Baldridge KK, Siegel JS. Of graphs and graphenes: molecular design and chemical studies of aromatic compounds. *Angew Chem Int Ed* 2013, 52:5436–5438. doi: 10.1002/anie.201300625.

38. Trinajstic N. *Chemical Graph Theory*. Boca Raton, FL: CRC Press; 1983.

39. Kotschik D. The topology and combinatorics of soccer balls. *Am Sci* 2006, 94:350–357. doi: 10.1511/2006.60.1001.

40. Cataldo F, Graovac A, Ori O. *The mathematics and topology of fullerenes*. Berlin: Springer; 2011.

41. Dresselhaus MS, Dresselhaus G, Eklund PC. *Science of Fullerenes and Carbon Nanotubes*. New York: Academic Press; 1995.

42. Curl RF. Dawn of the fullerenes: experiment and conjecture. *Rev Mod Phys* 1997, 69:691–702. doi: 10.1103/RevModPhys.69.691.

43. Kadish KM, Ruoff RS, eds. *Fullerenes: Chemistry, Physics, and Technology*. New York: Wiley-Interscience; 2000.

44. Hirsch A, Brettreich M, Wudl F. *Fullerenes: Chemistry and Reactions*. Weinheim: Wiley-VCH; 2005.

45. Rodríguez-Fortea A, Irle S, Poblet JM. Fullerenes: formation, stability, and reactivity. *WIREs Comput Mol Sci* 2011, 1:350–367. doi: 10.1002/wcms.21.

46. Sheka EF. *Fullerenes: Nanochemistry, Nanomagnetism, Nanomedicine, Nanophotonics*. Boca Radon, FL: CRC Press, Taylor & Francis; 2011.

47. Darwish AD. Fullerenes. *Annu Rep Prog Chem, Sect A Inorg Chem* 2012, 108:464–477. doi: 10.1039/C2IC90017C.

48. Whitney H. Non-separable and planar graphs. *Trans Am Math Soc* 1932, 34:339–362. doi: 10.1090/S0002-9947-1932-1501641-2.

49. Steinitz E. Polyeder und Raumeinteilungen. In: Klein F, Meyer W, eds. *Encyclopädie der mathematischen Wissenschaften*. Geometrie, vol. 3. Leipzig: B.G. Teubner Verlag; 1922, 1–139.

50. Schmalz TG, Seitz WA, Klein DJ, Hite GE. Elemental carbon cages. *J Am Chem Soc* 1988, 110:1113–1127. doi: 10.1021/ja00212a020.

51. Grünbaum G, Motzkin TS. The number of hexagons and the simplicity of geodesics on certain polyhedra. *Can J Math* 1963, 15:744–751. doi: 10.4153/CJM-1963-071-3.

52. Killblane C, Gao Y, Shao N, Zeng XC. Search for lowest-energy nonclassical fullerenes III: C_{22}. *J Phys Chem A* 2009, 113:8839–8844. doi: 10.1021/jp9016745.

53. Janežič D, Miličević A, Nikolić S. Trinajstić N. In: Gutman I, ed. *Graph Theoretical Matrices in Chemistry*. Mathematical Chemistry Monographs, vol. 3. Kragujevac, Serbia: University of Kragujevac; 2007.

54. Tutte WT. How to draw a graph. *Proc Lond Math Soc* 1963, 13:743–767.

55. Brandenburg FJ, Himsolt M, Rohrer C. An experimental comparison of force-directed and randomized graph drawing algorithms. In: Brandenburg FJ, ed. *Graph Drawing*. Lecture Notes in Computer Science, vol. 1027. Berlin Heidelberg: Springer; 1996, 76–87.

56. Fruchterman TMJ, Reingold EM. Graph drawing by force-directed placement. *Softw Pract Exp* 1991, 21:1129–1164. doi: 10.1002/spe.4380211102.

57. Plestenjak B. An algorithm for drawing Schlegel diagrams. Available at: http://www-lp.fmf.uni-lj.si/plestenjak/Papers/NICEGR.pdf 1996, 1–10. (Accessed July 1, 2014)

58. Manolopoulos DE, May JC, Down SE. Theoretical studies of the fullerenes: C_{34} to C_{70}. *Chem Phys Lett* 1991, 181:105–111. doi: 10.1016/0009-2614(91)90340-F.

59. Wirz LN, Avery JE, Schwerdtfeger P. Structure and properties of the non-face-spiral fullerenes T-C_{380}, D_3-C_{384}, D_3-C_{440} and D_3-C_{672} and their halma and leapfrog transforms. *J Chem Inf Model* 2014, 54:121–130. doi: 10.1021/ci4005578.

60. Manolopoulos DE, Fowler PW. A fullerene without a spiral. *Chem Phys Lett* 1993, 204:1–7. doi: 10.1016/0009-2614(93)85597-H.

61. Brinkmann G, Goedgebeur J, McKay BD. The smallest fullerene without a spiral. *Chem Phys Lett* 2012, 522:54–55. doi: 10.1016/j.cplett.2011.11.056.

62. Fowler P, Cremona J. Fullerenes containing fused triples of pentagonal rings. *J Chem Soc Faraday Trans* 1997, 93:2255–2262. doi: 10.1039/A701271C.

63. Yoshida M, Fowler PW. Dihedral fullerenes of three-fold symmetry with and without face spirals. *J Chem Soc Faraday Trans* 1997, 93:3289–3294. doi: 10.1039/A702351K.

64. Brinkmann G, Fowler PW, Yoshida M. New non-spiral fullerenes from old: generalised truncations of isolated-pentagon-triple carbon cages. *MATCH Commun Math Comput Chem* 1998, 7–17.

65. Brinkmann G. Problems and scope of spiral algorithms and spiral codes for polyhedral cages. *Chem Phys Lett* 1997, 272:193–198. doi: 10.1016/S0009-2614(97)88009-8.

66. Fowler PW, Graovac A, Žerovnik J, Pisanski T. A generalized ring spiral algorithm for coding fullerenes and other cubic polyhedra. Preprint series/Institute of Mathematics, Physics and Mechanics, Department of Mathematics, University of Ljubljana, 1998.

67. Fowler PW, Horspool D, Myrvold W. Vertex spirals in fullerenes and their implications for nomenclature of fullerene derivatives. *Chem Eur J* 2007, 13:2208–2217. doi: 10.1002/chem.200601107.

68. Cozzi F, Powell WH, Thilgen C. Numbering of fullerenes (IUPAC recommendations 2005). *Pure Appl Chem* 2005, 77:843–923. doi: 10.1351/pac200577050843.

69. Liu X, Klein DJ, Schmalz TG, Seitz WA. Generation of carbon-cage polyhedra. *J Comput Chem* 1991, 12:1252–1259. doi: 10.1002/jcc.540121013.

70. Brinkmann G, Dress AW. A constructive enumeration of fullerenes. *J Algor* 1997, 23:345–358. doi: 10.1006/jagm.1996.0806.

71. Brinkmann G, Franceus D, Fowler PW, Graver JE. Growing fullerenes from seed: growth transformations of fullerene polyhedra. *Chem Phys Lett* 2006, 428:386–393. doi: 10.1016/j.cplett.2006.07.040.

72. Hasheminezhad M, Fleischner H, McKay BD. A universal set of growth operations for fullerenes. *Chem Phys Lett* 2008, 464:118–121. doi: 10.1016/j.cplett.2008.09.005.

73. Balaban AT, Schmalz TG, Zhu H, Klein DJ. Generalizations of the Stone-Wales rearrangement for cage compounds, including fullerenes. *J Mol Struct THEOCHEM* 1996, 363:291–301. doi: 10.1016/0166-1280(95)04448-5.

74. Graver JE, Graves CM, Graves SJ. Fullerene patches II. *Ars Math Contemp* 2014, 7:405–421.

75. Brinkmann G, Goedgebeur J, McKay BD. The generation of fullerenes. *J Chem Inf Model* 2012, 52:2910–2918. doi: 10.1021/ci3003107.

76. Brinkmann G, Goedgebeur J, Van Cleemput N. The history of the generation of cubic graphs. *J Chem Inf Model* 2013, 5:67–89.

77. Goldberg M. A class of multi-symmetric polyhedra. *Tohoku Math J* 1937, 43:104–108.

78. Coxeter HSM. Virus macromolecules and geodesic domes. In: Butcher JC, ed. *A Spectrum of mathematics—Essays Presented to H. G. Forder*. Oxford, UK: Oxford University Press; 1971, 98–107.

79. Guo X, Hansen P, Zheng M. Boundary uniqueness of fusenes. *Discrete Appl Math* 2002, 118:209–222. doi: 10.1016/S0166-218X(01)00180-9.

80. Graver JE. The (m,k)-patch boundary code problem. *MATCH Commun Math Comput Chem* 2003, 48:189–196.

81. Brinkmann G, Graver JE, Justus C. Numbers of faces in disordered patches. *J Math Chem* 2009, 45:263–278. doi: 10.1007/s10910-008-9403-6.

82. Graver JE, Graves CM. Fullerene patches I. *Ars Math Contemp* 2010, 3:109–120.

83. Brinkmann G, Fowler PW, Justus C. A catalogue of isomerization transformations of fullerene polyhedra. *J Chem Inf Comput Sci* 2003, 43:917–927. doi: 10.1021/ci020069l.

84. Brinkmann G, Fowler PW. A catalogue of growth transformations of fullerene polyhedra. *J Chem Inf Comput Sci* 2003, 43:1837–1843. doi: 10.1021/ci030017b.

85. Bornhöft J, Brinkmann G, Greinus J. Pentagon–hexagon-patches with short boundaries. *Eur J Comb* 2003, 24:517–529. doi: 10.1016/S0195-6698(03)00034-9.

86. Stone AJ, Wales DJ. Theoretical studies of icosahedral C_{60} and some related species. *Chem Phys Lett* 1986, 128:501–503. doi: 10.1016/0009-2614(86)80661-3.

87. Babić D, Bassoli S, Casartelli M, Cataldo F, Graovac A, Ori O, York B. Generalized Stone-Wales transformations. *Mol Simulat* 1995, 14:395–401. doi: 10.1080/08927029508022032.

88. Astakhova TY, Vinogradov GA. New isomerization operations for fullerene graphs. *J Mol Struct THEOCHEM* 1998, 430:259–268. doi: 10.1016/S0166-1280(98)90253-6.

89. Ori O, Putz MV, Gutman I, Schwerdtfeger P. Generalized Stone-Wales transformations for fullerene graphs derived from Berge's switching theorem. In: Gutman I, Pokric B, Vukicevic D, eds. *Ante Graovac—Life and Works*. Mathematical Chemistry Monographs, vol. 16. Kragujevac, Serbia: University of Kragujevac; 2014, 259–272.

90. Berge C. *Graphs and Hypergraphs*. New York: Elsevier; 1973.

91. Endo M, Kroto HW. Formation of carbon nanofibers. *J Phys Chem* 1992, 96:6941–6944. doi: 10.1021/j100196a017.

92. Yoshida M, Fowler PW. Systematic relationships between fullerenes without spirals. *Chem Phys Lett* 1997, 278:256–261. doi: 10.1016/S0009-2614(97)00980-9.

93. Podlivaev A, Openov L. Stone-Wales transformation paths in fullerene C_{60}. *J Exp Theoret Phys Lett* 2005, 81:533–537. doi: 10.1134/1.1996764.

94. Ori O, Cataldo F, Putz MV. Topological anisotropy of Stone-Wales waves in graphenic fragments. *Int J Mol Sci* 2011, 12:7934–7949. doi: 10.3390/ijms12117934.

95. Saha B, Irle S, Morokuma K. Hot giant fullerenes eject and capture C_2 molecules: QM/MD simulations with constant density. *J Phys Chem C* 2011, 115:22707–22716. doi: 10.1021/jp203614e.

96. Murry RL, Strout DL, Odom GK, Scuseria GE. Role of sp^3 carbon and 7-membered rings in fullerene annealing and fragmentation. *Nature* 1993, 366:665–667. doi: 10.1038/366665a0.

97. Walsh TR, Wales DJ. Relaxation dynamics of C_{60}. *J Chem Phys* 1998, 109:6691–6700. doi: 10.1063/1.477319.

98. Dunk PW, Kaiser NK, Hendrickson CL, Quinn JP, Ewels CP, Nakanishi Y, Sasaki Y, Shinohara H, Marshall AG, Kroto HW. Closed network growth of fullerenes. *Nature Commun* 2012, 3:855. doi: 10.1038/ncomms1853.

99. Irle S, Zheng G, Wang Z, Morokuma K. The C_{60} formation puzzle "solved": QM/MD simulations reveal the shrinking hot giant road of the dynamic fullerene self-assembly mechanism. *J Phys Chem B* 2006, 110:14531–14545. doi: 10.1021/jp061173z.

100. Tan YZ, Chen RT, Liao ZJ, Li J, Zhu F, Lu X, Xie SY, Li J, Huang RB, Zheng LS. Carbon arc production of heptagon-containing fullerene[68]. *Nature Commun* 2011, 2:420. doi: 10.1038/ncomms1431.

101. Austin SJ, Fowler PW, Manolopoulos DE, Zerbetto F. The Stone-Wales map for C_{60}. *Chem Phys Lett* 1995, 235:146–151. doi: 10.1016/0009-2614(95)00082-F.

102. Budyka MF, Zyubina TS, Ryabenko AG, Muradyan VE, Esipov SE, Cherepanova NI. Is C_2 cluster ingested by fullerene C_{60}? *Chem Phys Lett* 2002, 354:93–99. doi: 10.1016/S0009-2614(02)00113-6.

103. Dutour M, Deza M. Goldberg-Coxeter construction for 3- and 4-valent plane graphs. *Electron J Comb* 2004, 11:1–49.

104. Bakowies D, Bühl M, Thiel W. Can large fullerenes be spherical? *J Am Chem Soc* 1995, 117:10113–10118. doi: 10.1021/ja00145a025.

105. Bakowies D, Bühl M, Thiel W. A density functional study on the shape of C_{180} and C_{240} fullerenes. *Chem Phys Lett* 1995, 247:491–493. doi: 10.1016/S0009-2614(95)01222-2.

106. Senn P. Computation of the cartesian coordinates of buckminsterfullerene. *J Chem Educ* 1995, 72:302–303. doi: 10.1021/ed072p302.

107. Manolopoulos DE, Fowler PW. Molecular graphs, point groups, and fullerenes. *J Chem Phys* 1992, 96:7603–7614. doi: 10.1063/1.462413.

108. Cvetković D, Fowler P, Rowlinson P, Stevanović D. Constructing fullerene graphs from their eigenvalues and angles. *Linear Algebra Appl* 2002, 356:37–56. doi: 10.1016/S0024-3795(02)00280-X.

109. Pisanski T, Shawe-Taylor J. Characterizing graph drawing with eigenvectors. *J Chem Inf Comput Sci* 2000, 40:567–571. doi: 10.1021/ci9900938.

110. Fowler P, Pisanski T, Shawe-Taylor J. Graph drawing. In: Tamassia R, Tollis I, eds. *Lecture Notes in Computer Science*, vol. 894. Berlin: Springer; 1995, 282–285.

111. László I, Graovac A, Pisanski T, Plavšić D. Graph drawing with eigenvectors. In: Putz MV, ed. *Carbon Bonding and Structures, Vol. 5: Carbon Materials: Chemistry and Physics*. Netherlands: Springer; 2011, 95–115. doi: 10.1007/978-94-007-1733-6_6.

112. Graver JE. Kekulé structures and the face independence number of a fullerene. *Europ J Combin* 2007, 28:1115–1130. doi: 10.1016/j.ejc.2006.03.003.

113. Kardoš F, Král' D, Miškuf J, Sereni JS. Fullerene graphs have exponentially many perfect matchings. *J Math Chem* 2009, 46:443–447. doi: 10.1007/s10910-008-9471-7.

114. Wu Z, Jelski DA, George TF. Vibrational motions of buckminsterfullerene. *Chem Phys Lett* 1987, 137:291–294. doi: 10.1016/0009-2614(87)80221-X.

115. Weeks DE, Harter WG. Rotation-vibration spectra of icosahedral molecules. II. Icosahedral symmetry, vibrational eigenfrequencles, and normal modes of buckminsterfullerene. *J Chem Phys* 1989, 90:4744–4771. doi: 10.1063/1.456571.

116. Cyvin SJ, Brendsdal E, Cyvin BN, Brunvoll J. Molecular vibrations of footballene. *Chem Phys Lett* 1988, 143:377–380. doi: 10.1016/0009-2614(88)87050-7.

117. Jishi RA, Mirie RM, Dresselhaus MS. Force-constant model for the vibrational modes in C_{60}. *Phys Rev B* 1992, 45:13685–13689. doi: 10.1103/PhysRevB.45.13685.

118. Feldman JL, Broughton JQ, Boyer LL, Reich DE, Kluge MD. Intramolecular-force-constant model for C_{60}. *Phys Rev B* 1992, 46:12731–12736. doi: 10.1103/PhysRevB.46.12731.

119. Ceulemans A, Fowler PW, Vos I. C_{60} vibrates as a hollow sphere. *J Chem Phys* 1994, 100:5491–5500. doi: 10.1063/1.467167.

120. Hands ID, Dunn JL, Bates CA. A complete nearest-neighbor force field model for C_{60}. *J Chem Phys* 2004, 120:6912–6923. doi: 10.1063/1.1683105.

121. Ceulemans A, Titeca BC, Chibotaru LF, Vos I, Fowler PW. Complete bond force field for trivalent and deltahedral cages: group theory and applications to cubane, closo-dodecahedrane, and buckminsterfullerene. *J Phys Chem A* 2001, 105:8284–8295. doi: 10.1021/jp0036792.

122. Zheng G, Irle S, Morokuma K. Performance of the DFTB method in comparison to DFT and semiempirical methods for geometries and energies of C_{20}–C_{86} fullerene isomers. *Chem Phys Lett* 2005, 412:210–216. doi: 10.1016/j.cplett.2005.06.105.

123. Mani P. Automorphismen von polyedrischen Graphen. *Math Ann* 1971, 192:279–303. doi: 10.1007/BF02075357.

124. Deza M, Dutour-Sikirić M, Fowler PW. The symmetries of cubic polyhedral graphs with face size no larger than 6. *MATCH Commun Math Comput Chem* 2009, 61:589–602.

125. Balasubramanian K. Applications of combinatorics and graph theory to spectroscopy and quantum chemistry. *Chem Rev* 1985, 85:599–618. doi: 10.1021/cr00070a005.

126. Faghani M. Symmetry of a toroidal fullerene. *Optoelectron Adv Mater Rapid Commun* 2010, 4:1844–1846.

127. Fujita S. Application of coset representations to the construction of symmetry adapted functions. *Theoret Chim Acta* 1990, 78:45–63. doi: 10.1007/BF01112352.

128. King RB, Diudea MV. The chirality of icosahedral fullerenes: a comparison of the tripling (leapfrog), quadrupling (chamfering), and septupling (capra) transformations. *J Math Chem* 2006, 39:597–604. doi: 10.1007/s10910-005-9048-7.

129. David WIF, Ibberson RM, Matthewman JC, Prassides K, Dennis TJS, Hare JP, Kroto HW, Taylor R, Walton DRM. Crystal structure and bonding of ordered C_{60}. *Nature* 1991, 353:147–149. doi: 10.1038/353147a0.

130. Devadoss SL, O'Rourke J. *Discrete and Computational Geometry*. Princeton, NJ: Princeton University Press; 2011.

131. Pisanski T, Kaufman M, Bokal D, Kirby EC, Graovac A. Isoperimetric quotient for fullerenes and other

polyhedral cages. *J Chem Inf Comput Sci* 1997, 37:1028–1032. doi: 10.1021/ci970228e.

132. Sylvester JJ. A question in the geometry of situation. *Q J Pure Appl Math* 1857, 1:79.

133. Elzinga DJ, Hearn DW. The minimum covering sphere problem. *Manag Sci* 1972, 19:96–104.

134. Hopp TH, Reeve CP. An algorithm for computing the minimum covering sphere in any dimension. In: COMMERCE UDO ed. NIST IR5381, Gaithersburg, MD: NIST; 1996, 1–8.

135. Nielsen F, Nock R. Approximating smallest enclosing balls. In: Laganá A, Gavrilova M, Kumar V, Mun Y, Tan C, Gervasi O, eds. *Computational Science and Its Applications – ICCSA 2004.* Lecture Notes in Computer Science, vol. 3045. Berlin Heidelberg: Springer; 2004, 147–157.

136. Yıldırım E. Two algorithms for the minimum enclosing ball problem. *SIAM J Optimiz* 2008, 19:1368–1391. doi: 10.1137/070690419.

137. Fowler P. Cylindrical fullerenes: the smallest nanotubes? *J Phys Chem Solids* 1993, 54:1825–1833. doi: 10.1016/0022-3697(93)90295-3.

138. Kumar P, Yıldırım E. Minimum-volume enclosing ellipsoids and core sets. *J Optim Theory Appl* 2005, 126:1–21. doi: 10.1007/s10957-005-2653-6.

139. Kumar P, Yıldırım E. Computing minimum-volume enclosing axis-aligned ellipsoids. *J Optim Theory Appl* 2008, 136:211–228. doi: 10.1007/s10957-007-9295-9.

140. Sun P, Freund RM. Computation of minimum-volume covering ellipsoids. *Oper Res* 2004, 52:690–706. doi: 10.1287/opre.1040.0115.

141. Todd MJ, Yıldırım E. On Khachiyan's algorithm for the computation of minimum-volume enclosing ellipsoids. *Discrete Appl Math* 2007, 155:1731–1744. doi: 10.1016/j.dam.2007.02.013.

142. Nasu K, Taketsugu T, Nakano T, Nagashima U, Hosoya H. Stability of small fullerenes C_n ($n = 36, 40$ and 60): a topological and molecular orbital approach. *Theoret Chim Acta* 1995, 90:75–86. doi: 10.1007/BF01113841.

143. Díaz-Tendero S, Martín F, Alcamí M. Structure and electronic properties of fullerenes C_{52}^{q+}: is C_{52}^{2+} an exception to the pentagon adjacency penalty rule? *ChemPhysChem* 2005, 6:92–100. doi: 10.1002/cphc.200400273.

144. Díaz-Tendero S, Alcamí M, Martín F. Fullerene C_{50}: sphericity takes over, not strain. *Chem Phys Lett* 2005, 407:153–158. doi: 10.1016/j.cplett.2005.03.065.

145. Fowler PW, Heine T, Zerbetto F. Competition between even and odd fullerenes: C_{118}, C_{119}, and C_{120}. *J Phys Chem A* 2000, 104:9625–9629. doi: 10.1021/jp0019815.

146. Fischer JE, Heiney PA, Smith AB. Solid-state chemistry of fullerene-based materials. *Acc Chem Res* 1992, 25:112–118. doi: 10.1021/ar00015a003.

147. Heiney PA, Fischer JE, McGhie AR, Romanow WJ, Denenstein AM, McCauley JP Jr, Smith AB, Cox DE. Orientational ordering transition in solid C_{60}. *Phys Rev Lett* 1991, 66:2911–2914. doi: 10.1103/PhysRevLett.66.2911.

148. Liu S, Lu YJ, Kappes MM, Ibers JA. The structure of the C_{60} molecule: X-ray crystal structure determination of a twin at 110 K. *Science* 1991, 254:408–410. doi: 10.1126/science.254.5030.408.

149. Vaughan GBM, Heiney PA, Fischer JE, Luzzi DE, Ricketts-Foot DA, McGhie AR, Hui YW, Smith AL, Cox DE, Romanow WJ, et al. Orientational disorder in solvent-free solid C_{70}. *Science* 1991, 254: 1350–1353. doi: 10.1126/science.254.5036.1350.

150. Kauczor J, Norman P, Saidi WA. Non-additivity of polarizabilities and van der Waals C_6 coefficients of fullerenes. *J Chem Phys* 2013, 138:114107. doi: 10.1063/1.4795158.

151. Lundin A, Sundqvist B, Skoglund P, Fransson A, Pettersson S. Compressibility, specific heat capacity, and Grüneisen parameter for C_{60}/C_{70}. *Solid State Commun* 1992, 84:879–883. doi: 10.1016/0038-1098(92)90451-E.

152. Kawamura H, Akahama Y, Kobayashi M, Shinohara H, Sato H, Saito Y, Kikegawa T, Shimomura O, Aoki K. Solid C_{70} high pressure and high temperature. *J Phys Chem Solids* 1993, 54:1675–1678. doi: 10.1016/0022-3697(93)90281-U.

153. Zettl A, Cumings J. Elastic properties of fullerenes. In: Levy M, Bass H, Stern R, eds. *Handbook of Elastic Properties of Solids, Liquids, and Gases.* Lecture Notes in Computer Science, vol. 2. San Diego, CA: Academic Press; 2001, 163–170.

154. Schwerdtfeger P, Gaston N, Krawczyk RP, Tonner R, Moyano GE. Extension of the Lennard-Jones potential: theoretical investigations into rare-gas clusters and crystal lattices of He, Ne, Ar, and Kr using many-body interaction expansions. *Phys Rev B* 2006, 73:064112. doi: 10.1103/PhysRevB.73.064112.

155. Cohen ML. Calculation of bulk moduli of diamond and zinc-blende solids. *Phys Rev B* 1985, 32:7988–7991. doi: 10.1103/PhysRevB.32.7988.

156. Faccio R, Denis PA, Pardo H, Goyenola C, Mombrú AW. Mechanical properties of graphene nanoribbons. *J Phys Condens Mat* 2009, 21:285304. doi: 10.1088/0953-8984/21/28/285304.

157. Milyavskiy VV, Borodina TI, Sokolov SN. Phase transitions of C_{70} fullerite with hexagonal closed-packed structure under shock-wave loading. *Fuller Nanotub Carbon Nanostruct* 2008, 16:494–498. doi: 10.1080/15363830802282433.

158. Hales TC. A computer verification of the Kepler conjecture. In: *Proceedings of the International Congress of Mathematicians*, vol. III. Beijing: Higher Ed. Press; 2002, 795–804.

159. Hales TC. A proof of the Kepler conjecture. *Ann Math* 2005:1065–1185. doi: 10.4007/annals.2005.162.1065.

160. Stoyan Y, Gil N, Scheithauer G, Pankratov A, Magdalina I. Packing of convex polytopes into a parallelepiped. Tech. Rep. MATH-NM-04-2004, Technische Universität Dresden, 2003.

161. Stoyan Y, Gil N, Pankratov A. Packing of nonconvex polytopes into a parallelepiped. Tech. Rep. MATH-NM-06-2004, Technische Universität Dresden, 2004.

162. Yıldırım E. On the minimum volume covering ellipsoid of ellipsoids. *SIAM J Optimiz* 2006, 17:621–641. doi: 10.1137/050622560.

163. Donev A, Stillinger FH, Chaikin PM, Torquato S. Unusually dense crystal packings of ellipsoids. *Phys Rev Lett* 2004, 92:255506. doi: 10.1103/PhysRevLett.92.255506.

164. Wiener H. Structural determination of paraffin boiling points. *J Am Chem Soc* 1947, 69:17–20. doi: 10.1021/ja01193a005.

165. Ori O, D'Mello M. A topological study of the structure of the C_{76} fullerene. *Chem Phys Lett* 1992, 197:49–54. doi: 10.1016/0009-2614(92)86020-I.

166. Ori O, Cataldo F, Vukičević D, Graovac A. Wiener way to dimensionality. *Iranian J Math Chem* 2010, 1:5–15.

167. Graovac A, Ori O, Faghani M, Ashrafi A. Distance property of fullerenes. *Iranian J Math Chem* 2011, 2:99–107.

168. Koorepazan-Moftakhar F, Ashrafi AR, Ori O, Putz MV. Sphericality of some classes of fullerenes measured by topology. In: *Fullerenes: Chemistry, Natural Sources and Technological Applications*. New York: NIST. Nova Publications; 2014.

169. Vukičević D, Cataldo F, Ori O, Graovac A. Topological efficiency of C_{66} fullerene. *Chem Phys Lett* 2011, 501:442–445. doi: 10.1016/j.cplett.2010.11.055.

170. Ori O, Cataldo F, Graovac A. Topological ranking of C_{28} fullerenes reactivity. *Fuller Nanotub Carbon Nanostruct* 2009, 17:308–323. doi: 10.1080/15363830902782332.

171. Wang CR, Kai T, Tomiyama T, Yoshida T, Kobayashi Y, Nishibori E, Takata M, Sakata M, Shinohara H. Materials science: C_{66} fullerene encaging a scandium dimer. *Nature* 2000, 408:426–427. doi: 10.1038/35044195.

172. Katritzky AR, Karelson M, Petrukhin R. The CODESSA PRO project, 2005.

173. Fowler PW, Caporossi G, Hansen P. Distance matrices, Wiener indices, and related invariants of fullerenes. *J Phys Chem A* 2001, 105:6232–6242. doi: 10.1021/jp0104379.

174. Hosoya H. On some counting polynomials in chemistry. *Discrete Appl Math* 1988, 19:239–257. doi: 10.1016/0166-218X(88)90017-0.

175. Gutman I. A formula for the Wiener number of trees and its extension to graphs containing cycles. *Graph Theory Notes NY* 1994, 27:9–15.

176. Balaban AT. Topological indices based on topological distances in molecular graphs. *Pure Appl Chem* 1983, 55:199–206. doi: 10.1351/pac198855020199.

177. Balaban AT. Chemical graphs: looking back and glimpsing ahead. *J Chem Inf Comput Sci* 1995, 35:339–350. doi: 10.1021/ci00025a001.

178. Zhang H, Balasubramanian K. Spectral moments of fullerene cages. *Mol Phys* 1993, 79:727–745. doi: 10.1080/00268979300101581.

179. Estrada E. Characterization of 3D molecular structure. *Chem Phys Lett* 2000, 319:713–718. doi: 10.1016/S0009-2614(00)00158-5.

180. de la Peña JA, Gutman I, Rada J. Estimating the Estrada index. *Linear Algebra Appl* 2007, 427:70–76. doi: 10.1016/j.laa.2007.06.020.

181. Diudea MV, Gutman I, Jantschi L. *Molecular Topolgy*. New York: Nova Science; 2001.

182. Ju Y, Liang H, Zhang J, Bai F. A note on Fowler-Manolopoulos predictor of fullerene stability. *MATCH Commun Math Comput Chem* 2010, 64:419–424.

183. Austin SJ, Fowler PW, Manolopoulos DE, Orlandi G, Zerbetto F. Structural motifs and the stability of fullerenes. *J Phys Chem* 1995, 99:8076–8081. doi: 10.1021/j100020a035.

184. Stevanović D. Remarks on Fowler-Manolopoulos predictor of fullerene stability. *MATCH Commun Math Comput Chem* 2011, 66:285–292.

185. Karton A, Chan B, Raghavachari K, Radom L. Evaluation of the heats of formation of corannulene and C_{60} by means of high-level theoretical procedures. *J Phys Chem A* 2013, 117:1834–1842. doi: 10.1021/jp312585r.

186. Perdew JP, Burke K, Ernzerhof M. Generalized gradient approximation made simple. *Phys Rev Lett* 1996, 77:3865–3868. doi: 10.1103/PhysRevLett.77.3865.

187. Weigend F, Ahlrichs R. Balanced basis sets of split valence, triple zeta valence and quadruple zeta valence quality for H to Rn: design and assessment of accuracy. *Phys Chem Chem Phys* 2005, 7:3297–3305. doi: 10.1039/B508541A.

188. Iranmanesh A, Alizadeh Y, Mirzaie S. Computing Wiener polynomial, Wiener index and Hyper Wiener index of C_{80} fullerene by GAP program. *Fuller Nanotub Carbon Nanostruct* 2009, 17:560–566. doi: 10.1080/15363830903133204.

189. Charlier JC, Eklund P, Zhu J, Ferrari A. Electron and phonon properties of graphene: their relationship with carbon nanotubes. In: Jorio A, Dresselhaus G, Dresselhaus M, eds. *Carbon Nanotubes: Advanced Topics in the Synthesis, Structure, Properties and Applications*. Berlin: Springer; 2008.

190. Khamatgalimov AR, Kovalenko VI. Electronic structure and stability of C_{80} fullerene IPR isomers. *Fuller Nanotub Carbon Nanostruct* 2011, 19:599–604. doi: 10.1080/1536383X.2010.504951.

191. Xu L, Cai W, Shao X. Prediction of low-energy isomers of large fullerenes from C_{132} to C_{160}. *J Phys Chem A* 2006, 110:9247–9253. doi: 10.1021/jp057181h.

192. Shao N, Gao Y, Yoo S, An W, Zeng XC. Search for lowest-energy fullerenes: C_{98} to C_{110}. *J Phys Chem A* 2006, 110:7672–7676. doi: 10.1021/jp0624092.

193. Shao N, Gao Y, Zeng XC. Search for lowest-energy fullerenes 2: C_{38} to C_{80} and C_{112} to C_{120}. *J Phys Chem C* 2007, 111:17671–17677. doi: 10.1021/jp0701082.

194. Klein DJ, Balaban AT. Clarology for conjugated carbon nano-structures: molecules, polymers, graphene, defected graphene, fractal benzenoids, fullerenes, nano-tubes, nano-cones, nano-tori, etc. *Open Org Chem J* 2011, 5:27–61. doi: 10.2174/1874364101105010027.

195. Klein DJ, Schmalz TG, Hite GE, Seitz WA. Resonance in C_{60} buckminsterfullerene. *J Am Chem Soc* 1986, 108:1301–1302. doi: 10.1021/ja00266a032.

196. Vukičević D, Kroto HW, Randić M. Atlas of Kekulé valence structures of buckminsterfullerene. *Croat Chem Acta* 2005, 78:223–234.

197. Randić M, Kroto HW, Vukičević D. Numerical Kekulé structures of fullerenes and partitioning of π-electrons to pentagonal and hexagonal rings. *J Chem Inf Model* 2007, 47:897–904. doi: 10.1021/ci600484u.

198. Austin S, Fowler P, Hansen P, Monolopoulos D, Zheng M. Fullerene isomers of C_{60}. Kekulé counts versus stability. *Chem Phys Lett* 1994, 228:478–484. doi: 10.1016/0009-2614(94)00965-1.

199. Esperet L, Kardoš F, King AD, Král' D, Norine S. Exponentially many perfect matchings in cubic graphs. *Adv Math* 2011, 227:1646–1664. doi: 10.1016/j.aim.2011.03.015.

200. Lovász L, Plummer MD. *Matching Theory*. Amsterdam: Elsevier; 1986.

201. Pauling L, Brockway LO, Beach J. The dependence of interatomic distance on single bond-double bond resonance. *J Am Chem Soc* 1935, 57:2705–2709. doi: 10.1021/ja01315a105.

202. Narita S, Morikawa T, Shibuya T. Linear relationship between the bond lengths and the Pauling bond orders in fullerene molecules. *J Mol Struct THEOCHEM* 2000, 532:37–40. doi: 10.1016/S0166-1280(00)00563-7.

203. Rogers KM, Fowler PW. Leapfrog fullerenes, Hückel bond order and Kekulé structures. *J Chem Soc, Perkin Trans 2* 2001:18–22. doi: 10.1039/B007520P.

204. Gross L, Mohn F, Moll N, Schuler B, Criado A, Guitián E, Peña D, Gourdon A, Meyer G. Bond-order discrimination by atomic force microscopy. *Science* 2012, 337:1326–1329. doi: 10.1126/science.1225621.

205. Graver JE, Hartung EJ, Souid AY. Clar and Fries numbers for benzenoids. *J Math Chem* 2013, 51:1981–1989. doi: 10.1007/s10910-013-0193-0.

206. Bernáth A, Kovács ER. NP-hardness of the Clar number in general plane graphs. Available at http://www.cseltehu/egres/qp/egresqp-11-07ps 2011, 1–3.

207. Ye D, Zhang H. Extremal fullerene graphs with the maximum Clar number. *Discrete Appl Math* 2009, 157:3152–3173. doi: 10.1016/j.dam.2009.06.007.

208. Zhang H, Ye D, Liu Y. A combination of Clar number and Kekulé count as an indicator of relative stability of fullerene isomers of C_{60}. *J Math Chem* 2010, 48:733–740. doi: 10.1007/s10910-010-9706-2.

209. Fowler PW. Localised models and leapfrog structures of fullerenes. *J Chem Soc, Perkin Trans 2* 1992:145–146. doi: 10.1039/P29920000145.

210. Došlić T. Leapfrog fullerenes have many perfect matchings. *J Math Chem* 2008, 44:1–4. doi: 10.1007/s10910-007-9287-x.

211. Hartung E. Fullerenes with complete Clar structure. *Discrete Appl Math* 2013, 161:2952–2957. doi: 10.1016/j.dam.2013.06.009.

212. Fowler PW, Austin SJ, Dunning OJ, Dias JR. Symmetry properties of the leapfrog transformation for fullerenes and benzenoids. *Chem Phys Lett* 1994, 224:123–130. doi: 10.1016/0009-2614(94)00525-7.

213. Zhang H, Ye D. An upper bound for the Clar number of fullerene graphs. *J Math Chem* 2007, 41:123–133. doi: 10.1007/s10910-006-9061-5.

214. Herndon WC. Resonance energies of aromatic hydrocarbons. Quantitative test of resonance theory. *J Am Chem Soc* 1973, 95:2404–2406. doi: 10.1021/ja00788a073.

215. Herndon WC, Ellzey JM. Lawrence. Resonance theory. V. Resonance energies of benzenoid and nonbenzenoid pi systems. *J Am Chem Soc* 1974, 96:6631–6642. doi: 10.1021/ja00828a015.

216. Babić D, Balaban AT, Klein DJ. Nomenclature and coding of fullerenes. *J Chem Inf Comput Sci* 1995, 35:515–526. doi: 10.1021/ci00025a020.

217. Liu Y, O'Brien S, Zhang Q, Heath J, Tittel F, Curl R, Kroto H, Smalley R. Negative carbon cluster ion beams: new evidence for the special nature of C_{60}. *Chem Phys Lett* 1986, 126:215–217. doi: 10.1016/S0009-2614(86)80042-2.

218. Slanina Z, Uhlík F, Zhao X, Adamowicz L, Nagase S. Relative stabilities of C_{74} isomers. *Fuller Nanotub Carbon Nanostruct* 2007, 15:195–205. doi: 10.1080/15363830701236423.

219. Beckhaus HD, Verevkin S, Rüchardt C, Diederich F, Thilgen C, Meer HUT, Mohn H, Müller W. C_{70} ist stabiler als C_{60}: experimentelle Bestimmung der Bildungswärme von C_{70}. *Angew Chem* 1994, 33:996–998. doi: 10.1002/ange.19941060916.

220. Wang Z, Ke X, Zhu Z, Zhu F, Ruan M, Chen H, Huang R, Zheng L. A new carbon solid made of the

world's smallest caged fullerene C_{20}. *Phys Lett A* 2001, 280:351–356. doi: 10.1016/S0375-9601(00)00847-1.

221. Lin F, Sorensen ES, Kallin C, Berlinsky AJ. C_{20}, the smallest fullerene. In: Sattler KD, ed. *Handbook of Nanophysics: Clusters and Fullerenes, Handbook of Nanophysics, chap. 29*. Boca Raton, FL: CRC Press; 2010.

222. Babić D, Brinkmann G, Dress A. Topological resonance energy of fullerenes. *J Chem Inf Comput Sci* 1997, 37:920–923. doi: 10.1021/ci9700283.

223. Bühl M, Hirsch A. Spherical aromaticity of fullerenes. *Chem Rev* 2001, 101:1153–1184. doi: 10.1021/cr990332q.

224. Haddon R, Brus L, Raghavachari K. Electronic structure and bonding in icosahedral C_{60}. *Chem Phys Lett* 1986, 125:459–464. doi: 10.1016/0009-2614(86)87079-8.

225. Haddon R, Brus L, Raghavachari K. Rehybridization and π-orbital alignment: the key to the existence of spheroidal carbon clusters. *Chem Phys Lett* 1986, 131:165–169. doi: 10.1016/0009-2614(86)80538-3.

226. Bakowies D, Thiel W. MNDO study of large carbon clusters. *J Am Chem Soc* 1991, 113:3704–3714. doi: 10.1021/ja00010a012.

227. Fowler PW, Hansen P, Stevanović D. A note on the smallest eigenvalue of fullerenes. *MATCH Commun Math Comput Chem* 2003, 48:37–48.

228. Došlić T. The smallest eigenvalue of fullerene graphs – closing the gap. *MATCH Commun Math Comput Chem* 2013, 70:73–78.

229. Randić M, Trinajstić N, Živković T. Molecular graphs having identical spectra. *J Chem Soc, Faraday Trans 2* 1976, 72:244–256. doi: 10.1039/F29767200244.

230. Aihara J. A new definition of Dewar-type resonance energies. *J Am Chem Soc* 1976, 98:2750–2758. doi: 10.1021/ja00426a013.

231. Gutman I, Milun M, Trinajstic N. Graph theory and molecular orbitals. 19. Nonparametric resonance energies of arbitrary conjugated systems. *J Am Chem Soc* 1977, 99:1692–1704. doi: 10.1021/ja00448a002.

232. Balasubramanian K. Exhaustive generation and analytical expressions of matching polynomials of fullerenes C_{20}-C_{50}. *J Chem Inf Comput Sci* 1994, 34:421–427. doi: 10.1021/ci00018a032.

233. Salvador JM, Hernandez A, Beltran A, Duran R, Mactutis A. Fast partial-differential synthesis of the matching polynomial of C_{72-100}. *J Chem Inf Comput Sci* 1998, 38:1105–1110. doi: 10.1021/ci9800155.

234. Randić M. Novel insight into Clar's aromatic π-sextets. *Chem Phys Lett* 2014, 601:1–5. doi: 10.1016/j.cplett.2014.03.073.

235. Lu X, Chen Z. Curved π-conjugation, aromaticity, and the related chemistry of small fullerenes ($<C_{60}$) and single-walled carbon nanotubes. *Chem Rev* 2005, 105:3643–3696. doi: 10.1021/cr030093d.

236. Chen Z, Wu JI, Corminboeuf C, Bohmann J, Lu X, Hirsch A, Schleyer PR. Is C_{60} buckminsterfullerene aromatic? *Phys Chem Chem Phys* 2012, 14:14886–14891. doi: 10.1039/C2CP42146A.

237. Hirsch A, Ruoff Z, Jiao H. Spherical aromaticity in I_h symmetrical fullerenes: the 2(n+1)2 rule. *Angew Chem Int Ed* 2000, 39:3915–3917. doi: 10.1002/1521-3773(20001103)39:21<3915::AID-ANIE3915>3.0.CO;2-O.

238. Fedorov AS, Fedorov DA, Kuzubov AA, Avramov PV, Nishimura Y, Irle S, Witek HA. Relative isomer abundance of fullerenes and carbon nanotubes correlates with kinetic stability. *Phys Rev Lett* 2011, 107:175506. doi: 10.1103/PhysRevLett.107.175506.

239. Fowler PW. Fullerene graphs with more negative than positive eigenvalues: the exceptions that prove the rule of electron deficiency? *J Chem Soc Faraday Trans* 1997, 93:1–3. doi: 10.1039/A605413G.

240. Manolopoulos DE, Woodall DR, Fowler PW. Electronic stability of fullerenes: eigenvalue theorems for leapfrog carbon clusters. *J Chem Soc Faraday Trans* 1992, 88:2427–2435. doi: 10.1039/FT9928802427.

241. Fowler PW, Austin SJ. Closed-shell carbon frameworks: leapfrog fullerenes and decorated spheriphane hydrocarbons. *J Chem Inf Comput Sci* 1994, 34:264–269. doi: 10.1021/ci00018a006.

242. Deza M, Fowler PW, Rassat A, Rogers KM. Fullerenes as tilings of surfaces. *J Chem Inf Comput Sci* 2000, 40:550–558. doi: 10.1021/ci990066h.

243. Fowler P, Rogers K, Fajtlowicz S, Hansen P, Caporossi G. Facts and conjectures about fullerene graphs: leapfrog, cylinder and Ramanujan fullerenes. In: Betten A, Kohnert A, Laue R, Wassermann A, eds. *Algebraic Combinatorics and Applications*. Berlin Heidelberg: Springer; 2001, 134–146.

244. Bakowies D, Gelessus A, Thiel W. Quantum-chemical study of C_{78} fullerene isomers. *Chem Phys Lett* 1992, 197:324–329. doi: 10.1016/0009-2614(92)85777-8.

245. Bakowies D, Kolb M, Thiel W, Richard S, Ahlrichs R, Kappes MM. Quantum-chemical study of C_{84} fullerene isomers. *Chem Phys Lett* 1992, 200:411–417. doi: 10.1016/0009-2614(92)87013-F.

246. Chen Z, Thiel W. Performance of semiempirical methods in fullerene chemistry: relative energies and nucleus-independent chemical shifts. *Chem Phys Lett* 2003, 367:15–25. doi: 10.1016/S0009-2614(02)01660-3.

247. Noël Y, De La Pierre M, Zicovich-Wilson CM, Orlando R, Dovesi R. Structural, electronic and energetic properties of giant icosahedral fullerenes up to C6000: insights from an ab initio hybrid DFT study. *Phys Chem Chem Phys* 2014, 16:13390–13401. doi: 10.1039/C4CP01442A.

248. Lu X, Chen Z, Thiel W, Schleyer PR, Huang R, Zheng L. Properties of fullerene[50] and D_{5h} decachlorofullerene[50]: a computational study. *J Am Chem Soc* 2004, 126:14871–14878. doi: 10.1021/ja046725a.

249. Fowler PW, Sandall JPB. Predictions of special signatures of fullerenes. Second-order Jahn-Teller effects on the structures of C_{44}, C_{56}, C_{68} and C_{92}. *J Chem Soc, Perkin Trans 2* 1994:1917–1921. doi: 10.1039/P29940001917.

250. Paulus B. Electronic and structural properties of the cage-like molecules C_{20} to C_{36}. *Phys Chem Chem Phys* 2003, 5:3364–3367. doi: 10.1039/B304539K.

251. Grossman JC, Mitas L, Raghavachari K. Structure and stability of molecular carbon: importance of electron correlation. *Phys Rev Lett* 1995, 75:3870–3873. doi: 10.1103/PhysRevLett.75.3870.

252. Zhang BL, Wang CZ, Ho KM, Xu CH, Chan CT. The geometry of small fullerene cages: C_{20} to C_{70}. *J Chem Phys* 1992, 97:5007–5011. doi: 10.1063/1.463854.

253. Chen Z, Jiao H, Bühl M, Hirsch A, Thiel W. Theoretical investigation into structures and magnetic properties of smaller fullerenes and their heteroanalogues. *Theoret Chem Acc* 2001, 106:352–363. doi: 10.1007/s002140100284.

254. Chen Z, Heine T, Jiao H, Hirsch A, Thiel W, Schleyer PR. Theoretical studies on the smallest fullerene: from monomer to oligomers and solid states. *Chem Eur J* 2004, 10:963–970. doi: 10.1002/chem.200305538.

255. Gerhardt P, Löffler S, Homann KH. Polyhedral carbon ions in hydrocarbon flames. *Chem Phys Lett* 1987, 137:306–310. doi: 10.1016/0009-2614(87)80889-8.

256. Zhang QL, O'Brien SC, Heath JR, Liu Y, Curl RF, Kroto HW, Smalley RE. Reactivity of large carbon clusters: spheroidal carbon shells and their possible relevance to the formation and morphology of soot. *J Phys Chem* 1986, 90:525–528. doi: 10.1021/j100276a001.

257. Smalley RE. Self-assembly of the fullerenes. *Acc Chem Res* 1992, 25:98–105. doi: 10.1021/ar00015a001.

258. Wakabayashi T, Achiba Y. A model for the C_{60} and C_{70} growth mechanism. *Chem Phys Lett* 1992, 190:465–468. doi: 10.1016/0009-2614(92)85174-9.

259. Wakabayashi T, Kikuchi K, Shiromaru H, Suzuki S, Achiba Y. Ring-stacking considerations on higher fullerene growth. *Z Phys D* 1993, 26:258–260. doi: 10.1007/BF01425683.

260. von Helden G, Gotts NG, Bowers MT. Experimental evidence for the formation of fullerenes by collisional heating of carbon rings in the gas phase. *Nature* 1993, 363:60–63. doi: 10.1038/363060a0.

261. George S, Hammond VJK, eds. *Fullerenes: Synthesis, Properties, and Chemistry of Large Carbon Clusters*. ACS Symposium Series. Washington DC: ACS; 1992.

262. Ōsawa E. Formation mechanism of C_{60} under nonequilibrium and irreversible conditions – an annotation. *Fuller Nanotub Carbon Nanostruct* 2012, 20:299–309. doi: 10.1080/1536383X.2012.655104.

263. Sasaki K, Wakasaki T, Matsui S, Kadota K. Distributions of C_2 and C_3 radical densities in laser-ablation carbon plumes measured by laser-induced fluorescence imaging spectroscopy. *J Appl Phys* 2002, 91:4033–4039. doi: 10.1063/1.1455151.

264. Curl RF, Lee MK, Scuseria GE. C_{60} buckminsterfullerene high yields unraveled. *J Phys Chem A* 2008, 112:11951–11955. doi: 10.1021/jp806951v.

265. Zhang J, Bowles FL, Bearden DW, Ray WK, Fuhrer T, Ye Y, Dixon C, Harich K, Helm RF, Olmstead MM, et al. A missing link in the transformation from asymmetric to symmetric metallofullerene cages implies a top-down fullerene formation mechanism. *Nature Chem* 2013, 5:880–885. doi: 10.1038/NCHEM.1748.

266. Shinohara H. Endohedral metallofullerenes. *Rep Prog Phys* 2000, 63:843–892. doi: 10.1088/0034-4885/63/6/201.

267. Chaur MN, Melin F, Ortiz AL, Echegoyen L. Chemical, electrochemical, and structural properties of endohedral metallofullerenes. *Angew Chem Int Ed* 2009, 48:7514–7538. doi: 10.1002/anie.200901746.

268. Kobayashi K, Nagase S, Yoshida M, Ōsawa E. Endohedral metallofullerenes. Are the isolated pentagon rule and fullerene structures always satisfied? *J Am Chem Soc* 1997, 119:12693–12694. doi: 10.1021/ja9733088.

269. Beavers CM, Zuo T, Duchamp JC, Harich K, Dorn HC, Olmstead MM, Balch AL. $Tb_3N@C_{84}$: an improbable, egg-shaped endohedral fullerene that violates the isolated pentagon rule. *J Am Chem Soc* 2006, 128:11352–11353. doi: 10.1021/ja063636k.

270. Rodríguez-Fortea A, Alegret N, Balch AL, Poblet JM. The maximum pentagon separation rule provides a guideline for the structures of endohedral metallofullerenes. *Nature Chem* 2010, 2:955–961. doi: 10.1038/nchem.837.

271. Ugarte D. Curling and closure of graphitic networks under electron-beam irradiation. *Nature* 1992, 359:707–709. doi: 10.1038/359707a0.

272. Ugarte D. Canonical structure of large carbon clusters: C_n, $n > 100$. *Europhys Lett* 1993, 22:45–50. doi: 10.1209/0295-5075/22/1/009.

273. Bühl M, Thiel W. Ab initio helium NMR chemical shifts of endohedral fullerene compounds He@C_n (n = 32–180). *Chem Phys Lett* 1995, 233:585–589. doi: 10.1016/0009-2614(94)01459-9.

274. Ugarte D. Onion-like graphitic particles. *Carbon* 1995, 33:989–993. doi: 10.1016/0008-6223(95)00027-B.

275. Bühl M, Patchkovskii S, Thiel W. Interaction energies and NMR chemical shifts of noble gases

in C_{60}. *Chem Phys Lett* 1997, 275:14–18. doi: 10.1016/S0009-2614(97)00733-1.

276. Heggie MI, Terrones M, Eggen BR, Jungnickel G, Jones R, Latham CD, Briddon PR, Terrones H. Quantitative density-functional study of nested fullerenes. *Phys Rev B* 1998, 57:13339–13342. doi: 10.1103/PhysRevB.57.13339.

277. Zhang M, He D, Ji L, Wei B, Wu D, Zhang X, Xu Y, Wang W. Macroscopic synthesis of onion-like graphitic particles. *Nanostruc Mat* 1998, 10:291–297. doi: 10.1016/S0965-9773(98)00069-5.

278. Tomita S, Fujii M, Hayashi S, Yamamoto K. Electron energy-loss spectroscopy of carbon onions. *Chem Phys Lett* 1999, 305:225–229. doi: 10.1016/S0009-2614(99)00374-7.

279. Iglesias-Groth S. Fullerenes and buckyonions in the interstellar medium. *Astrophys J Lett* 2004, 608:L37. doi: 10.1086/422216.

280. Grimme S, Mück-Lichtenfeld C, Antony J. Noncovalent interactions between graphene sheets and in multishell (hyper)fullerenes. *J Phys Chem C* 2007, 111:11199–11207. doi: 10.1021/jp0720791.

281. Yamada M, Akasaka T, Nagase S. Endohedral metal atoms in pristine and functionalized fullerene cages. *Acc Chem Res* 2010, 43:92–102. doi: 10.1021/ar900140n.

282. Korona T, Dodziuk H. Small molecules in C_{60} and C_{70}: which complexes could be stabilized? *J Chem Theory Comput* 2011, 7:1476–1483. doi: 10.1021/ct200111a.

283. Botkin N, Turova-Botkina V. An algorithm for finding the Chebyshev center of a convex polyhedron. *Appl Math Optim* 1994, 29:211–222. doi: 10.1007/BF01204183.

284. Mantina M, Chamberlin AC, Valero R, Cramer CJ, Truhlar DG. Consistent van der Waals radii for the whole main group. *J Phys Chem A* 2009, 113:5806–5812. doi: 10.1021/jp8111556.

285. Weiske T, Böhme DK, Hrušák J, Krätschmer W, Schwarz H. Endohedral cluster compounds: inclusion of helium within C_{60}^+ and C_{70}^+ through collision experiments. *Angew Chem Int Ed* 1991, 30:884–886. doi: 10.1002/anie.199108841.

286. Weiske T, Hrusak J, Böhme DK, Schwarz H. Formation of endohedral carbon-cluster noble-gas compounds with high-energy bimolecular reactions: $C_{60}He^{n+}$ ($n = 1,2$). *Chem Phys Lett* 1991, 186:459–462. doi: 10.1016/0009-2614(91)90209-R.

287. Weiske T, Schwarz H. Sequential insertion of ^{3}He and ^{4}He in C_{60}^+. *Angew Chem Int Ed* 1992, 31:605–606. doi: 10.1002/anie.199206051.

288. Weiske T, Wong T, Krätschmer W, Terlouw JK, Schwarz H. The neutralization of He@C_{60}^+ in the gas phase: compelling evidence for the existence of an endohedral structure for He@C_{60}. *Angew Chem Int Ed* 1992, 31:183–185. doi: 10.1002/anie.199201831.

289. Weiske T, Hrušák J, Böhme DK, Schwarz H. Endohedral fullerene-noble gas clusters formed with high-energy bimolecular reactions of C_x^{n+} ($x = 60, 70$; $n = 1, 2, 3$). *Helvet Chim Acta* 1992, 75:79–89. doi: 10.1002/hlca.19920750106.

290. Weiske T, Schwarz H, Giblin DE, Gross ML. High-energy collisions of Kr@C_{60}^+ with helium. Evidence for the formation of HeKr@C_{60}^+. *Chem Phys Lett* 1994, 227:87–90. doi: 10.1016/0009-2614(94)00786-1.

291. Saunders M, Jimenez-Vazquez HA, Cross RJ, Mroczkowski S, Gross ML, Giblin DE, Poreda RJ. Incorporation of helium, neon, argon, krypton, and xenon into fullerenes using high pressure. *J Am Chem Soc* 1994, 116:2193–2194. doi: 10.1021/ja00084a089.

292. Son MS, Sung YK. The atom-atom potential. exohedral and endohedral complexation energies of complexes of X@C_{60} between fullerene and rare-gas atoms (X = He, Ne, Ar, Kr, and Xe). *Chem Phys Lett* 1995, 245:113–118. doi: 10.1016/0009-2614(95)00952-Z.

293. Straka M, Lantto P, Vaara J. Toward calculations of the ^{129}Xe chemical shift in Xe@C_{60} at experimental conditions: relativity, correlation, and dynamics. *J Phys Chem A* 2008, 112:2658–2668. doi: 10.1021/jp711674y.

294. Autschbach J, Zurek E. Relativistic density-functional computations of the chemical shift of ^{129}Xe in Xe@C_{60}. *J Phys Chem A* 2003, 107:4967–4972. doi: 10.1021/jp0346559.

295. Kurotobi K, Murata Y. A single molecule of water encapsulated in fullerene C_{60}. *Science* 2011, 333:613–616. doi: 10.1126/science.1206376.

296. Thilgen C. A single water molecule trapped inside hydrophobic C_{60}. *Angew Chem Int Ed* 2012, 51:587–589. doi: 10.1002/anie.201107379.

297. Zhang RQ, Ma WY, Han KL, Lee CS. A thermodynamic and kinetic study of the formation of C_{20} compounds encapsulating H, He and Ne atoms. *Theoret Chem Acc* 2003, 109:278–283. doi: 10.1007/s00214-003-0438-2.

298. Breslavskaya N, Levin A, Buchachenko A. Endofullerenes: size effects on structure and energy. *Russian Chem Bull* 2004, 53:18–23. doi: 10.1023/B:RUCB.0000024824.35542.0e.

299. Pyykkö P, Wang C, Straka M, Vaara J. A London-type formula for the dispersion interactions of endohedral A@B systems. *Phys Chem Chem Phys* 2007, 9:2954–2958. doi: 10.1039/B704695B.

300. Ruoff RS, Ruoff AL. The bulk modulus of C_{60} molecules and crystals: a molecular mechanics approach. *Appl Phys Lett* 1991, 59:1553–1555. doi: 10.1063/1.106280.

301. Tonner R, Frenking G, Lein M, Schwerdtfeger P. Packed to the rafters: filling up C_{60} with rare gas

atoms. *ChemPhysChem* 2011, 12:2081–2084. doi: 10.1002/cphc.201100360.

302. Tomaněk D, Zhong W, Krastev E. Stability of multi-shell fullerenes. *Phys Rev B* 1993, 48:15461–15464. doi: 10.1103/PhysRevB.48.15461.

303. Bates KR, Scuseria GE. Why are buckyonions round? *Theoret Chem Acc* 1998, 99:29–33. doi: 10.1007/s002140050299.

304. Casella G, Bagno A, Saielli G. Spectroscopic signatures of the carbon buckyonions $C_{60}@C_{180}$ and $C_{60}@C_{240}$: a dispersion-corrected DFT study. *Phys Chem Chem Phys* 2013, 15:18030–18038. doi: 10.1039/C3CP53273A.

305. Mackay AL, Terrones H. Diamond from graphite. *Nature* 1991, 352:762. doi: 10.1038/352762a0.

306. Vanderbilt D, Tersoff J. Negative-curvature fullerene analog of C_{60}. *Phys Rev Lett* 1992, 68:511–513. doi: 10.1103/PhysRevLett.68.511.

307. Ching WY, Huang MZ, Yn X. Electronic and optical properties of the Vanderbilt-Tersoff model of negative-curvature fullerene. *Phys Rev B* 1992, 46:9910–9912. doi: 10.1103/PhysRevB.46.9910.

308. Ceulemans A, Fowler PW. Symmetry extensions of Euler's theorem for polyhedral, toroidal and benzenoid molecules. *J Chem Soc Faraday Trans* 1995, 91:3089–3093. doi: 10.1039/FT9959103089.

309. Chuang C, Fan Y, Jin B. Systematics of toroidal, helically-coiled carbon nanotubes, high-genus fullerenes, and other exotic graphitic materials. *Procedia Eng* 2011, 14:2373–2385. doi: 10.1016/j.proeng.2011.07.299.

310. Schein S, Gayed JM. Fourth class of convex equilateral polyhedron with polyhedral symmetry related to fullerenes and viruses. *Proc Natl Acad Sci U S A* 2014, 111:2920–2925. doi: 10.1073/pnas.1310939111.

311. Terrones H, Mackay A. The geometry of hypothetical curved graphite structures. *Carbon* 1992, 30:1251–1260. doi: 10.1016/0008-6223(92)90066-6.

312. Ayuela A, Fowler PW, Mitchell D, Schmidt R, Seifert G, Zerbetto F. C_{62}: theoretical evidence for a nonclassical fullerene with a heptagonal ring. *J Phys Chem* 1996, 100:15634–15636. doi: 10.1021/jp961306o.

313. Charlier JC, Ebbesen TW, Lambin P. Structural and electronic properties of pentagon-heptagon pair defects in carbon nanotubes. *Phys Rev B* 1996, 53:11108–11113. doi: 10.1103/PhysRevB.53.11108.

314. Kirby E, Pisanski T. Aspects of topology, genus and isomerism in closed 3-valent networks. *J Math Chem* 1998, 23:151–167. doi: 10.1023/A%1019104804788.

315. An J, Gan LH, Zhao JQ, Li R. A global search for the lowest energy isomer of C_{26}. *J Chem Phys* 2010, 132:154304. doi: 10.1063/1.3364801.

316. Vizitiu AE, Diudea MV. C_{60} structural relatives – an omega-aided topological study. In: Cataldo F, Graovac A, Ori O, eds. *The Mathematics and Topology of Fullerenes*, vol. 16. Berlin: Springer; 2011, 39–60.

317. Terrones H, Terrones M. The transformation of polyhedral particles into graphitic onions. *J Phys Chem Solids* 1997, 58:1789–1796. doi: 10.1016/S0022-3697(97)00067-X.

318. Avron JE, Berger J. Tiling rules for toroidal molecules. *Phys Rev A* 1995, 51:1146–1149. doi: 10.1103/PhysRevA.51.1146.

319. Berger J, Avron JE. Classification scheme for toroidal molecules. *J Chem Soc Faraday Trans* 1995, 91:4037–4045. doi: 10.1039/FT9959104037.

320. Tamura R, Ikuta M, Hirahara T, Tsukada M. Positive magnetic susceptibility in polygonal nanotube tori. *Phys Rev B* 2005, 71:045418. doi: 10.1103/PhysRevB.71.045418.

321. Borštnik B, Lukman D. Molecular mechanics of toroidal carbon molecules. *Chem Phys Lett* 1994, 228:312–316. doi: 10.1016/0009-2614(94)00944-9.

322. Diudea MV, Kirby EC. The energetic stability of tori and single-wall tubes. *Fuller Sci Technol* 2001, 9:445–465. doi: 10.1081/FST-100107148.

323. Kang MH. Toroidal fullerenes with the Cayley graph structures. *Discrete Math* 2011, 311:2384–2395. doi: 10.1016/j.disc.2011.06.018.

324. Yoshida M, Fujita M, Fowler PW, Kirby EC. Non-bonding orbitals in graphite, carbon tubules, toroids and fullerenes. *J Chem Soc Faraday Trans* 1997, 93:1037–1043. doi: 10.1039/A607401D.

325. Iijima S, Ichihashi T, Ando Y. Pentagons, heptagons and negative curvature in graphite microtubule growth. *Nature* 1992, 356:776–778. doi: 10.1038/356776a0.

326. Diudea MV, Nagy CL, Silaghi-Dumitrescu I, Graovac A, Janežić D, Vikic-Topiić D. Periodic cages. *J Chem Inf Model* 2005, 45:293–299. doi: 10.1021/ci049738g.

327. Diudea MV, Bende A, Nagy CL. Carbon multi-shell cages. *Phys Chem Chem Phys* 2014, 16:5260–5269. doi: 10.1039/C3CP55309D.

328. Terrones H, Terrones M. Quasiperiodic icosahedral graphite sheets and high-genus fullerenes with nonpositive Gaussian curvature. *Phys Rev B* 1997, 55:9969–9974. doi: 10.1103/PhysRevB.55.9969.

329. Ricardo-Chávez JL, Dorantes-Dávila J, Terrones M, Terrones H. Electronic properties of fullerenes with nonpositive Gaussian curvature: finite zeolites. *Phys Rev B* 1997, 56:12143–12146. doi: 10.1103/PhysRevB.56.12143.

330. Bandow S, Takizawa M, Hirahara K, Yudasaka M, Iijima S. Raman scattering study of double-wall carbon nanotubes derived from the chains of fullerenes in single-wall carbon nanotubes. *Chem Phys Lett* 2001, 337:48–54. doi: 10.1016/S0009-2614(01)00192-0.

331. Terrones H. Beyond carbon nanopeapods. *ChemPhysChem* 2012, 13:2273–2276. doi: 10.1002/cphc.201200321.

332. Donadio D, Colombo L, Milani P, Benedek G. Growth of nanostructured carbon films by cluster assembly. *Phys Rev Lett* 1999, 83:776–779. doi: 10.1103/PhysRevLett.83.776.

333. Barborini E, Piseri P, Milani P, Benedek G, Ducati C, Robertson J. Negatively curved spongy carbon. *Appl Phys Lett* 2002, 81:3359–3361. doi: 10.1063/1.1516635.

334. Benedek G, Vahedi-Tafreshi H, Barborini E, Piseri P, Milani P, Ducati C, Robertson J. The structure of negatively curved spongy carbon. *Diamond Relat Mater* 2003, 12:768–773. doi: 10.1016/S0925-9635(03)00082-7.

335. Benedek G. The topological background of schwarzite physics. In: Cataldo F, Graovac A, Ori O, eds. *The Mathematics and Topology of Fullerenes*, vol. 16. Berlin: Springer; 2011, 214–247.

336. Schwarz HA. Sur une définition erronée de l'aire d'une surface courbe. In: *Gesammelte Mathematische Abhandlungen*. Berlin: Springer; 1933.

337. Dierkes U, Hildebrandt S. *Global Analysis of Minimal Surfaces*, vol. 341. Berlin: Springer; 2010.

338. Terrones H, Terrones M. Curved nanostructured materials. *New J Phys* 2003, 5:126.1–126.37. doi: 10.1088/1367-2630/5/1/126.

339. Lenosky T, Gonze X, Teter M, Elser V. Energetics of negatively curved graphitic carbon. *Nature* 1992, 355:333–335. doi: 10.1038/355333a0.

340. Weierstrass K. Untersuchungen über die Flächen, deren mittlere Krümmung überall gleich Null ist. *Monatsber Akad Wiss Berlin* 1866, 612–625.

341. Terrones H, Mackay A. Negatively curved graphite and triply periodic minimal surfaces. *J Math Chem* 1994, 15:183–195. doi: 10.1007/BF01277558.

342. Gonzalez Szwacki N, Sadrzadeh A, Yakobson BI. B_{80} fullerene: an ab initio prediction of geometry, stability, and electronic structure. *Phys Rev Lett* 2007, 98:166804. doi: 10.1103/PhysRevLett.98.166804.

343. Enyashin AN, Ivanovskii AL. Graphene allotropes. *Phys Status Sol (b)* 2011, 248:1879–1883. doi: 10.1002/pssb.201046583.

344. Sundholm D. C_{72}: gaudiene, a hollow and aromatic all-carbon molecule. *Phys Chem Chem Phys* 2013, 15:9025–9028. doi: 10.1039/C3CP51042E.

345. Bulusu S, Li X, Wang LS, Zeng XC. Evidence of hollow golden cages. *Proc Natl Acad Sci U S A* 2006, 103:8326–8330.

346. Johansson MP, Sundholm D, Vaara J. Au_{32}: a 24-carat golden fullerene. *Angew Chem Int Ed* 2004, 43:2678–2681. doi: 10.1002/anie.200453986.

347. Gao Y, Zeng XC. Au_{42}: an alternative icosahedral golden fullerene cage. *J Am Chem Soc* 2005, 127:3698–3699. doi: 10.1021/ja050435s.

348. Karttunen AJ, Linnolahti M, Pakkanen TA, Pyykkö P. Icosahedral Au_{72}: a predicted chiral and spherically aromatic golden fullerene. *Chem Commun* 2008, 465–467. doi: 10.1039/B715478J.

349. Assadollahzadeh B, Schwerdtfeger P. A systematic search for minimum structures of small gold clusters Au_n (n = 2-20) and their electronic properties. *J Chem Phys* 2009, 131:064306. doi: 10.1063/1.3204488.

350. Zhai HJ, Zhao YF, Li WL, Chen Q, Bai H, Hu HS, Piazza ZA, Tian WJ, Lu HG, Wu YB, et al. Observation of an all-boron fullerene. *Nature Chem* 2014, 6:727–731. doi: 10.1038/nchem.1999.